Numerical modeling of rapidly varying flow conditions in collection systems

by

Robson Leo Pachaly

Dissertation submitted to the Graduate Faculty of
Auburn University
in partial fulfillment of the
requirements for the Degree of
Doctor of Philosophy

Auburn, Alabama
December 11, 2021

Keywords: Collection systems, Computational hydraulics, SWMM, HEC-RAS, OpenFOAM

Approved by

José G. Vasconcelos, Chair, Associate Professor of Civil Engineering
Xing Fang, Professor of Civil Engineering
Frances O'Donnell, Assistant Professor of Civil Engineering
Jay Khodadadi, Alumni Professor of Mechanical Engineering

Abstract

The design, operation and maintenance of urban water infrastructure depends on the urban runoff flow characteristics. Many modeling tools are being applied for predicting the flow characteristics and their accuracy are essential for more resilient, cost-effective, and safer operation of urban water infrastructures. Engineers and practitioners around the world face difficulties in applying such modeling tools due to the large number of models currently available, the necessary set up parameters, and the required precision to achieve the modeling goals. This research focused in applying well-known models in the context of urban drainage, aiming for improvements in their hydraulic accuracy and in more efficient applications of these models.

The Stormwater Management Model (SWMM) is one of the most used tools to simulate different components of urban water systems. Typical unsteady flow conditions are well represented by SWMM, but its capability to precisely simulate more complex phenomena such as regime transition, mixed flows, closed pipe transients, and surges were unknown. The introduction of artificial spatial discretization in SWMM, by increasing the number of computational cells in each link, and the addition of the Preissmann slot pressurization algorithm have the potential to expand SWMM's applications. Hence, artificial spatial discretization and pressurization algorithms were systematically investigated using the conditions presented in the SWMM 5 Quality Assurance Program report. General improvements were achieved in terms of continuity error and numerical stability when artificial spatial discretization was introduced along with the Preissmann slot pressurization algorithm.

The rapid filling of collection systems can lead to the development of fast transients, specially caused by unexpected situations such as pump failure or sudden flow blockage. Significant pressure and velocity variations may occur during these events. It was unknown whether SWMM could accurately represent such situations. For this reason, a modification for the new Preissmann slot pressurization algorithm that enforces a celerity value close to the ones anticipated in transient flows was proposed along with artificial spatial discretization. An

analytical solution of a hydraulic transient and a model comparison of a real-world situation where a hydraulic transient is expected were used to assess the potential benefits of these modifications. The results demonstrated that SWMM is capable to represent certain types of hydraulic transients when set up accordingly.

Stormwater tunnels under rapid filling conditions caused by intense rain events might face operational problems, such as surging. The SWMM capability to represent such situation was never investigated and the addition of artificial spatial discretization as well modifications on the Preissmann slot algorithm are expected to improve SWMM's representation of surging. Using part of the Chicago's TARP tunnel system, a combination of artificial spatial discretization and pressurization algorithms in SWMM was compared to the HAST model, which was specifically designed to represent surges in stormwater tunnels. It was shown that, with adequate model set up, SWMM can represent surging in stormwater tunnels more precisely.

Urban areas tend to experience flooding events, especially during intense heavy rain events and/or when the drainage system has limited hydraulic conveyance. Combining a 1D model to represent the key hydrological aspects of the watershed and a 2D model to simulate the flooding extent would enable a better representation of flooding in urban areas as well as faster model set up. Therefore, a 1D PCSWMM was used to represent the surface hydrology and a 2D HEC RAS model was used to simulate the flooding extent based on 1D PCSWMM results. Field data was collected for calibration purposes and possible conceptual approaches that could mitigate the extent of flooding were assessed. This modeling framework predicted the flooded areas according to reported flooding events and it demonstrated that flooding depth and duration was reduced when the conceptual approaches were employed.

In large stormwater tunnels, rapid filling conditions may lead to the formation of air pockets and its discharge through vertical structures can cause damages to the system. The pressure variation of uncontrolled air release in complex dropshaft structures was little known. Hence, an investigation of a multiphase rapid filling condition in a tunnel system in Columbus, OH was performed. The methodology coupled a 1D and a 3D model to determine the magnitude of surges, possibility of air pocket entrapment, air–water surging, and the consequences of uncontrolled air pocket release. Results demonstrated that proper ventilation is required to

reduce the growth of air phase pressure to safe levels since the air compressibility can cause damages to the dropshaft top slab.

Finally, the methodologies proposed in this dissertation improved the accuracy of flow simulation in a range of dynamic, transient, and multiphase flow conditions. We hope that the findings of this research will aid in future applications of simulating flows in collection systems, leading to better operational conditions and greater resiliency.

Table of Contents

List of Figures

List of Tables

List of Abbreviations

$1D$	One-dimensional
$2D$	Two-dimensional
$3D$	Three-dimensional
ASD	Artificial Spatial Discretization
CFD	Computational Fluid Dynamics
CFL	Courant-Friedrich-Lewy stability condition
CHI	Computational Hydraulics International
CN	Curve Number
CSO	Combined Sewer Overflow
CV	Control Volume
DEM	Digital Elevation Model
DWE	Diffusion Wave Equations
EPA	Environmental Protection Agency
$HAST$	Hydraulic Analysis of Sewers and Tunnels
HEC	Hydrological Engineering Center
$JCDH$	Jefferson County Department of Health

$LiDAR$ Light Detection And Ranging

LOT Lower Olentangy Tunnel

$M\&E$ Metcalf & Eddy Inc. of Palo Alto

$MNSA$ Minimum Nodal Surface Area

MOC Method of Characteristics

$MWRD$ Metropolitan Water Reclamation of the District of the Greater Chicago

$NLCD$ National Land Cover Database

$NOAA$ National Oceanic and Atmospheric Administration

$NRCS$ Natural Resources Conservation Service

$OARS$ OSIS Augmentation and Relief Sewer

OBJ Wavefront Object

$OSIS$ Olentangy Scioto Interceptor River

QA Quality Assurance

$RANS$ Reynolds-averaged Navier–Stokes

$SRTC$ Sensitivity-based Radio Tunning Calibration

$SSURGO$ Soil Survey Geographic Database

STL Stereolithography

SWE Shallow Water Equations

$SWMM$ Storm Water Management Model

$TARP$ Tunnel and Reservoir Plan

TPA Two-component Pressure Approach

UDP Upper Des Plaines Tunnel

UF University of Florida

$USDA$ United States Department of Agriculture

$USGS$ United States Geological Survey

VOF Volume of Fluid

Eu sou apenas um rapaz

Latino-americano

Sem dinheiro no banco

Sem parentes importantes

E vindo do interior

Belchior

Chapter 1

Introduction and literature review

The development of urban areas over recent years, converting pervious areas into impervious, led to an excessive quantity of runoff being generated (Wanielista & Yousef, 1992). This overflow must be conveyed by the cities' collection systems and/or infiltrated over green areas. Quantifying this runoff involves many variables, such as land cover, soil type, rainfall, and others (Mays, 2001). Some of these variables may change over time, for instance, land cover could change so significantly since the construction of a collection system that the system cannot convey the runoff anymore. Also, depending on the age of the collection system, it could experience damages such as blocked pipes or detritus that decreases the capacity of conveying runoff (Yen, 1986). These changes within the systems can lead to different types of hydraulics transients that may result in economical and social impacts to the cities (Wright et al., 2011; Zhou et al., 2002).

One way to predict these phenomena and propose design solutions is the usage of rainfall-runoff models (Wanielista & Yousef, 1992). In general, a model can be defined as a simplified, schematic representation of the real world (Popescu, 2014). The necessity of design and plan drainage structures more economically and quickly as possible led to the development of many rainfall-runoff models and software. These models were significantly transformed and improved over the past centuries by advances in technology and computing (Cunge, 1980; Popescu, 2014), nowadays considered an important engineering tool. They are used to aid engineers, scientists, and decision-makers to understand what is happening in the present and predict scenarios of what may happen in the future (Popescu, 2014).

Hydrological models couple hydrological calculations to estimate the runoff quantity and hydraulic calculations to route the flow through a system of reaches. Nowadays, there are many modeling tools available, some developed by governmental agencies and others by private companies, with different modeling objectives. However, these models can be based on simple mathematical equations and have a very simplified engine and fast computations while others can be based on complex mathematical equations and require high computational efforts. The degree of complexity required by these models depends on the phenomena being analysed by the modeler. For example, the operation of a collection system under a weak rainfall event can be represented by a simpler model, but when the same collection system is operating under heavy rainfall, a more robust model may be required to accurately predict the flow characteristics.

1.1 Stormwater systems modeling

Due to its complexity, the flow in sewers, stormwater systems, or combined systems is a complicated phenomenon to be properly modeled. There are many conditions in these systems that can cause instabilities problems (Yen, 1986). According to Cunge (1980), some particular features of drainage network flow demand special requirements for a precise modeling. The design of collection systems usually considers gravity or free surface flow. However, in some situations such as severe floods, inadequate pumping capacity, unsteady inflows to the system, blockage of the line, occurrence of hydraulic jump, and others, the system can become partially or completely surcharged (Yen, 1986). Geysering (Muller et al., 2017; Vasconcelos & Wright, 2011; Wright et al., 2011), manhole blow-off (Wang & Vasconcelos, 2020), sharp-peaked overflow, structural damages (Zhou et al., 2002), waterhammer pressure peaks (Wylie & Streeter, 1993) are problems that might occur due to this transition and are scope of study by many authors.

Flooding is another issue caused by intense rain events. When modeling flooding areas, one usually relies in two-dimensional (2D) models for predicting the flooding extent. In urban areas, the collection systems comprise both natural and manmade channels. A precise representation of the manmade drainage network as well as the natural drainage network is required to represent problems such as flash floods and river floods (Wanielista & Yousef, 1992). Furthermore, in

regions where the flow path is not completely known or where the streams are highly braided, the usage of 2D models could provide better results than an one-dimensional (1D) model.

In some large collection systems, the air-water interactions may also cause significant damages to the collection system (Muller et al., 2017; Vasconcelos & Wright, 2011; Wright et al., 2011). The formation and release of entrapped air pockets within these systems have been extensively studied over the last years (Schulz et al., 2020; Vasconcelos & Leite, 2012; Vasconcelos & Wright, 2006; Zhou et al., 2002). However, only a few 1D models can predict the formation and motion of these air pockets, and modeling their release through vertical structures is complex, usually requiring three-dimensional (3D) models. The 3D models typically solve the Navier-Stokes equations and require significant computational efforts. To date, a widespread application of 3D models for predicting the formation, motion, and release of air pockets in stormwater systems is limited.

Even though all fluid flows are 3D by nature, some phenomena can be simplified as 1D or 2D for modeling purposes. The balance between computational effort, applicability, and accuracy will depend on the physical process being modeled and the modeling goal. Higher dimensions and more complex mathematical formulations will require more computational effort for its solution. Therefore, dropping one or two dimensions or simplifying its mathematical formulation could significantly reduce its computational effort. However, care should be taken to not oversimplify to a point where the mathematical formulation is not applicable anymore or when the accuracy is impaired.

The following sections will describe in more detail the formulation and simplifications of 1D, 2D, and 3D models mostly used in civil and environmental engineering applications. It is important to highlight that no derivation will be shown in this dissertation for the sake of brevity. Only the equations used in each modeling approach and its simplifications will be presented.

1.2 One-dimensional flows

Some types of flow can be assumed as 1D, such as the case of flows where the flow characteristics vary only on longitudinal direction and have well-defined boundaries. A good example of this simplification is the flow in pipes or open-channel flows. The conservation laws of mass,

momentum and, energy are used to describe open-channel flows (Chaudhry, 2007; Sturm, 2001). However, to define flow conditions at a channel cross section only two flow variables such as depth and velocity are sufficient. The equations of continuity and momentum are commonly used to determine the characteristics of open-channel flows (Chaudhry, 2007, 2013; Cunge, 1980; Popescu, 2014; Sturm, 2001). These equations, known as the Saint-Venant equations, incorporate only the most important aspects of flow to describe open-channel flows in a simple way (Cunge, 1980).

The open-channel governing equations adopt the following assumptions (Chaudhry, 2007; Cunge, 1980; Sturm, 2001):

- The flow is one-dimensional;
- Pressure distribution is hydrostatic;
- Channel bottom slope is small;
- Flow velocity over the entire channel cross section is uniform;
- Channel is prismatic;
- Head losses may be simulated by using the steady-state resistance laws.

The next sections will explain the Saint-Venant equations and its most common solutions techniques.

1.2.1 Governing equations

Continuity Equation

For any control volume, during a small time interval (Δt), the law of conservation of mass states that the difference between the mass entering and leaving the control volume is equal to the change of mass inside the control volume (Popescu, 2014). According to Chaudhry (2007), in open-channel flows the water is assumed to be incompressible and have a constant mass density. Because of that, the conservation of mass can be expressed as the continuity equation (Equation 1.1) (Sturm, 2001):

$$\frac{\partial A}{\partial t} + \frac{\partial Q}{\partial x} = q_L \tag{1.1}$$

where *A* is the cross sectional area of the flow, *Q* is the channel flow rate, q_L is the lateral contribution per unit length of the channel. Both the flow rate and depth are functions of distance *x* and time *t*.

The continuity equation shows that the channel flow rate is balanced with temporal changes in cross sectional area at a point (Sturm, 2001). If the right-hand side of this equation is zero, the mass is conserved in any closed contour in the $x - t$ plane. On the other hand, if the right-hand side of this equation is not zero, the q_L term is used as a source or a sink of water depending of its sign (Chaudhry, 2007; Cunge, 1980; Sturm, 2001).

Momentum equation

The Momentum Equation is based on the Newton's second law of motion. This law states that the resultant force acting on the control volume is equal to the rate of change of momentum (Chaudhry, 2007). The assumptions used in open-channel flows to simplify the momentum equation include neglecting shear stresses due to wind and the effects of Coriolis acceleration. In many engineering applications, particularly 1D flows, these assumptions are commonly used (Chaudhry, 2007; Sturm, 2001). The Momentum Equation considering the lateral inflow as zero, channels is shown in the Equation 1.2:

$$\frac{1}{A}\frac{\partial Q}{\partial t} + \frac{1}{A}\frac{\partial}{\partial x}(\frac{Q^2}{A}) + g\frac{\partial y}{\partial x} = g(S_o - S_f) \tag{1.2}$$

where *g* is the gravity, *y* is the water depth, S_o the channel bottom slope, S_f is the friction slope, and *A* the cross-sectional area on which the force acts (Sturm, 2001). This equation is valid for unsteady, nonuniform flow and it is commonly referred as the dynamic equation since it does not genuinely describe the conservation of momentum (Chaudhry, 2007; Sturm, 2001).

1.2.2 Numerical solution techniques

The set of differential equations explained in the previous section are too complex to be solved by analytical methods (Chaudhry, 2007; Cunge, 1980). Because of that, approximate solutions of the derivatives can be obtained by numerical techniques either in the characteristic form or in the original partial differential form (Sturm, 2001).

Method of Finite Differences

The Method of Finite Differences is used to find numerical solutions for Partial Differential Equations (PDE) and it is based on the Taylor series. The method replaces functions of continuous arguments which describe the state of flow by functions defined on a structured grid of points (Bates et al., 2005; Causon & Mingham, 2010; Popescu, 2014). This grid is called computational grid (Figure 1.1) and it has a finite set of points sharing the same domain in the $x - t$ plane. Then, these functions are combined to give an equation for the derivative at the given point in terms of those around it (Abbott & Basco, 1997; Bates et al., 2005; Causon & Mingham, 2010; Popescu, 2014).

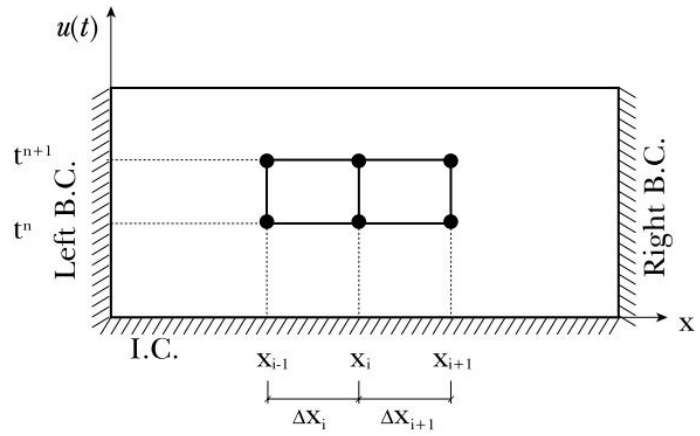

Figure 1.1: Computational grid. Adapted from Popescu (2014).

Explicit finite difference methods use an explicit function of dependent variables already determined for several grid nodes at the beginning of the time step to advance the solution to

the end of the time step at a single grid node (Abbott & Basco, 1997). Even though the explicit finite difference techniques are easy to program, they need to obey the Courant condition to maintain stability. This condition depends of the flow velocity and celerity, which are functions of flow depth and the spatial grid spacing (Equation 1.3) (Chaudhry, 2007; Courant et al., 1928; Cunge, 1980). Thus, as the flow depth and velocity change during the computations, the time step might need to be altered at each computational interval to maintain stability. Hence, the time step should be selected in a way that the Courant Number (C_n) be below and as close to unity as possible (Abbott & Basco, 1997; Chaudhry, 2007; Cunge, 1980; Popescu, 2014).

$$C_n = \frac{|V| \pm c}{\Delta x / \Delta t} \tag{1.3}$$

where V is velocity, c is celerity, and Δx and Δt are, respectively, spatial and temporal discretization.

Differently from the explicit methods, the implicit methods use more than one grid value of the dependent variable at the future time in the computational grid. As a result, a system of equations that include multiple variables at the unknown time level exists, requiring thus simultaneous solution (Chaudhry, 2007; Popescu, 2014; Sturm, 2001; Yen, 1986). The advantage of these methods against the explicit methods are their inherent stability without having to satisfy the Courant condition, yielding sometime very small time steps (Sturm, 2001). However, implicit methods are relatively more difficult to formulate and program than the explicit methods due to the need to solve simultaneously these flow equations (Yen, 1986).

In addition, the Method of Finite Differences needs to use numerical schemes to be implemented. There are many finite difference schemes used in unsteady flow modeling. These schemes can be grouped in distinct classes depending of its main features such as the way in which physical coefficients in the flow equations are discretized or the number of grid points used. Numerical schemes such as Lax-Diffusive, Leapfrog, and Lax-Wendroff for explicit methods and Preissmann, Beam and Warming, and Vasiliev for implicit methods can be cited as the ones usually used in hydraulic modeling (Abbott & Basco, 1997; Chaudhry, 2007; Cunge, 1980). Also, these schemes are referred as linear schemes because, as the solution progresses

over time and space, the results of the conserved variables can be written as a linear combination of the variable already calculated. These schemes contrast with non-linear schemes that are often applied in Finite-Volume models.

Method of Characteristics

The method of characteristics (MOC) can be defined as graphical procedure for the integration of partial differential equations. The MOC eliminates the one independent variable in the continuity and momentum equations, transforming the PDE's into ODE's. Then, the ODE's are integrated on specific locations in the solution domain, called characteristics lines. This concept is mainly used in transient analysis in closed conduits and its application in open-channel analysis is unusual (Chaudhry, 2007; Sturm, 2001). However, this method is used in special cases such as the representation of boundary conditions or to check on some other method. The reason for that is the capability of following individual perturbations and the physical significance of its parameters (Abbott & Basco, 1997; Chaudhry, 2007; Cunge, 1980; Sturm, 2001). More information regarding the MOC can be found at Sturm (2001) and Chaudhry (2007).

Finite volume

The Finite Volume method is a numerical method for solving differential equations that can be used on structured and unstructured grids (Popescu, 2014). While the Method of Finite Differences uses a structured grid of points, the Finite Volume Method evaluates the average value of the solution over a volume. According to Popescu (2014), the computational domain is discretized into Control Volumes (CV) and the differential equations are integrated using numerical integration for each CV. Then, the values of the unknown function and their derivatives are approximated at the nodes of the CV. Finally, the solution is obtained by assembling the equations at the nodes over the CV into an algebraic system of equations. Figure 1.2 shows the 2D cell centered Finite Volume Method.

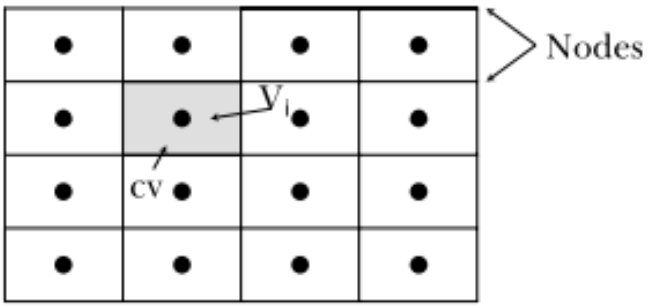

Figure 1.2: 2D Finite Volume. Adapted from Popescu (2014).

Even though the Finite Volume Method can be implemented with linear numerical schemes, it is not usual in practical cases. Usually, non-linear numerical schemes are applied on Finite Volume methods. Differently from the linear numerical schemes, the update of flow values in non-linear numerical schemes is not a linear combinations from the variables already calculated. In these schemes, more physics is introduced, improving the overall computational accuracy.

1.2.3 One-dimensional models

Storm Water Management Model

The University of Florida (UF) along the CDM consulting firm (formerly WRE) and Metcalf & Eddy Inc. of Palo Alto (M&E) started in 1969, funded by the Environmental Protection Agency (EPA), the initial development of Storm Water Management Model (SWMM). At this time, SWMM focused only in combined sewer overflow (CSO) but through several upgrades since its first version the model turned into a dynamic rainfall-runoff simulator. Nowadays, distributed and maintained by EPA, SWMM 5.1 has been complete re-written and added many more features. SWMM is a dynamic hydrologic-hydraulic model that can be used to simulate runoff quantity and quality for a single event or continuous simulation. The model estimates the runoff generated by subcatchments, transporting it through collection systems and computing the flow rate, flow depth, and water quality in each component of the collection system. Planning, analysis, and design of storm water runoff, combined sewers, sanitary sewers, and other drainage systems in urban areas and non-urban areas are tasks commonly performed by the SWMM users

around the world (Rossman, 2015b). One of the many advantages of SWMM against other models is that its code is open-source and it can be downloaded directly from the EPA website (www.epa.gov), allowing many users around the world to help the development of the model and add new features.

SWMM accounts many hydrological processes to simulate runoff quality and quantity from primarily urban areas. Dividing the study area into a collection of small areas with particular characteristics, the model can represent accurately the spatial variability of hydrological processes. Time-varying rainfall, evaporation, infiltration, interception, snow accumulation and melting, and many other processes are used to perform the SWMM hydrological simulation (Rossman & Huber, 2016). Furthermore, the user can select different methods for estimating these processes, such as Curve Number, Green-Ampt, Horton, and others for infiltration, Hargreaves for evaporation, and so on.

SWMM transports the runoff generated by the hydrological processes through system of pipes, channels, storage/treatment devices, pumps, and regulators. The model represents this collection system components using nodes and links. The SWMM's hydraulic solver uses one-dimensional, gradually varied, and unsteady flow equations to determine at each time step the water level at each node, and flow rate and flow depth at each link (Rossman, 2017a). For unsteady flow analysis, SWMM uses the Saint-Venant equations for solving the conservation of mass and momentum for each link coupled with a conservation of mass each node.

The Saint-Venant equations are not able to simulate pressurized flows because the two-phase flow is not in accordance with the assumptions of Saint-Venant equations (Popescu, 2014; Trajkovic et al., 1999). For that, one needs to use a conceptual model. Some approaches have been developed to deal with the transition from open-channel to pressurized flows. One of the most used methods to avoid the change of equations between open-channel and pressurized flow is the Preissmann slot. This method considers a small vertical slot over each pipe allowing the application of open-channel equations throughout the surcharged situation (Cunge, 1980), as shown in Figure 1.3. Two limitations of this method is that it does not sustain negative pressures and spurious numerical oscillations may occur during the transition from open-channel to pressurized flow (Bousso et al., 2013).

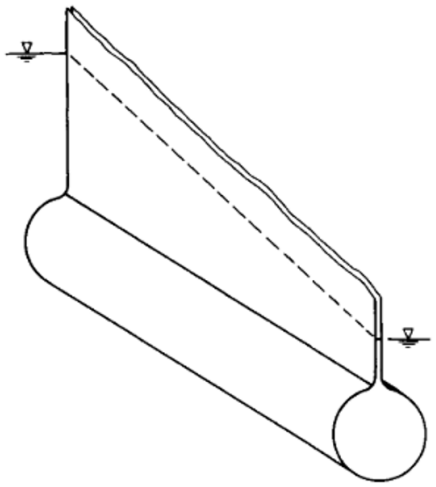

Figure 1.3: Preissmann slot concept. Adapted from Yen (1986).

Another method to handle this transition is to use a different set of equations when the flow becomes pressurized. Assuming that pipe cross sectional elasticity and water compressibility are negligible, the continuity (Eq. 1.4a) and momentum (Eq. 1.4b) become:

$$\frac{\partial H}{\partial t} = \sum Q/A_s \tag{1.4a}$$

$$\frac{\partial Q}{\partial H} = (\frac{gA}{L})\frac{\Delta t}{1 + \Delta Q_{losses}} \tag{1.4b}$$

where A_s denotes the surface area of the junction, L denotes the conduit length, and ΔQ_{losses} denotes a term that accounts for local and friction losses. Changing the equations during a simulation, specially when simulating dynamic flow conditions, may cause a significant impact on the simulation in terms of numerical stability. It is important to highlight that both methods described here cannot simulate two-phase flows.

HAST model

The Hydraulic Analysis Stormwater Tunnels (HAST) is a model that implements a non-linear finite volume numerical scheme that uses an approximate Riemann solver associated with the Saint-Venant Equations to model stormwater conduits and open channel flow. Due to its formulation, HAST is able to properly simulate all flow conditions of a tunnel filling process, including locations where air can potentially be trapped and the transition from open channel

to surcharged flow (Lautenbach et al., 2008; Vasconcelos et al., 2015). Problems related to smearing of flow discontinuities associated with shock phenomena such as hydraulic bores are minimized, mainly by the use of non-linear numerical schemes (Lautenbach et al., 2008).

This solving technique has a number of advantages in terms of conservativeness, geometric flexibility, and conceptual simplicity when compared to more simple methods (Bousso et al., 2013; Chaudhry, 2007; Popescu, 2014; Roe, 1981; Sturm, 2001; Toro, 2013). The models which use Riemann Solver or approximate Riemann Solvers have many benefits such as the possibility of handle different discontinuities. Also, these models are insensitive to low Courant numbers as far as the hydraulics' modeling accuracy is concerned. As stated by Bousso et al. (2013), complex episodes and discontinuities such as mixed flow, two-phase flow, roll waves, shock waves, expansion waves, and others are able to be accurately modeled by these solvers. However, the combination of finite volume and non-linear numerical schemes for flow modeling is a relatively new approach and a limited number of studies has been performed (Vasconcelos et al., 2015).

HAST uses the Two-component Pressure Approach (TPA) (Vasconcelos & Wright, 2006). The TPA represents the effects of pressurization in a single set of equations, starting from the set of mass and momentum equations in traditional pressurized pipe flows and assuming an elastic behavior to the pipe wall while neglecting water compressibility. This leads to the following set of equations:

$$\frac{\partial \overrightarrow{U}}{\partial t} + \frac{\partial \overrightarrow{F}}{\partial x} = S(\overrightarrow{U}) \tag{1.5a}$$

$$\overrightarrow{U} = \begin{bmatrix} A \\ Q \end{bmatrix} \quad F(\overrightarrow{U}) = \begin{bmatrix} Q \\ \frac{Q^2}{A} + gAh_c + gAh_s \end{bmatrix} \quad S(\overrightarrow{U}) = \begin{bmatrix} 0 \\ gA(S_o - S_f) \end{bmatrix} \tag{1.5b}$$

where h_c denotes the depth of the centroid of the cross-sectional flow area; and h_s denotes the pressure head associated with pressurized flows (positive or negative). Equations 1.5a and 1.5b differ from the traditional Saint-Venant formulation because a surcharge head h_s is included. This term is zero if the pipeline flows in a free surface flow regime, and relates to the

cross-sectional flow area A, the original pipe wall A_{pipe} and the acoustic wave speed a when the flow regime is pressurized.

1.3 Two-dimensional flows

In some situations, the 1D flow assumption may not be representative of the physical process being analysed and the 3D flow calculations could require excessive not necessary computational power. In such cases, a 2D model could be employed for results of reasonable accuracy and a simpler mathematical formulation (Chaudhry, 2007). Mapping flooding, dam break analysis, wide floodplains, and other analysis are examples where the 2D assumption can be employed. The 2D assumption simplifies the 3D flows by using vertically averaged quantities (Chaudhry, 2007). The next sections will present the governing equations.

1.3.1 Governing equations

The 2D governing equations are derived from the Navier-Stokes equations for an incompressible fluid (Chaudhry, 2007). These equations are often referred as the Shallow Water Equations (SWE). The basic assumptions for deriving the governing equations are the same as the previous section but considering 2D flows. Also, the SWE can be solved with the same numerical techniques as the Saint Venant equations.

Continuity equation

The continuity equation for 2D flows is derived by integrating the Navier-Stokes continuity equation over the flow depth. This integration results in Equation 1.6:

$$\frac{\partial h}{\partial t} + \frac{\partial (uh)}{\partial x} + \frac{\partial (vh)}{\partial y} = 0 \tag{1.6}$$

where u and v are the mean values of velocity in $x - y$ directions over the depth of the channel h (Chaudhry, 2007).

Momentum equation

Assuming uniform density and velocity distribution, hydrostatic pressure and small channel bottom, the turbulent motion is approximated using eddy viscosity and effective stresses dominated by the bottom shear stresses (Chaudhry, 2007). The momentum equations in the $x - y$ directions are shown in the following equations (Eq. 1.7a & 1.7b):

$$\frac{\partial(uh)}{\partial t} + \frac{\partial(u^2h + gh^2/2)}{\partial x} + \frac{\partial(uvh)}{\partial y} = gh(S_{ox} - S_{fx}) \tag{1.7a}$$

$$\frac{\partial(vh)}{\partial t} + \frac{\partial(uvh)}{\partial x} + \frac{\partial(v^2h + gh^2/2)}{\partial y} = gh(S_{oy} - S_{fy}) \tag{1.7b}$$

where S_{ox} and S_{oy} are the channel slopes the S_{fx} and S_{fy} are the friction slopes.

1.3.2 Two-dimensional modeling tools

PCSWMM

PCSWMM is a third party software developed by the Computational Hydraulics International (CHI) that uses SWMM engine together with has the capability to perform 1D-2D and quasi-2D modeling procedures (Beck, 2016). As a result, it is a software that allows the user to not only perform the same calculations present in SWMM but extends its usage to broader applications. Furthermore, PCSWMM has GIS features integrated with its interface that allows for a faster model setup and a calibration tool named SRTC that aids in model calibration.

The 1D-2D modeling procedure implemented in PCSWMM considers a 1D channel network and a 2D floodplain. It employs a connection between the 1D network and 2D mesh by using or a direct connection between the junctions or a bottom orifice. At these specific connection points is where the floodplain will start to receive water or when the water accumulated on the 2D mesh will contribute to the conveyance of the 1D network (Beck, 2016). The full quasi-2D modeling procedure within PCSWMM uses a no-wall rectangular channel that represents the whole 2D mesh. According to Beck (2016), one drawback of this method is the channel wetted perimeter could be misrepresented.

As SWMM, PCSWMM can be employed in a wide range of applications. Over the last years, this software is been employed for analysing Low Impact Development techniques (Ahiablame & Shakya, 2016; Goncalves et al., 2018; Palermo et al., 2020), flood analysis (Munir et al., 2020; Nazari et al., 2016; Pinos & Timbe, 2019), stormwater systems design and analysis (Bi et al., 2015; Panos et al., 2018; Paule-Mercado et al., 2018), and other applications.

HEC-RAS

HEC-RAS is a powerful model capable of performing many hydrological, hydraulic, and water quality modeling. The software is developed at the Hydrological Engineering Center (HEC) by the U.S. Army Corps of Engineers (Brunner, 2021a). HEC-RAS is constantly updated since its first version in 1995 and the current version (6.0) has many hydrodynamic flow routing capabilities (Brunner, 2021a). The software is designed for 1D, 2D, or combined 1D-2D hydraulic calculations for natural and constructed channels (Brunner, 2021a).

The 1D calculations in HEC-RAS allows for water surface profile calculations in subcritical, supercritical and mixed flow regimes. For the steady flow, the water surface profiles are calculated in each cross-section by solving the Energy Equation using the standard step method (Brunner, 2021a). For unsteady flow, HEC-RAS uses the principles of mass conservation and momentum conservation for calculating the water surface profiles. More information about its mathematical formulation and solution techniques can be found in (Brunner, 2021b).

The 2D unsteady flow calculations performed by HEC-RAS solve either the 2D Shallow Water equations or the 2D Diffusion Wave equations (Brunner, 2021a). Using an Implicit Finite Volume algorithm, the routing time step required for maintaining the stability can be larger than when a explicit method is employed. As in the 1D calculations, the subcritical, supercritical and mixed flows regimes can be solved, allowing for the correct representation of hydraulic jumps and flows passing through critical depth (Brunner, 2021a). HEC-RAS can also combine the 1D and the 2D hydraulic calculations, an advantage when modeling 1D structures such as culverts and bridges.

Many studies have been performed using this software lately. Its applications range from flooding events (Benito et al., 2003; Quirogaa et al., 2016; Timbadiya et al., 2011), dam break

analysis (Butt et al., 2013; Haltas et al., 2016; Yi, 2011), bridge and culvert design and analysis (Larsen et al., 2011; Lee et al., 2006; Seckin et al., 2007), and other applications.

1.4 Three-dimensional flows

In the past sections, it was discussed that the fluid flow could be considered 1D or 2D depending on the physical process that is being modeled and the simplifications assumed. However, any fluid flow is 3D by nature and it follows three fundamental principles: conservation of mass, momentum, and energy (Wendt, 2008). These principles are expressed in partial differential equations and the act of replacing these equations with numbers and advancing its solutions in space and time is called Computational Fluid Dynamics (CFD) (Wendt, 2008). The next sections will show a brief discussion of these equations and solutions techniques.

1.4.1 Governing equations

The 3D fluid motion follows the three fundamental physical principles from the laws of physics, the conservation of mass, momentum, and energy (Wendt, 2008). Its properties, such as velocity, pressure, temperature, density, and others, should be solved simultaneously at each time step and at each cell of the computational domain. The next sections will present the equations for incompressible flows. More information regarding the derivation of these equations can be found in Wendt (2008).

Mass conservation

The continuity equation states that the mass is conserved. It means that the difference between the mass that enters and leaves the system is zero. Considering an incompressible fluid, the continuity equation can be expressed in conservation form as Equation 1.8.

$$\frac{\partial u}{\partial x} + \frac{\partial v}{\partial y} + \frac{\partial w}{\partial z} = 0 \tag{1.8}$$

where u, v, and w are the velocities in the x, y, and z directions.

Momentum conservation

The momentum equation is based on the Newton's 2nd law, which states that the force on the fluid element is equal to its mass times the element's acceleration (Wendt, 2008). There are two forces acting on the fluid element: body forces and surface forces. The first is caused by gravitational, electric and magnetic forces and the latter is caused by the pressure distribution and by the shear and normal stresses acting on the element surface (Wendt, 2008). The momentum equations in the x, y, and z directions are presented in Equations 1.9a, 1.9b, and 1.9c:

$$\rho(\frac{\partial u}{\partial t} + u\frac{\partial u}{\partial x} + v\frac{\partial u}{\partial y} + w\frac{\partial u}{\partial z}) = \rho g_x - \frac{\partial P}{\partial x} + \mu(\frac{\partial^2 u}{\partial x^2} + \frac{\partial^2 u}{\partial y^2} + \frac{\partial^2 u}{\partial z^2}) \tag{1.9a}$$

$$\rho(\frac{\partial v}{\partial t} + u\frac{\partial v}{\partial x} + v\frac{\partial v}{\partial y} + w\frac{\partial v}{\partial z}) = \rho g_y - \frac{\partial P}{\partial y} + \mu(\frac{\partial^2 v}{\partial x^2} + \frac{\partial^2 v}{\partial y^2} + \frac{\partial^2 v}{\partial z^2}) \tag{1.9b}$$

$$\rho(\frac{\partial w}{\partial t} + u\frac{\partial w}{\partial x} + v\frac{\partial w}{\partial y} + w\frac{\partial w}{\partial z}) = \rho g_z - \frac{\partial P}{\partial z} + \mu(\frac{\partial^2 w}{\partial x^2} + \frac{\partial^2 w}{\partial y^2} + \frac{\partial^2 w}{\partial z^2}) \tag{1.9c}$$

where ρ is the fluid's density, μ is the viscosity coefficient, and P is the pressure.

Energy conservation

The energy conservation states that the rate of change of energy in a fluid's element is equal to the summation of the net flux of heat into the element and the rate of working done on the element due to body and surface forces (Wendt, 2008). The energy equation is shown in Equation 1.10.

$$\rho c_p(\frac{\partial T}{\partial t} + u\frac{\partial T}{\partial x} + v\frac{\partial T}{\partial y} + w\frac{\partial T}{\partial z}) = k(\frac{\partial^2 T}{\partial x^2} + \frac{\partial^2 T}{\partial y^2} + \frac{\partial^2 T}{\partial z^2}) + \phi \tag{1.10}$$

Where T is temperature, c_p is specific heat, k is thermal conductivity, and ϕ is viscous dissipation rate.

Turbulence modeling

Von Karman (1937) was one of the first authors that tried to define turbulence. His definition of turbulence stated that: "Turbulence is an irregular motion which in general makes its appearance

in fluids, gaseous or liquid, when they flow past solid surfaces or even when neighboring streams of the same fluid flow past or over one another". According to Wilcox et al. (1998), this definition can be imprecise because of the term "irregular motion". Then, another definition proposed by Hinze (1975) has a better description of turbulence: "Turbulent fluid motion is an irregular condition of flow in which the various quantities show a random variation with time and space coordinates, so that statistically distinct average values can be discerned".

Turbulent flows are very relevant in many engineering applications. The turbulence can enhance the fluid's diffusivity since the transfer of mass, momentum, and energy is increased in turbulent flows (Wilcox et al., 1998). Turbulent flows are present in daily situations, such as the airflow over an aircraft wind, the flow in pipes, and others. The CFD models rely on turbulent models to predict the evolution of turbulence. Nowadays, these turbulent models are called n-equation models, where n is the number of additional differential transport equations beyond those expressing conservation of mass, momentum, and energy (Wilcox et al., 1998). The zero-equation models are based on mixing-length hypothesis. The one-equation models depend on the kinetic energy of the turbulent fluctuations (k). The two-equation models use k and the turbulence length scale or equivalent (Wilcox et al., 1998). The two-equation models will be discussed in detail on section 1.4.3, where the CFD solver applied in this dissertation is presented. More information regarding turbulence modeling can be found in Wilcox et al. (1998).

1.4.2 Numerical solution techniques

Volume of Fluid

The numerical method named Volume of Fluid (VOF) is employed for free surface approximation. The surfaces where discontinuities exist in one or more variables are called free boundaries (Hirt & Nichols, 1981). Many problems arise in these situations, such as in their boundary conditions, discrete representation, and evolution in time (Hirt & Nichols, 1981). For this reason, the VOF came out to be a simple and efficient method for tracking and locating the free boundaries.

This method considers a function F that its numerical value depends on the fluid that is occupying that point (Hirt & Nichols, 1981). In a multiphase - air & water - simulation, a point occupied by water is considered 1 and 0 is occupied by air. For the points where the F values range between 0 and 1, it is considered a free surface. The advantage of using this method is that it can locate free boundaries with a minimum of stored information (Hirt & Nichols, 1981). The time dependence of F is governed by Equation 1.11:

$$\frac{\partial F}{\partial t} + u\frac{\partial F}{\partial x} + v\frac{\partial F}{\partial y} = 0 \tag{1.11}$$

More information regarding the VOF method can be found in Hirt and Nichols (1981).

1.4.3 Three-dimensional models

Nowadays, there are many CFD packages available that can perform a variety of simulations. However, many of them require a commercial license, such as ANSYS fluent (Matsson, 2020) or Star-CCM+ (CD-adapco, 2017). A free-to-use and well-known package is OpenFOAM (OpenFOAM, 2021). This CFD software will be described in more detail in the following section.

OpenFOAM

One of the most used CFD software in many areas of engineering and science, considering applications in industry and academy, is OpenFOAM. It is an open source C++ object-oriented library that has been developed primarily by OpenCFD Ltd and it has many features that allow the solution of many complex fluid flows, including chemical reactions, turbulence, heat transfer, and other applications (OpenFOAM, 2021). OpenFOAM has frequent updates that include customer developments and contributions by its community. At every update, and independent and rigorous quality assurance is prepared before the release of a new version, guaranteeing progressive development and maintenance (OpenFOAM, 2021).

There are various multiphase flow solvers within OpenFOAM, such as *interFoam*, *InterDyMFoam*, *twoPhaseEulerFoam*, *compressibleInterFoam*, and others (Schulze & Thorenz,

2014). The solver selection depends on the problem that will be analysed and in its simplifications. For instance, in some simulations the air and water compressibility plays a major role, requiring a solver that handles this compressibility accordingly. However, in other simulations, this may not be as relevant and a solver that considers the fluids as incompressible can be used. In the following section, the solver named *compressibleInterFoam* will be discussed in more detail.

compressibleInterFoam

The *compressibleInterFoam* is a solver for two compressible, non-isothermal immiscible fluids using the VOF phase-fraction based on the interface capturing approach (Hirt & Nichols, 1981; OpenFOAM, 2021). The thermodynamic and transport properties - viscosity, density, and specific heat - are derived from properties of the mixture components (Svenungsson, 2016). There are many applications in the context of air-water interactions in closed conduits using this solver, such as the works of Eldayih and Vasconcelos (2018), Huang et al. (2021), Muller et al. (2017), Vasconcelos (2019), and Wang and Vasconcelos (2018).

The *compressibleInterFoam* solves the Navier–Stokes equations. Equations 1.12a, 1.12b and 1.12c present the two-phase continuity, momentum, and energy expressions solved by the *compressibleInterFoam* in OpenFOAM. Equation 1.12d is used to track the free surface and it is modified to reduce issues associated with the convection of the step function.

$$\frac{\partial \rho}{\partial t} = \bigtriangledown \cdot (\rho U) = 0 \tag{1.12a}$$

$$\frac{\partial (\rho U)}{\partial t} + \bigtriangledown \cdot (\rho U U) = - \bigtriangledown p + \bigtriangledown \cdot (\mu \bigtriangledown U) + S_U \tag{1.12b}$$

$$\frac{\partial (\rho C_p T)}{\partial t} + \bigtriangledown \cdot (\rho U C_p T) = \bigtriangledown \cdot (k \bigtriangledown T) + S_T \tag{1.12c}$$

$$\frac{\partial \alpha}{\partial t} + \bigtriangledown \cdot (\alpha U) + \bigtriangledown \cdot ((1-\alpha)\alpha U r) = 0 \tag{1.12d}$$

where rho is the fluid density, t is the time, U is the 3D velocity vector, p is the pressure μ is the dynamic viscosity, S_U is the momentum source term, C_p is the specific heat, T is the temperature, S_T is the energy source term, α is the volume fraction ($0 \leq \alpha \leq 1$), and U_r is the

velocity field to compress the interface. The values of α represent the liquid fraction within a cell, with unity representing pure water and zero pure air. The velocity field U_r is included to counter a disadvantage of VOF in solving for the free surface that is related to interface smearing near the free surface, as described by Rusche (2003).

This solver allows the user to define which turbulence model will be used for solving the fluid flow. The most used turbulence models are $k-\epsilon$, $k-\omega$, and $k-\omega\ SST$. The $k-\epsilon$ is a two-equation model which motivation was to improve the mixing-length model, as well as to find an alternative to algebraically prescribing turbulent length scales in moderate to high complexity flows. It gives a general description of turbulence by means of two transport equations. Equations 1.13a and 1.13b show the two-equations in conservation form.

$$\frac{\partial(\rho k)}{\partial t}+\frac{\partial(\rho u_j k)}{\partial x_j}=P-\rho\epsilon+\frac{\partial}{\partial x_j}[(\mu+\frac{\mu_t}{\sigma_k})\frac{\partial k}{\partial x_j}]+\rho L_k \tag{1.13a}$$

$$\frac{\partial(\rho \epsilon)}{\partial t}+\frac{\partial(\rho u_j \epsilon)}{\partial x_j}=C_{\epsilon_1}f_1\frac{\epsilon}{k}P-C_{\epsilon_2}f_2\frac{\rho\epsilon^2}{k}+\frac{\partial}{\partial x_j}[(\mu+\frac{\mu_t}{\sigma_\epsilon})\frac{\partial \epsilon}{\partial x_j}]+\rho L_\epsilon \tag{1.13b}$$

$k-\omega$ is a common two-equation turbulence model that is used as a closure for the Reynolds-averaged Navier–Stokes equations (RANS equations). The model attempts to predict turbulence by two partial differential equations (Equations 1.14a and 1.14b) for k and ω, which is the specific rate of dissipation.

$$\frac{\partial(\rho k)}{\partial t}+\frac{\partial(\rho u_j k)}{\partial x_j}=P-\beta^*\rho\omega k+\frac{\partial}{\partial x_j}[(\mu+\sigma_k\frac{\rho k}{\omega})\frac{\partial k}{\partial x_j}] \tag{1.14a}$$

$$\frac{\partial(\rho \omega)}{\partial t}+\frac{\partial(\rho u_j \omega)}{\partial x_j}=\frac{\gamma\omega}{k}P-\beta\rho\omega^2+\frac{\partial}{\partial x_j}[(\mu+\sigma_\omega\frac{\rho k}{\omega})\frac{\partial \omega}{\partial x_j}]+\frac{\rho\sigma_d}{\omega}\frac{\partial k}{\partial x_j}\frac{\partial \omega}{\partial x_j} \tag{1.14b}$$

Finally, $k-\omega\ SST$ combines the $k-\omega$ turbulence model and $k-\epsilon$ turbulence model such that the $k-\omega$ is used in the inner region of the boundary layer and switches to the $k-\epsilon$ in the free stream. This two turbulence model combination is performed by a blending function called F_1. When $F_1=1$ the $k-\omega$ is activated and when $F_1=0$ the $k-\epsilon$ is activated. Equations 1.15a and 1.15b show the $k-\omega\ SST$ turbulence model.

$$\frac{\partial(\rho k)}{\partial t} + \frac{\partial(\rho u_j k)}{\partial x_j} = P - \beta^* \rho \omega k + \frac{\partial}{\partial x_j}[(\mu + \sigma_k \mu_t)\frac{\partial k}{\partial x_j}] \tag{1.15a}$$

$$\frac{\partial(\rho \omega)}{\partial t} + \frac{\partial(\rho u_j \omega)}{\partial x_j} = \frac{\gamma}{\nu_t} P - \beta \rho \omega^2 + \frac{\partial}{\partial x_j}[(\mu + \sigma_\omega \mu_t)\frac{\partial \omega}{\partial x_j}] + 2(1 - F_1)\frac{\rho \sigma_{\omega_2}}{\omega}\frac{\partial k}{\partial x_j}\frac{\partial \omega}{\partial x_j} \tag{1.15b}$$

For the sake of brevity, all the terms presented in these equations are not thoroughly explained in this section. The objective of presenting these equations is to give a brief overview of the turbulence models employed in the following sections of this dissertation. More information regarding these turbulence models as well as its derivation and explanation of all terms and constants can be found in Wilcox et al. (1998).

1.5 Knowledge gap

Facing the necessity of more effective stormwater systems designs, hydrological/hydraulic models have been extensively used over the last years. However, these models have limitations when trying to model more complex flows conditions. Currently, situations such as the pressurization of flows or pressurization bores, incorrect peak and frequency of surges, flooding, air-water interactions, and others are not well-represented by most 1D urban stormwater models, specially in system-wide applications. Also, the potential benefits of coupling 1D models with 2D and 3D models to address such situations is unknown.

1.6 Objectives and hypothesis

1.6.1 Main objective

This dissertation proposes innovative approaches and methodologies in numerical modeling and model setup methodologies of stormwater systems, specially in rapidly varying flow conditions. As a result, it will aid engineers and modelers to have more precise analysis of collection systems' operation and more accurate design solutions.

1.6.2 Specific objectives

- Assess a new model setup methodology to represent unsteady flows conditions in SWMM by changing different numerical modeling variables such as spatial & temporal discretization and modifications on pressurization algorithms.
- Evaluate the accuracy and potential limitations of SWMM to represent cases of closed-pipe transient flows by comparing its results against analytical solutions and a benchmark model.
- Apply SWMM in the context of rapid filling of a large-scale stormwater tunnel and evaluate its capacity to predict surges.
- Predict flooding in urban watersheds and propose conceptual design approaches to mitigate the flooding extent by employing a combination of 1D and 2D models.
- Propose a methodology that combines 1D and 3D models to represent the air discharge in stormwater tunnel systems.

1.7 Dissertation's structure

This dissertation contains seven chapters, organized as follows:

Chapter 1: Introduction and literature review provides background on stormwater systems modeling and in its mathematical formulations. This chapter explains when a 1D model is suitable for modeling a specific physical process or when a 2D or 3D models may be required for representing other types of physical processes occurring in stormwater systems. Also, some of the most used software and packages for modeling processes within stormwater systems and their formulations and current limitations are discussed.

Chapter 2: Comparing SWMM 5.1 calculation alternatives to represent unsteady stormwater sewer flows is a paper published on the *ASCE Journal of Hydraulic Engineering* where artificial spatial discretization was introduced in SWMM to represent unsteady flows in stormwater systems. This new modeling approach was evaluated in terms of continuity errors and numerical

stability. Improvements were achieved in modeling results when the proposed methodology was employed.

Chapter 3: Evaluating SWMM capabilities to simulate closed pipe transients was published on the *IAHR Journal of Hydraulic Research*. This chapter proposed a modification on the SWMM's Preismann slot algorithm allowing for a more precise simulation in the context of closed pipe transients. The modification resulted in a more precise closed pipe transient simulations.

Chapter 4: Surge predictions in a large stormwater tunnel system using SWMM is a paper published on the *IAHR Urban Water Journal* and it is an evaluation of the SWMM capability of predicting surges in large stormwater tunnel systems. The combination of the modified Preismann slot algorithm and artificial spatial discretization in SWMM allowed for a better SWMM representation of surging.

Chapter 5: Numerical modeling study of flooding in Brighton and Midfield presents results from a hydrological and hydraulic numerical study for the Jefferson County Department of Health (JCDH) on urban flooding in two areas of the Jefferson County, AL. This study comprised 1D PCWSMM and 2D HEC RAS modeling efforts to estimate the flooding extent as well as proposed conceptual approaches to mitigate the flooding extent.

Chapter 6: Multiphase Rapid Filling Conditions of Tunnel System in Columbus, Ohio describes a methodology that employed a combination of a 1D model for tracking the formation and motion of air pockets and a 3D model to predict the discharge of this air pocket through vertical shafts. This paper was accepted for publication on the *CHI Journal of Water Management and Modeling*. The employed methodology was able to track the formation, motion, and discharge of air pockets within the collection system.

Chapter 7: Conclusions and future research contains a summary of the most important conclusions drawn for each one of the dissertation's chapters. Also, in this section presents recommendations of future research on the topics covered in this dissertation.

Chapter 2

Comparing SWMM 5.1 Calculation Alternatives to Represent Unsteady Stormwater Sewer Flows[†]

Abstract - The Storm Water Management Model 5.1 (SWMM) is a widely-adopted dynamic hydrologic and hydraulic model often used to estimate runoff quantity and quality in urban drainage systems. SWMM unsteady flow algorithm, EXTRAN, is based on a link-node solution that enables it to represent well typical stormwater inflows. Yet, for rapid inflow conditions associated with more extreme inflows, predictions yielded by SWMM underestimate surges and sometimes under-represent sudden changes sewer flow conditions. Recent research showed the benefits of introducing in SWMM models artificial spatial discretization (ASD) to represent rapid inflows in sewers. However, with the recent addition of the Preissmann slot algorithm in SWMM formulation, a systematic evaluation of the performance of this pressurization algorithm in complex and highly dynamic inflow scenarios is still missing. The present work applied the conditions presented in the SWMM 5 Quality Assurance Program (QA) report and compared the use of either link-node or ASD along the original EXTRAN and the new Preissmann slot algorithm in modeling results. The performance of each of the selected modeling alternatives was evaluated in terms of continuity errors and numerical stability. The findings obtained here indicate modeling results improvements with an adequate selection of temporal and spatial discretization.

[†]**Published in**: Pachaly, R. L., Vasconcelos, J. G., Allasia, D. G., Tassi, R., & Bocchi, J. P. P. (2020). Comparing SWMM 5.1 Calculation Alternatives to Represent Unsteady Stormwater Sewer Flows. *Journal of Hydraulic Engineering*, 146(7). DOI: https://doi.org/10.1061/(ASCE)HY.1943-7900.0001762

2.1 Introduction and objectives

The Environmental Protection Agency (EPA) Stormwater Management Model 5.1 (SWMM) is one of the most successful and popular hydrologic-hydraulic models currently in use worldwide (Niazi et al., 2017; Obropta & Kardos, 2007). This model, which results from a multi-decade development effort (Huber & Roesner, 2012), is able to simulate runoff quantity and quality for single-event or continuous hydrologic modeling (EPA, 2018). Operating on a collection of subcatchments areas which receives precipitation and generates runoff, SWMM transports this runoff through system of pipes, channels, and others using its unsteady flow formulation presented by Roesner et al. (1988) and Rossman (2006).

SWMM unsteady formulation solves the flow conditions in a network of conduits (also referred as links) and junctions (also referred as nodes) through the Saint-Venant equations (EPA, 2018). In this work, this standard SWMM approach is referred as link-node solution. The Saint-Venant equations are a system of two partial differential equations based on the conservation of mass and linear momentum that represent the unsteady open-channel flows (Sturm, 2010). SWMM applies these equations to solve the flow along an individual conduit and an additional continuity relationship for the junctions, such as manholes, that connect two or more conduits together (Rossman, 2006). Even though SWMM is able to apply simplified versions of the Saint-Venant equations, such as the Zero-Inertia Wave or the Kinematic Wave, the complete Saint-Venant equations are frequently necessary when modeling rapid filling scenarios leading to pressurization (EPA, 2018). However, when very long conduits are present or when highly dynamic flow conditions happen, SWMM modeling results may yield significant flow continuity errors and/or numerical instabilities (Hodges et al., 2019; Pachaly et al., 2019; Ridgway, 2008; Vasconcelos et al., 2018).

In its version 5.1.013, SWMM allows the selection between two options to represent pressurized flows in conduits: EXTRAN and SLOT. EXTRAN denotes the traditional pressurization algorithm initially present in earlier SWMM versions ($<$ 5.1.012) (Roesner et al., 1988), which uses a variation of the surcharge algorithm to update nodal heads and link flows when the node's water level exceeds the crown of the highest conduit connected to it (Rossman, 2006).

When this situation occurs, an alternative nodal continuity condition expressed in the form of a perturbation equation is used to update nodal heads at the new time step. When both upstream and downstream nodes are surcharged, another set of equations is applied because the flow is considered pressurized (Rossman, 2006).

The SLOT pressurization algorithm is based on the Preissmann slot concept (Preissmann, 1961), which adds an hypothetical vertical and narrow slot at the pipe crown. This artificial slot allows the maintenance of free surface flow conditions, but also enables the increasing of cross-sectional pressure force in the momentum equation when conduit flow is pressurized. Using this method, SWMM's normal procedure for updating nodal heads can continue to be used (EPA, 2018). While there are significant differences in the solution procedure adopted by the EXTRAN and SLOT algorithms, to date no studies have been conducted comparing eventual differences yielded by these algorithms when extreme flow conditions are considered.

Parallel to the comparison between pressurization algorithms, some studies (e.g. Ridgway (2008), Vasconcelos et al. (2018), Pachaly et al. (2019)) evaluated the SWMM accuracy in hydraulic computations by the means of adding artificial spatial discretization (ASD) between SWMM nodes. ASD implies in splitting links into smaller ones by placing intermediate nodes as extra calculation points, often performed with the selection of smaller routing time steps to ensure numerical stability. Ridgway (2008) simulated force main transients using SWMM 5 and other programs. The findings of this work showed that reducing the link length by placing intermediate nodes can produce more realistic results. Vasconcelos et al. (2018) evaluated the SWMM accuracy to simulate mixed flows using experimental investigations. The authors concluded that the combination of spatial and temporal discretization in SWMM has a major impact in the accuracy of the simulation. Pachaly et al. (2019) tested several spatial discretizations approaches in SWMM using data from a field evaluation of a rapid filling situation in a real stormwater system. Their findings showed that adding spatial discretization in SWMM improves the simulation of rapid filling conditions but it has a significant impact on the computational time to perform the simulations. This is in accordance with Popescu (2014) that stated that reducing the approximation error by using small temporal and spatial discretization when solving the Saint-Venant equations can lead to significant improvements in accuracy.

Simultaneously to these studies, different SWMM applications have emerged. Some of them allowed SWMM to simulate situations that the model was not originally conceived to perform. In some cases it might require alterations in its source code (Burger et al., 2014; Cho & Seo, 2007) or coupling it with other software (Buahin & Horsburgh, 2018; Riaño-Briceño et al., 2016; Seyoum et al., 2012), but sometimes only adjusting the model setup (Pachaly et al., 2019; Ridgway, 2008; Vasconcelos et al., 2018) is enough. For example, some studies have shown that SWMM is able to represent intermittent water distribution systems (Campisano et al., 2019), mixed flows (Vasconcelos et al., 2018), rapid inflows (Pachaly et al., 2019), or force main transients (Ridgway, 2008) when coupling it with other software or setting the model properly for these specific situations.

Back in 2006, when SWMM was being upgraded from version 4.4 to version 5, a rigorous Quality Assurance (QA) report (Rossman, 2006) was elaborated to assure that the numerical results obtained by the SWMM's new version were compatible with the results from the previous version, specially regarding the dynamic wave routing (i.e. solution by Saint-Venant equations). The examples used in this QA are available online and contain many characteristics that are useful for testing highly dynamic flows in SWMM, including the newly implemented SLOT surcharge method and the additional spatial discretization. For the sake of brevity, many figures and information regarding the QA examples were suppressed in this work. Therefore, the reader should refer to the QA report (Rossman, 2006) for figures and locations of links and nodes.

The objective of this work is to present results related to a systematic analysis in terms of continuity errors and numerical stability by comparing the existing surcharge algorithms present in SWMM and the use of ASD versus the traditional link-node modeling approach. This systematic evaluation was performed using the modeling conditions presented in the SWMM QA report by Rossman (2006). Besides the comparison in terms of continuity and stability, this work includes a comparison of computational effort associated with ASD usage and different surcharge algorithms. Since adding ASD to SWMM models is a very time-demanding task, a software named ReSWMM was developed in order to automatize this task and it is available for download.

2.2 Methodology

2.2.1 SWMM formulation

The unsteady flow solver is one of the key modules presented in SWMM (EPA, 2018). This module is based on the EXTRAN algorithm originally proposed by Roesner et al. (1988) and, due to its simplicity and versatility, SWMM 5.1 continues to use this solution technique. However, some modifications were implemented in order to bring improvements in the model stability (Rossman, 2017b). Using a link-node approach, SWMM solves the complete form of Saint-Venant equations for unsteady free surface flow through a channel or pipe (Roesner et al., 1988; Rossman, 2006, 2017b). The Saint-Venant equations, conservation of mass (Eq. 2.1) and momentum (Eq. 2.2), can be expressed as:

$$\frac{\partial A}{\partial t} + \frac{\partial Q}{\partial x} = 0 \tag{2.1}$$

$$\frac{\partial Q}{\partial t} + \frac{\partial (Q^2/A)}{\partial x} + gA\frac{\partial H}{\partial x} + gAS_f + gAh_L = 0 \tag{2.2}$$

where A denotes cross-sectional area; t denotes time; Q denotes flow rate; x denotes distance; H denotes the hydraulic head of water in the conduit; g denotes gravity; h_L denotes the local energy loss per unit length of conduit; and S_f denotes the friction slope, which is implemented with the Manning equation (Rossman, 2006).

Within SWMM, these equations are converted into an explicit set of finite difference formulas and then solved using a method of successive approximations with under relaxation (Rossman, 2006). To compute the flow in each conduit and head in each node, SWMM uses, respectively, Eq. 2.3 and Eq. 2.4 for time $t + \Delta t$ as function of known values at time t (Rossman, 2006).

$$Q_{t+\Delta t} = \frac{Q_t + \Delta Q_{gravity} + \Delta Q_{inertial}}{1 + \Delta Q_{friction} + \Delta Q_{losses}} \tag{2.3}$$

$$H_{t+\Delta t} = H_t + \frac{\Delta Vol}{(A_{store} + \sum A_s)_{t+\Delta t}} \tag{2.4}$$

Where $\Delta Q_{gravity}$, $\Delta Q_{inertial}$, $\Delta Q_{friction}$, and ΔQ_{losses} denote the type of force they represent; ΔVol denotes net volume flowing through the node over the time step; A_{store} denotes surface area of the node; and $\sum A_s$ denotes surface area contributed by the conduits connected to the node. More details are provided in Rossman (2006).

When the nodal water level exceeds the crown of the highest conduit connected to it, the surcharge condition exists (Rossman, 2006, 2017b). In this situation, the current SWMM version (5.1.013) allows for the selection between two surcharge methods to handle pressurized conditions: EXTRAN or SLOT (EPA, 2018). Also, SWMM version 5.1.013 modified the calculation of the Minimum Nodal Surface Area (MNSA) during unsteady flow calculations. In previous SWMM versions (<5.1.012), the MNSA was being used as a surface area always available at a node instead of an amount of area available only when the surface area of the node's connecting links fells below it. To date, the impact of this modification in dynamic flow conditions was not investigated.

In both versions of the EXTRAN pressurization algorithm, when the surcharge condition exists, the surface area contributed by any closed conduits would be zero and an additional formulation is needed to update nodal head at new time steps (Roesner et al., 1988; Rossman, 2006). Using a form of a perturbation equation (Eq. 2.5) when the flow depth is greater than 96% of link diameter (EPA, 2018), this pressurization algorithm enforces the flow continuity condition.

$$\Delta H = \frac{-\sum Q}{\sum \partial Q / \partial H} \tag{2.5}$$

Where ΔH is the adjustment to the node's head that must be made to achieve a flow balance (Rossman, 2017b). Within a conduit, the combination of Eq. 2.5 and Eq. 2.3 results in:

$$\frac{\partial Q}{\partial H} = \frac{-g\overline{A}\Delta t / L}{1 + \Delta Q_{friction} + \Delta Q_{losses}} \tag{2.6}$$

where the negative sign is because the flow directed out of a node is considered negative while the flow into the node is considered positive (Rossman, 2006).

The SLOT surcharge method is based on the Preissmann Slot concept. This technique has been extensively used since 1960 (Chaudhry, 2008) and eliminates the need to switch to the surcharge algorithm for surcharged nodes (EPA, 2018). Using a vertical and narrow slot over each pipe, the free surface flow condition prevails allowing the use of Saint-Venant Equations (Cunge et al., 1980). When using this method in SWMM, the Preissmann Slot is attached to closed conduits flowing more than 98.5% full (EPA, 2018) using the Sjöberg equation (Jackson et al., 1986) for a smooth transition between the pipe crown and the slot, until a final slot width of 1% of link diameter.

Surcharge conditions frequently occur during rapid fillings and/or highly dynamic situations. Therefore, differences in modeling results between both versions (5.1.012 and 5.1.013) of the EXTRAN pressurization algorithm and the SLOT pressurization algorithm are expected. A comparison between these pressurization algorithms were performed.

Routing time-step and artificial discretization

The routing time-step recommendation originally proposed by Roesner et al. (1988) to ensure SWMM numerical stability was shown to be inadequate to represent modeling conditions involving rapid filling and ASD (Vasconcelos et al., 2018). Vasconcelos et al. (2018) suggested a simple modification of the original recommendation by Roesner et al. (1988), presented in Eq. 2.7, which was shown to reduce continuity errors in extreme inflows and pressurization conditions.

$$\Delta t = 0.1 \, \frac{\Delta x}{\sqrt{gD}} \tag{2.7}$$

Where Δt denotes recommended routing time-step; Δx denotes size of the spatial discretization; g denotes gravity acceleration; and D denotes link diameter. Eq. 2.7 is used to set routing time-step for the discretized examples presented in this work. To ensure that this smaller time step was always adopted by SWMM simulations, the use of variable time step was disabled.

The routing-time step was not modified for the original link-node examples presented in the QA, except when mentioned.

According to Ridgway (2008), Vasconcelos et al. (2018), and Pachaly et al. (2019), adding ASD in the links could lead to significant improvements in SWMM accuracy to simulate dynamic conditions. Therefore, an alternative modelling setup was conceived for each example considered in this work placing intermediate nodes between actual nodes. For a given link with length L, the discretization length is:

$$\Delta x = \frac{L}{n+1} \, , \tag{2.8}$$

where n is the number of intermediate junctions being calculated based on a ratio (Eq. 2.9) between the conduit length and diameter/max depth:

$$n = \max\left[\text{round}\left(0.1 \, \frac{L}{D}\right) - 1, 0\right] \, . \tag{2.9}$$

For instance, in the case of a 100-m long, 0.5-m diameter sewer, the number of intermediate junctions n would be 19, resulting in 20 links with a length of $\Delta x = 5$ m and unchanging the overall conduit length. However, in the case of short conduits (i.e. $L/D < 15$), there is no need of ASD and the results of Eq. 2.9 and Eq. 2.8 are $n = 0$ and $\Delta x = L$, respectively. The advantage of this approach is that long and short conduits will have the discretization based on its own characteristics and not in a general pattern. The 0.1 coefficient in Eq. 2.9 can be changed in order to produce a finer discretization but, in this work, this value was kept constant in all cases. According Pachaly et al. (2019), this method for discretizing links is the one that produces better results with less computational effort when compared to other discretization methods such as adding a fixed number of intermediate nodes between actual nodes independently of the link length.

The linear momentum is preserved given that the intermediate nodes have practically no storage, and thus no diversion of linear momentum occurs. This is confirmed in the works by Ridgway (2008) and Vasconcelos et al. (2018), who both studied mass oscillation simulations with SWMM. The entry loss is accounted only on the upstream link connecting the actual

node to the first intermediate node and the exit loss is accounted only in the downstream link connecting the last intermediate node to the actual node. If the model does not have any local losses, then the discretized model will also not have local losses. Therefore, there is no extra head loss accounted when the ASD is adopted. The maximum depth of the intermediate nodes is set as the terrain elevation (i.e., an artificial line connecting the maximum depth of the actual nodes) and the invert elevation of the intermediate nodes is set to match the slope of the original link. Also, the links generated by the ASD inherit the original link roughness.

Due to the time-consuming operation of creating manually the intermediate nodes, a software/add-on called ReSWMM (Pachaly et al., 2018) was used to perform this discretization automatically. Commercial implementations of SWMM model have similar features that enable the discretization of conduits.

2.2.2 Quality Assurance examples

The original link-node approach in SWMM implies that stormwater structures such as manholes and storage units are represented through nodes, while sewers, channels and other conduits are represented through links. These conditions are also present in a set of examples provided by the SWMM QA report (Rossman, 2006). Using several examples, this report compares the dynamic wave flow routing procedures of SWMM 4.4 against SWMM 5 in order to assure that the numerical results obtained by SWMM 5 were compatible with the results from the previous version (Rossman, 2006). Three set of examples were present in the QA report:

1. Models that were presented in SWMM-EXTRAN 4.4 User's Manual (Roesner et al., 1988). These examples include conditions that are representative of stormwater systems, such as side orifices, weirs, storage units, pumps, surcharged flows, etc. The great majority of these examples modifies hydraulic elements present in 2 branches of circular conduits that converge into a pair of trapezoidal channels.

2. Challenge Test Cases, which are a set of conditions compiled by Robert E. Dickinson for the QA report. These cases consist of circular pipes arranged in way that challenges the dynamic flow modeling including flat and adverse slopes, steep drops, etc. A total of

five models are present: (1) 10 pipes with 30.5 m lengths of 1.23 m diameter on a flat slope; (2) 5 pipes with 305 m lengths alternating sections of 3.66 m diameter into a 1.23 m diameter with a slope of 0.05 %; (3) 12 pipes with 152.4 m lengths with the first 6 having 1.83 diameter and the last 6 having 0.91 m diameter with a 12.2 m drop between them and a slope of 0.10 %; (4) inverted siphon with 10 pipes with 30.5 m lengths of 1.22 m diameter; and (5) 10 conduits with 30.5 m lengths of 1.22 m diameter with adverse slopes of 3 %.

3. Real-world models representing storm sewer systems, combined sewer systems, and natural channel systems, corresponding to the User-Submitted Test Cases in the SWMM QA report. Valuable results are accounted when analyzing the modeling performance in real-world cases due to the variety of situations and the large number of nodes and links occurring in these datasets.

Because of very irregular geometries or due to the absence of links, four of the twenty QA examples were not used in this work. Table 2.1 summarizes the elements present in each example for both traditional and discretized layouts and Fig. 2.1 shows samples of the first and third set of examples and Fig. 2.2 shows samples of the second set of examples. More information about these examples are presented in Rossman (2006).

For each of the 16 examples studied here, three surcharge algorithms were used (EXTRAN 5.1.012 / EXTRAN 5.1.013 / SLOT), along with traditional (i.e. link-node) and discretized approaches. A total of 96 simulations were thus performed in this investigation. Since there are many links and nodes that simulation data could be retrieved, the exact same links and nodes used by the QA report were chosen for display.

2.2.3 Criteria for evaluation of numerical solutions

In the present study, three different criteria were used to evaluate numerical solutions yielded by the modeling performed with SWMM 5.1: flow continuity errors, numerical stability and computational effort analyses. According to the SWMM User's Manual Version 5.1 (Rossman, 2015a), the flow continuity error represents the sum of the all outflow from the network divided

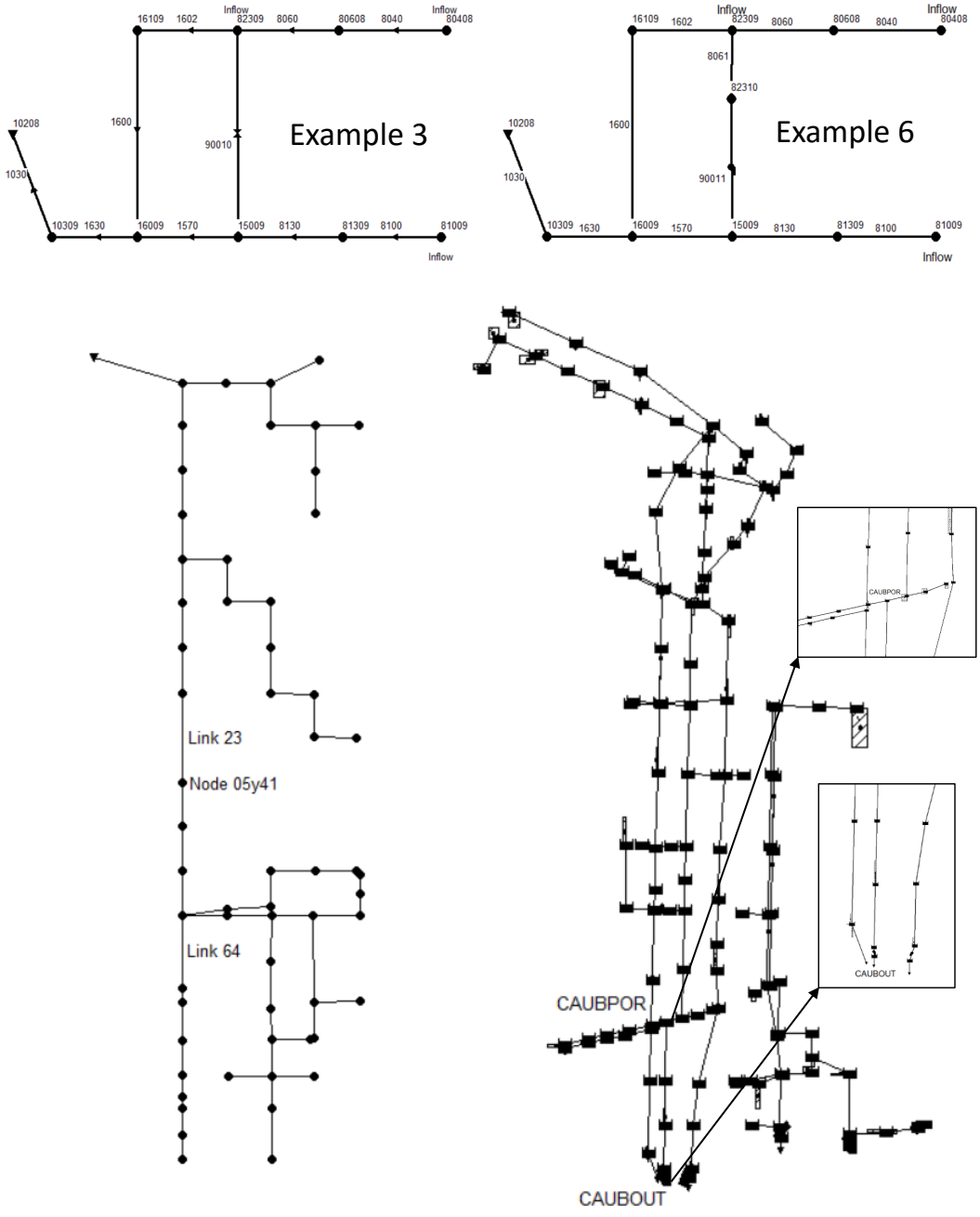

Figure 2.1: Samples of the first and third set of examples.

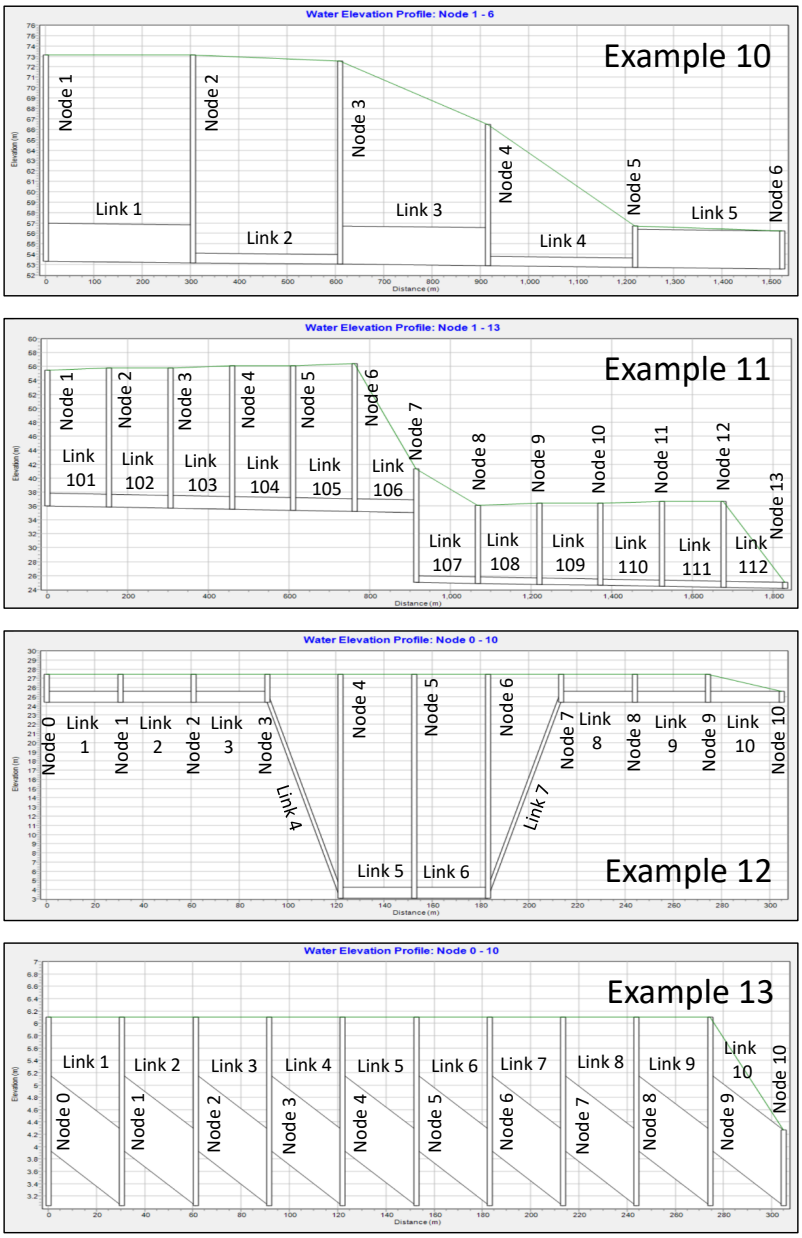

Figure 2.2: Samples of the second set of examples.

Table 2.1: QA report test cases summary. Adapted from Rossman (2006).

Example	Layout	Junctions	Stor. Unit	Outfalls	Conduits	Δt	Simulation Time
1	Trad.	9	-	1	9	20 s	8:00:00
	Disc.	540	-	1	540	0.64 s	8:00:00
2	Trad.	9	-	1	9	20 s	8:00:00
	Disc.	540	-	1	540	0.64 s	8:00:00
3	Trad.	9	-	1	9	20 s	8:00:00
	Disc.	540	-	1	540	0.53 s	8:00:00
4	Trad.	9	-	1	9	20 s	8:00:00
	Disc.	540	-	1	540	0.53 s	8:00:00
5	Trad.	9	1	1	9	20 s	8:00:00
	Disc.	540	1	1	540	0.53 s	8:00:00
6	Trad.	10	-	1	10	20 s	8:00:00
	Disc.	548	-	1	548	0.60 s	8:00:00
7	Trad.	9	-	1	9	20 s	8:00:00
	Disc.	540	-	1	540	0.64 s	8:00:00
8	Trad.	-	2	1	1	60 s	5:00:00
	Disc.	24	2	1	25	0.64 s	5:00:00
9	Trad.	10	-	1	10	5 s	5:00:00
	Disc.	20	-	1	20	0.80 s	5:00:00
10	Trad.	5	-	1	5	5 s	6:00:00
	Disc.	90	-	1	90	0.56 s	6:00:00
11	Trad.	12	-	1	12	5 s	6:00:00
	Disc.	150	-	1	150	0.54 s	6:00:00
12	Trad.	10	-	1	10	5 s	5:00:00
	Disc.	20	-	1	20	0.80 s	5:00:00
13	Trad.	10	-	1	10	5 s	12:00:00
	Disc.	20	-	1	20	0.80 s	12:00:00
14	Trad.	59	-	1	59	5 s	7:00:00
	Disc.	1116	-	1	1116	0.15 s	7:00:00
15	Trad.	5	130	6	134	0.5 s	6:00:00
	Disc.	2094	130	6	2223	0.25 s	6:00:00
16	Trad.	208	-	1	209	5 s	24:00:00
	Disc.	1520	-	1	1521	0.02 s	24:00:00

by the sum of all of the inflow to the network. Likewise, the manual states that continuity errors greater than ± 10% must be examined to guarantee the validity of the simulation. Too short conduits or too long time-steps are likely to be a reason for larger flow continuity errors. In order to evaluate eventual improvements achieved by using ASD, a comparison between flow continuity errors from the traditional approach and those from discretized approach was realized. Differences in flow continuity errors were grouped according to the surcharging algorithm used in the simulation.

Rossman (2015a) states that, due to the explicit nature of the numerical methods used in its solution, the flow in some links or water depth may fluctuate or oscillate as a result of numerical instabilities. SWMM is fitted with the ability to adjust and reduce the routing time step as a means to reduce instability in the simulation. Often times, reducing routing time or increasing short length links tend to help mitigate stability issues. Also, a more severe action of dampening or ignoring the inertial terms of the Saint-Venant equation can be implemented but his action can affect the modeling accuracy. Since SWMM 5, a criteria for determining if a nodal head has converged is used. This criteria is called Head Convergence Tolerance and reducing this value can lead to improvements in terms of numerical stability. Therefore, this work compares differences in numerical stability between the surcharge algorithms for selected cases.

Moreover, the size, complexity, and dynamic situations occurring in a system may require small time steps (Vasconcelos et al., 2018), and the combination of small time steps along with the presence of many nodes must demand higher computational time to perform a single simulation when compared to the traditional link-node approach. In order to analyze this additional computational effort, a comparison between the computational time spent to execute the traditional and discretized simulations with different surcharge methods was performed using the QA examples.

2.3 Results and discussion

Results presented in this section are grouped by discretization approach (link-node vs discretized) and by surcharge algorithm used in calculations (EXTRAN 5.1.012, EXTRAN 5.1.013 and SLOT). Initially a comparison of continuity errors is presented, followed by a discussion on

numerical stability of the solutions yielded by the different modeling strategies in SWMM, and concluding with a comparison of the computational effort associated with the modeling of each approach.

2.3.1 Evaluation of flow continuity errors

After running the SWMM QA report examples present in Table 2.1, results for continuity errors were extracted and summarized on Table 2.2. As it is noticed, most continuity errors are small, only Example 12 using the traditional link-node approach with the SLOT pressurization algorithm exceeded more than 68% of continuity error. The reason for this high value of continuity error was the routing time-step, reducing it from 5 s to 1 s decreased the continuity error to almost 0%. However, it is important to highlight that for 12 out of 16 examples the continuity errors were equal or smaller when spatial discretization was used.

For practical purposes, most of these continuity error values are not larger than other error sources in a modeling effort, and thus possibly acceptable in actual modeling applications. Yet, these comparisons with the SWMM QA cases indicate that both SLOT and the latest EXTRAN algorithms have a tendency of presenting smaller continuity errors. Adding ASD, which was shown to improve modeling results of flows involving surges, appears to also reduce continuity errors when routing time step was selected according to Eq. 2.7. In these cases, the routing time-steps selected were always smaller than those values reported in the original QA report, which should help in increasing the stability of the solutions.

2.3.2 Evaluation of numerical stability

Numerical stability, in the context of the present work, is reflected in a numerical solution that yields predictions that would be theoretically anticipated, without presenting spurious spikes and/or oscillations. Results in this way were observed for simulation conditions performed for Examples 1, 2, 4, 5, 7, 8, 9 and 16. The following results presented are focused on QA report examples in which differences between the modeling approaches were noticed, and when numerical stability issues were detected. It is important to highlight that no field data was available and, therefore, only comparisons between different simulation conditions and their

Table 2.2: Flow continuity error summary.

Example	Traditional Layout			Spatial Discretized Layout		
	EXTRAN (5.1.012)	**EXTRAN (5.1.013)**	**SLOT (5.1.013)**	**EXTRAN (5.1.012)**	**EXTRAN (5.1.013)**	**SLOT (5.1.013)**
1	-0.03 %	0.01 %	0.01 %	-0.13 %	-0.04 %	-0.01 %
2	-4.08 %	-4.05 %	-4.23 %	-0.10 %	-0.06 %	-0.05 %
3	0.09 %	0.09 %	0.10 %	-0.01 %	-0.04 %	-0.01 %
4	0.02 %	0.02 %	-0.10 %	-0.01 %	0.00 %	0.00 %
5	-0.22 %	-0.20 %	-0.41 %	-0.12 %	-0.06 %	-0.01 %
6	-0.05 %	-0.05 %	-0.16 %	-0.01 %	-0.13 %	-0.00 %
7	0.10 %	0.05 %	-0.11 %	0.12 %	0.10 %	-0.01 %
8	0.13 %	0.13 %	-0.18 %	0.09 %	0.03 %	0.04 %
9	-0.01%	-0.01%	-2.20%	-0.02%	-0.02%	-0.03%
10	-0.06%	-0.05%	-0.29%	-0.12%	-0.05%	-0.09%
11	-0.17%	-0.20%	-0.12%	-0.01%	-0.21%	0.03%
12	0.36%	0.34%	-68.16%	0.07%	0.03%	0.38%
13	-0.02%	-0.01%	-0.01%	-0.06%	-0.05%	-0.02%
14	-0.08%	0.13%	0.10%	-0.12%	0.78%	0.81%
15	-0.03%	-0.02%	-0.13%	-0.16%	-0.15%	-0.36%
16	0.05%	0.05%	0.05%	-0.02%	0.01%	0.04%

impact on the numerical stability were performed. As a result, there is no guarantee of which scenario best represented the real flow propagation, although some authors (Pachaly et al., 2019; Ridgway, 2008; Vasconcelos et al., 2018) showed that discretized models represented more accurately the flow propagation in terms of water peak level and arrival of inflow fronts in monitored cases.

Different simulation results obtained for Example 3 are presented in Fig. 2.3 (A, B, C). This example contains 7 circular conduits arranged in 2 branches with a bottom circular orifice to eliminate flooding converging into a pair of trapezoidal channels with a free outfall. The results show that there are no apparent spikes in the solution although it is noticed differences between solutions obtained with discretized and non-discretized modeling. The latter approach tends to show a delayed arrival of inflow fronts, as well a delayed recession curve during the dewatering of the system. The differences in total volume in links (A and B) and nodes (C) are because the analyzed links are in one side of the branch (Fig. 2.1) and adopting ASD changes how the flow is divided between the two branches. This result, which was also noticed in Example 7, is consistent with Vasconcelos et al. (2018), who pointed out that the use of ASD in SWMM helped to create a sharp description of inflow fronts. It can also be noticed that peak depths yielded by discretized approaches are smaller.

Example 6 in the SWMM QA report changes conditions in Example 3 by placing an off-line pump station (SWMM Type 1 pump) where formerly the orifice connected two junctions. In Fig. 2.4 (A), it is possible to observe the same delayed recession curve during the dewatering of the system for all non-discretized models. Some signs of numerical spikes are noticed in the solution in Fig. 2.4 (B) and Fig. 2.4 (C) using ASD along with the EXTRAN 5.0.13 pressurization algorithm. These instabilities may be reduced using a more strict routing time-step. Additionally, the total volume for some links are different between the traditional and discretized solutions due to the flow partition at the branches. It is noticed that the discretized model solution conveys more flow toward link 1602 when compared to the traditional model. On the other hand, the traditional approach conveys more flow toward link 8061. Interestingly, when Eq. 2.7 is used to estimate the routing time-step ($\Delta t = 3.19s$) for the non-discretized models instead of the original routing time step presented in the QA, the solution produces many

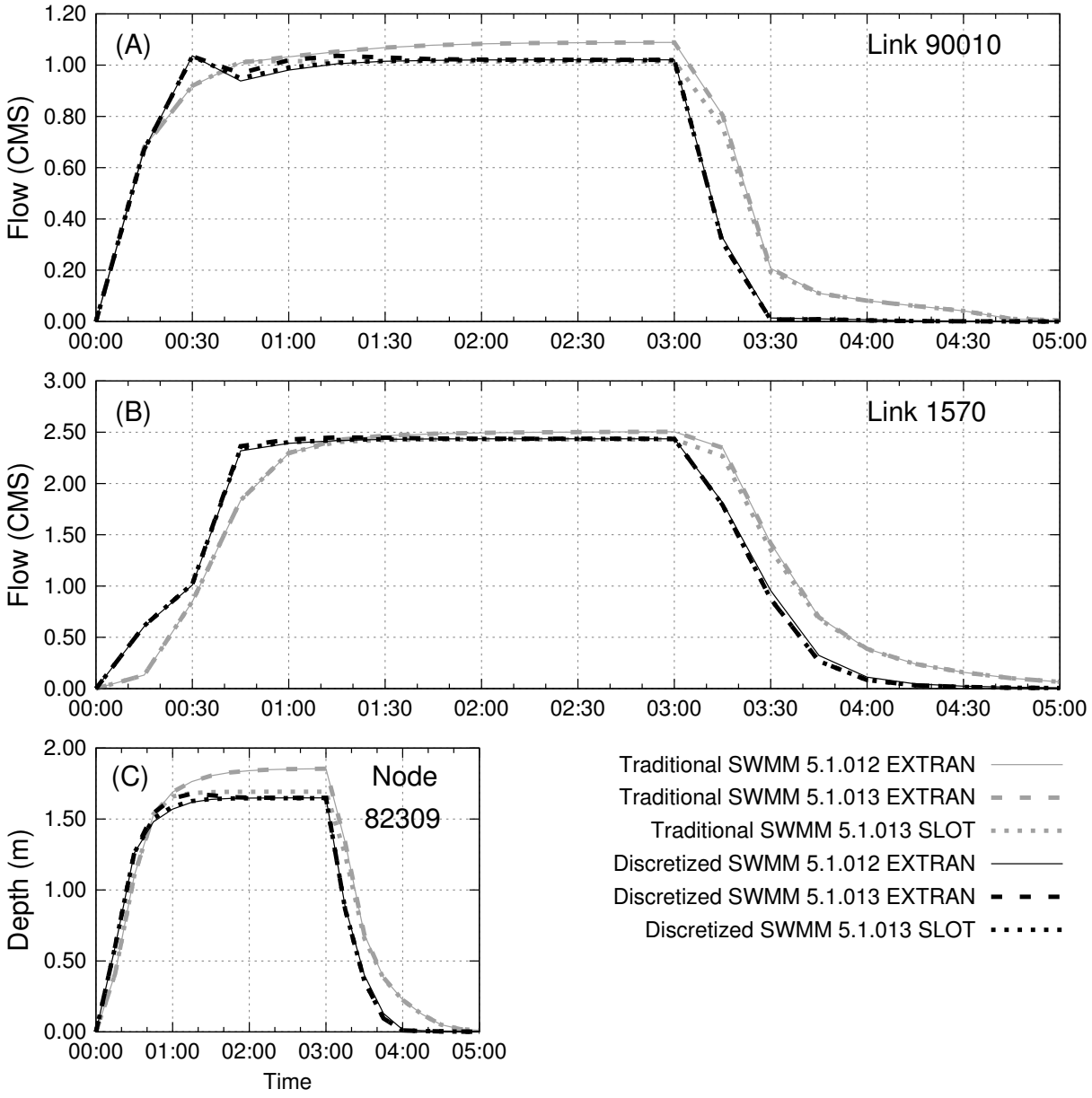

Figure 2.3: Example 3 SWMM results showing delayed flow arrivals and recession of traditional (i.e. link-node) approaches, compared to discretized modeling.

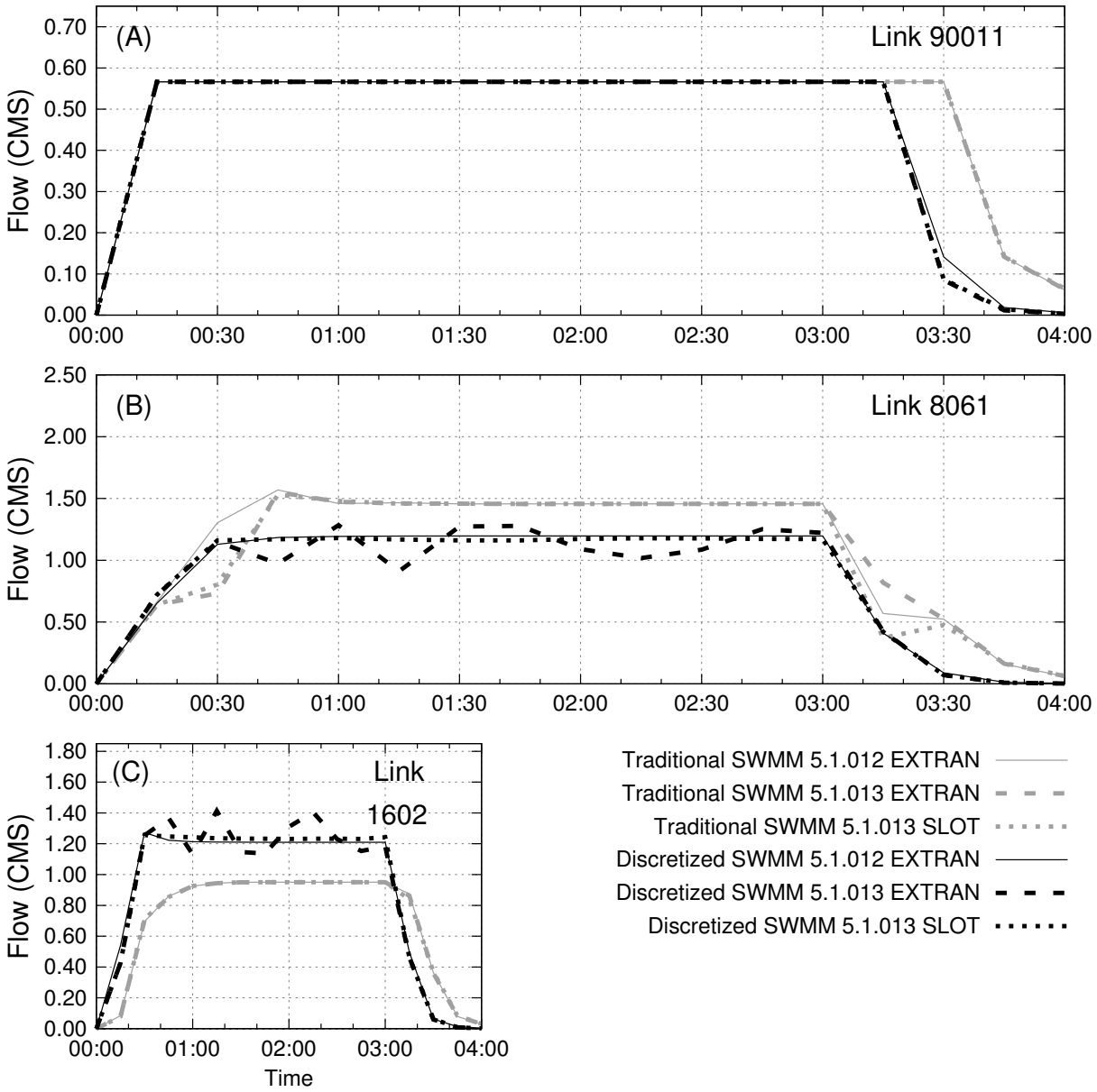

Figure 2.4: Selected SWMM results for Example 6 for all modeling conditions tested.

numerical spikes as can be seen in Fig. 2.5. It is speculated that in these cases the local Courant number for link 8061 is much decreased, and this impacts negatively the simulation.

Fig. 2.6 shows the most relevant results generated by Example 10. This example consists of alternating sections of 3.66 m diameter circular pipe flowing into a 0.91 m diameter pipe with each pipe having a slope of 0.05% and 305 m long. In Fig. 2.6 (A), all discretized models diminished the oscillations presented in the traditional layouts. Yet in Fig. 2.6 (B), the SLOT algorithm produced results without apparent numerical instability for both traditional and discretized models, with the first showing smaller flow values than the latter. The oscillations

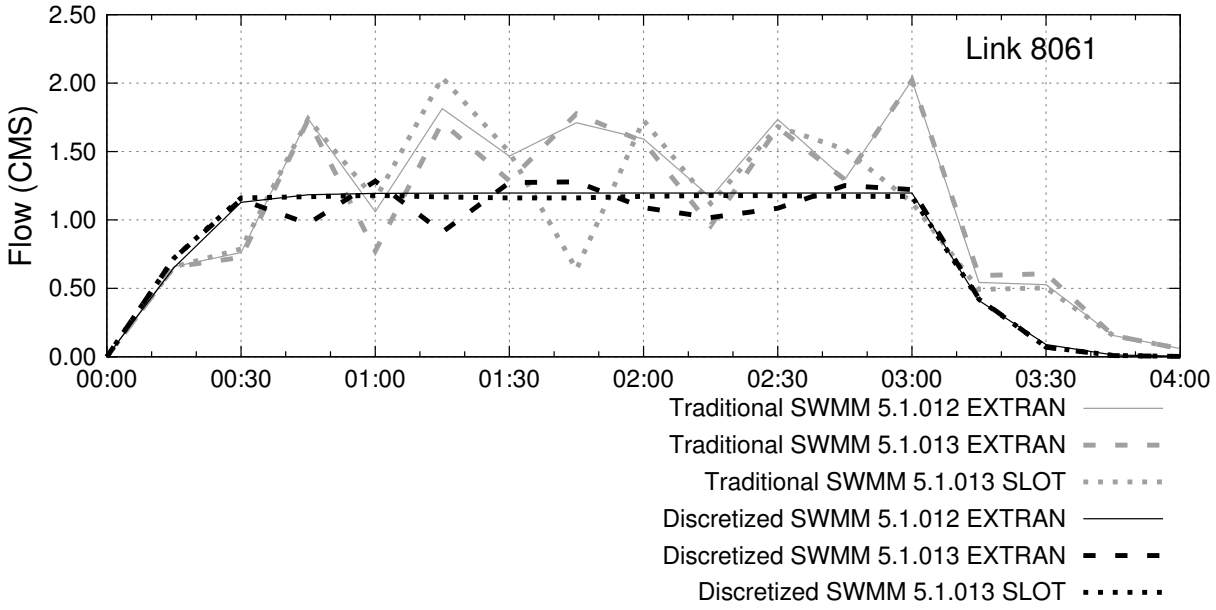

Figure 2.5: Example 6 link 8061 results showing numerical instabilities when Eq.2.7 is used to estimate the routing time-step for both traditional and discretized approaches.

observed in EXTRAN modeling occur when the flow transits from free surface to pressurized conditions in link 1-2 and then propagates these oscillations to link 3-4. EXTRAN algorithm applies different set of equations for free surface and pressurized flow regimes. Thus, it is speculated that during this transition between flow regimes, these oscillations take place as the flow solution algorithms alternate. This is not seen in the SLOT solution, given that the same set of equations for pressurized and free surface flow regimes are used. This situation is easier to visualize in Fig. 2.7, which shows Fig. 2.6 (B) in detail during the simulation period of 01:30-03:00. Still, the oscillations found in the discretized models using EXTRAN pressurization algorithm are less intense than the oscillations found in the non-discretized models using EXTRAN pressurization algorithm. Furthermore, it is important to highlight that the discretized results have, in general, higher values of flow and water depth than the traditional ones. Lastly, Fig. 2.6 (C) shows that the selection of the surcharge method impairs directly in the water level in this example.

Fig. 2.8 shows the most pertinent results of Example 11. This example consists of six sections of 1.83 m diameter circular pipe that drop 12.2 m to connect with another six sections of 0.91 diameter. Each pipe has a slope of 0.10% and a length of 152.4 m. In Fig. 2.8 (A), it is possible to identify that all the non-discretized models results showed oscillations not observed

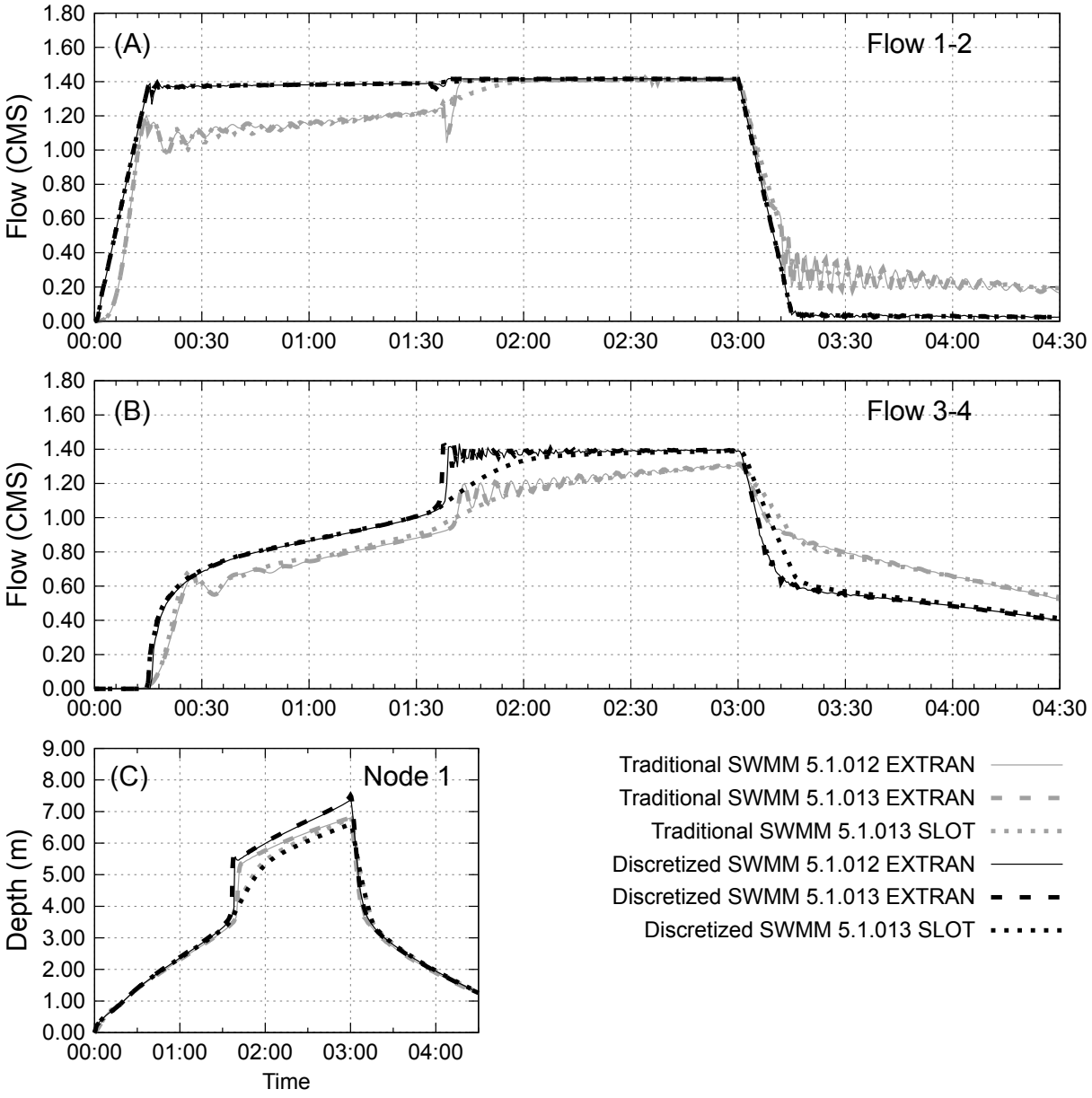

Figure 2.6: Selected SWMM results for Example 10 indicating numerical oscillations in traditional modeling approaches.

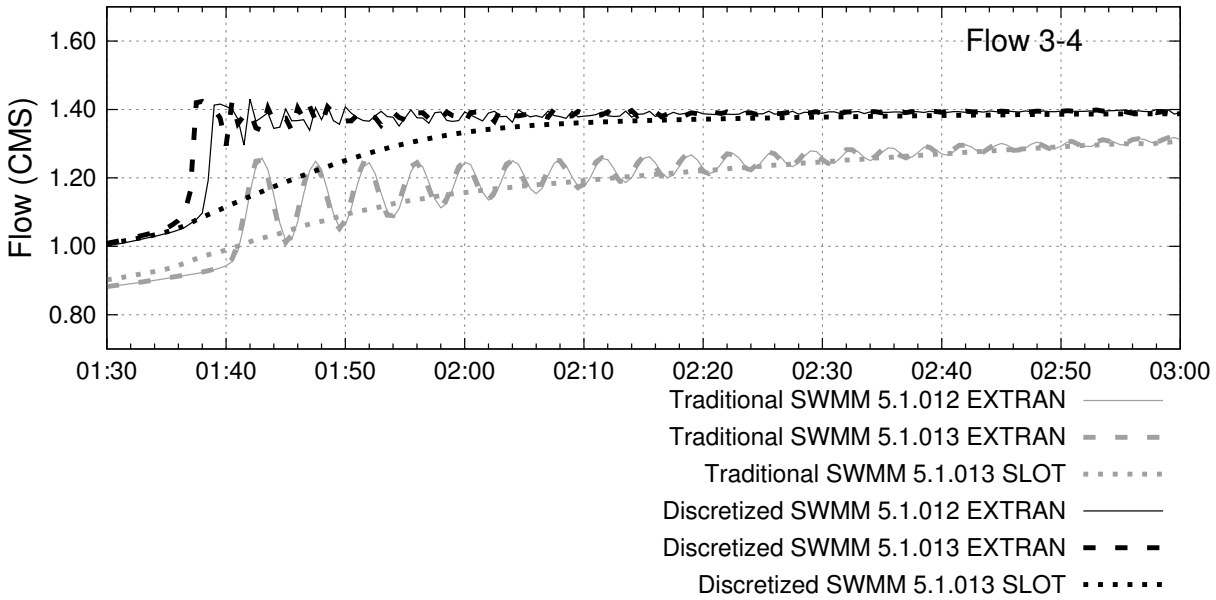

Figure 2.7: Detail of the predicted flows between nodes 3 and 4 in Example 10.

on discretized layouts. Fig. 2.9 magnifies Fig. 2.8 (A) during the simulation period of 00:45-1:25 in order to elucidate this statement. Moreover, there are differences between the EXTRAN and SLOT pressurization algorithm. These discrepancies do not exist until the moment when the conduits becomes pressurized. Fig. 2.8 (B) and (C) confirm that there are differences in the results obtained from these surcharge algorithms, mainly in the timing where the peak occurs. The SLOT algorithm overestimates the flow (Fig. 2.8 (B)) and underestimates the water depth (Fig. 2.8 (C)) for both traditional and discretized layouts. The discrepancies are thus attributed to the differences in the pressurized flow solution algorithm used by EXTRAN and by SLOT. There is as of yet no documentation on the SLOT algorithm in SWMM. However, it is speculated that one possible factor could be an additional cross-sectional area that is artificially provided by the slot when it pressurizes. The SLOT formulation is implemented in SWMM using the Sjöberg Equation (Jackson et al., 1986) to create a smooth transition from the pipe crown to the final slot width of 1% of link diameter.

Example 12 simulates an inverted siphon and its results are presented in Fig. 2.10. All the conduits are 30.5 m lengths of 1.23 m diameter circular pipe. In general, the results from both discretized and non-discretized models are alike, excepting the non-discretized model using the SLOT pressurization algorithm. Only this pressurization algorithm produced instabilities that crashed the simulation. When the system starts to watering, all models have similar behavior,

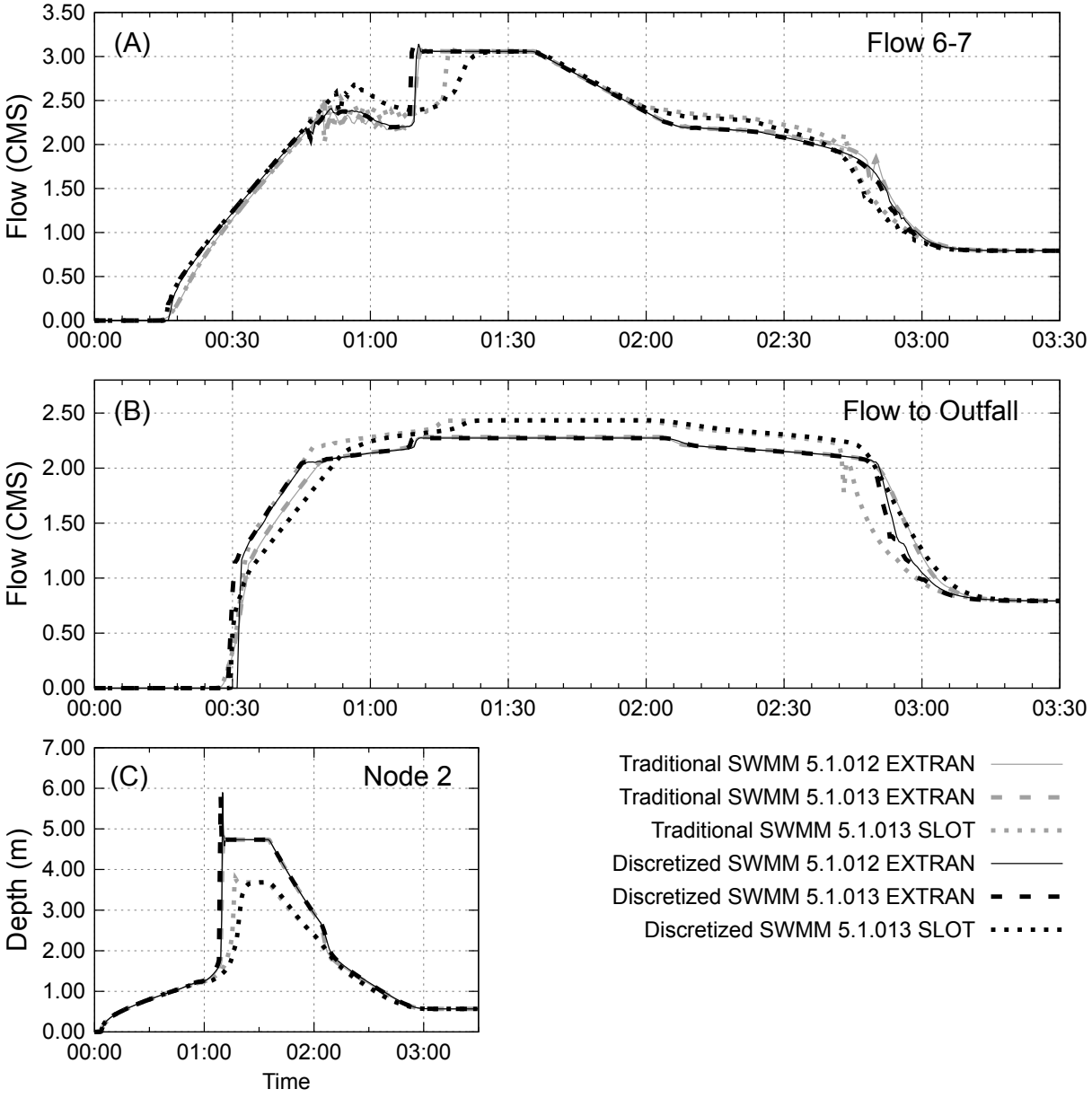

Figure 2.8: Example 11 results.

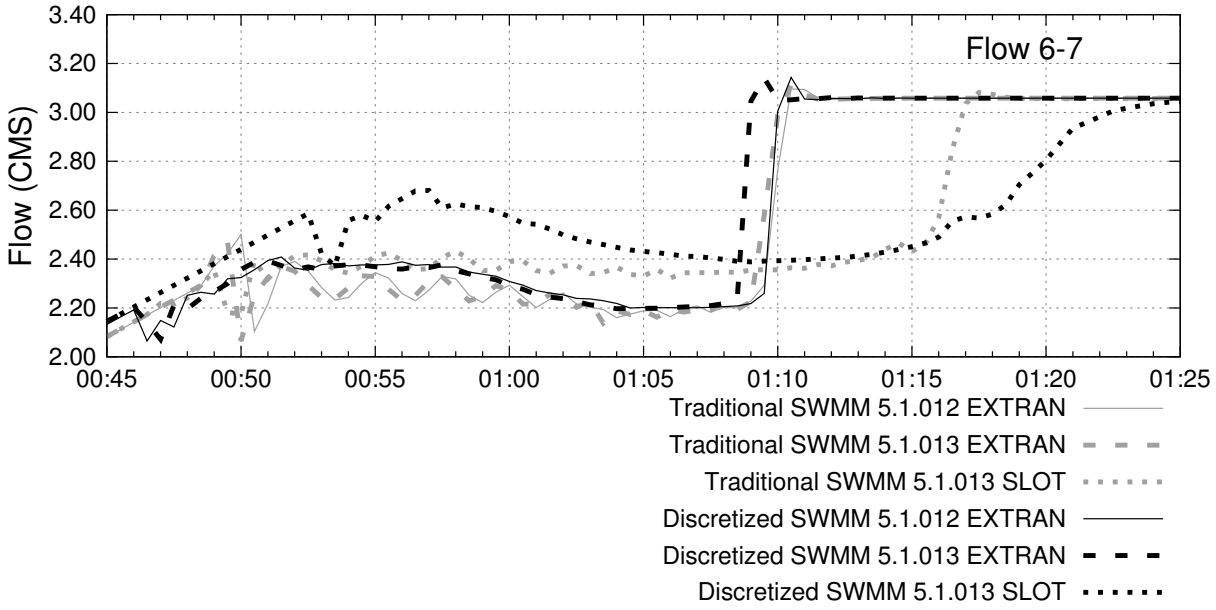

Figure 2.9: Example 11 - Fig. 2.8 (A) in detail.

however, the non-discretized model with the SLOT pressurization algorithm becomes highly unstable in the moment that the water touches the siphon crown. Using Eq.2.7 to estimate routing time-step ($\Delta t = 1.60s$) for the link-node approach, the instability produced by SLOT pressurization algorithm was removed and the flow continuity error was reduced to 0.21%.

Example 13 is a sequence of 30.5 m long, 1.23 m diameter circular pipes with a slope of 3% that each of them has a 0.91 m offset from the invert of its inlet node. The results obtained in Example 13 were unsatisfactory for the discretized layouts (Fig. 2.11). Fig. 2.11 (A) shows that discretized models have numerical spikes in the solution that are not present in the non-discretized layouts. This example is very challenging to dynamic flow modeling since there are adverse slopes in the order of 3%, a situation hardly present in real-world cases. Dampening or ignoring the inertial terms of the Saint-Venant equations could be a good procedure to try to avoid these numerical spikes (EPA, 2018). However, instead of dropping the inertial terms and, consequently, losing some accuracy, the strategy used was to reduce the head convergence tolerance. First, the head convergence tolerance was divided by 100 and improved results were found but still some numerical spikes were present. Then, the original head convergence tolerance was divided by 10^6 and the results had improvements, as can be seen in Fig. 2.11 (B). There are some numerical spikes around 08:00 but nothing compared to the ones presented using

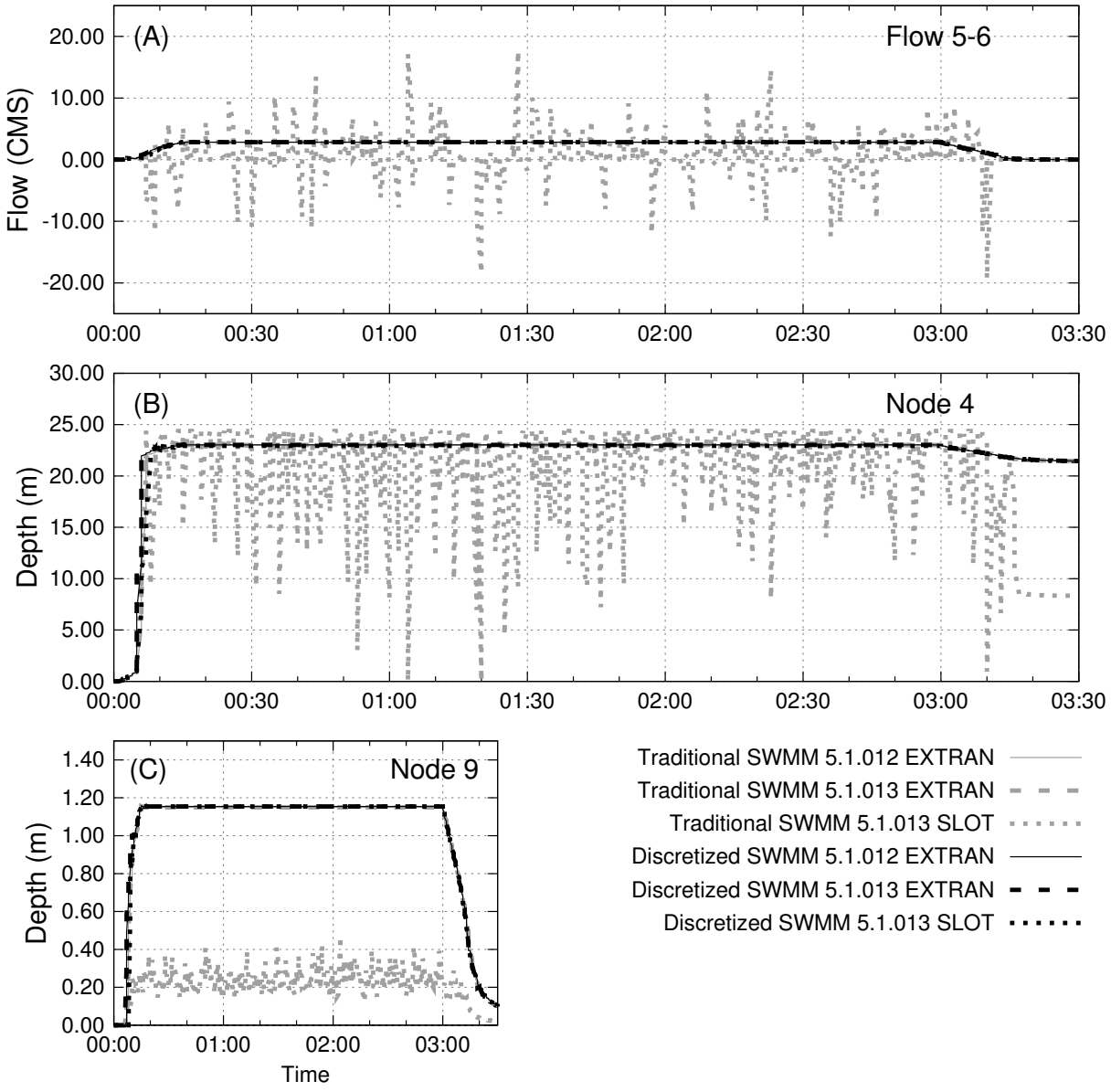

Figure 2.10: Example 12 results showing instabilities using the non-discretized model with the SLOT pressurization algorithm. Other simulations generated the same results.

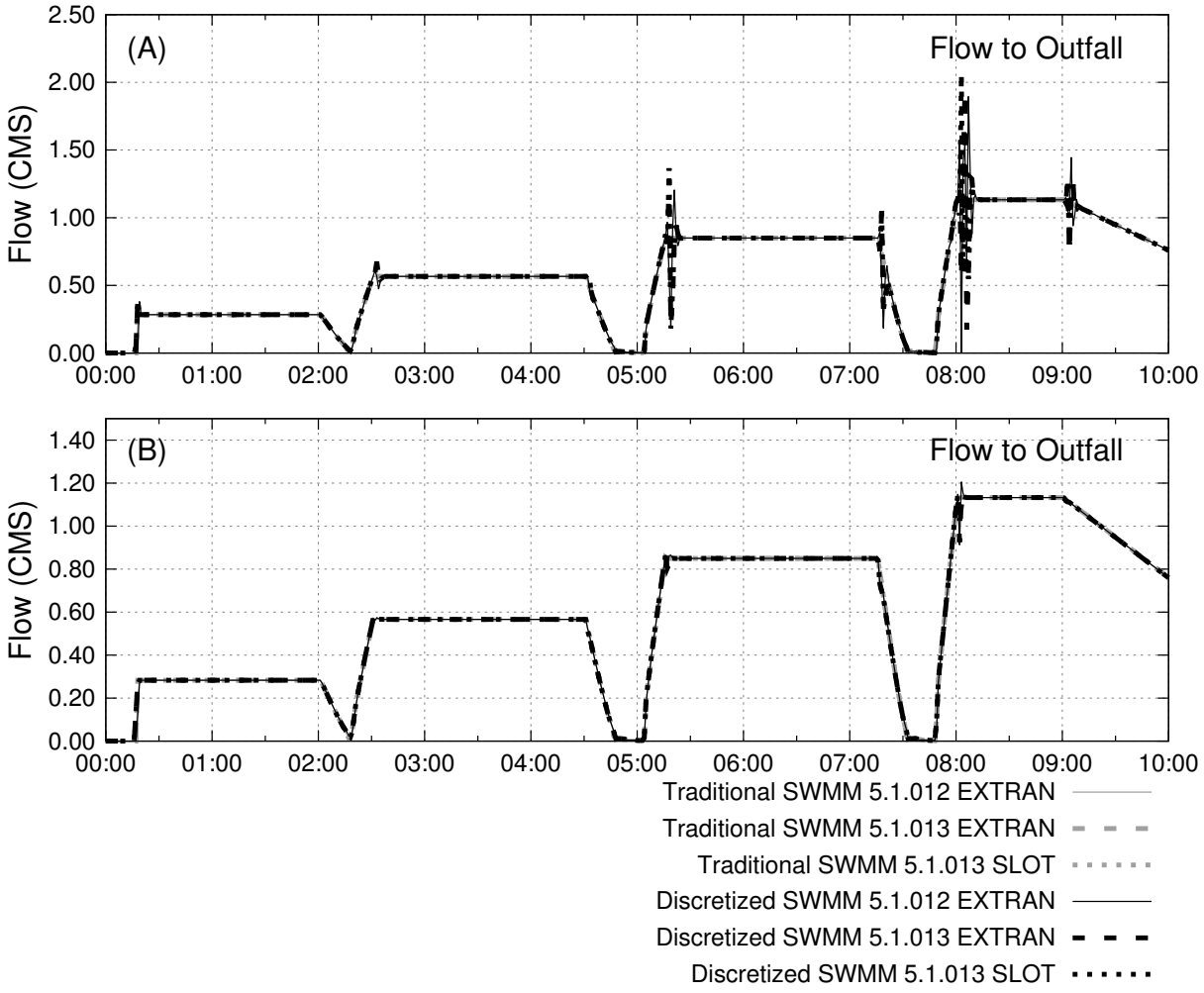

Figure 2.11: Example 13 results using the original head convergence tolerance (A) and the improvements achieved in terms of numerical stability when reducing the head convergence tolerance (B).

the original head convergence tolerance. Hence, the head convergence tolerance needs to be more stringent when ASD is added to the model since smaller Δt or Δx could led to truncation and rounding error.

Example 14 results are demonstrated in Fig. 2.12. This example consists of a real-world conveyance system containing 59 circular conduits connected to 59 junctions and a single outfall. Fig. 2.12 (A) and (B) show that, in general, the water rise and decline are different between the discretized and non-discretized models. The first show a delay of water rise during the system watering and a longer recession curve during the system dewatering. The latter show the opposite, an advanced water rise during the system watering and a shorter recession curve during the system dewatering. This is in accordance with Pachaly et al. (2019), which showed

that non-discretized simulations led to earlier arrival of inflow fronts when compared with field measurements of a sudden flow admission in a collection system. Fig. 2.12 (C) shows water depth results allowing to identify accentuated difference between discretized and non-discretized models. The discretized models show small water depth values while non-discretized show high ones. Probably these results are related to the wave produced when discretization is added to the model that is not captured by the SWMM traditional link-node approach (Pachaly et al., 2019). In the discretized models, the wave passes through several intermediate nodes until it arrives at the downstream node, representing more accurately the wave. In non-discretized models, the water depth starts to rise at the next node when the link connecting two nodes starts to fill. This can speed up the system filling and, at the same time, it promotes more water storage specially within the nodes, increasing water depth values. The system used in this case has many nodes ($>$1000), amplifying this situation not so evident in the previous examples. Moreover, in this example, EXTRAN 5.1.012 surcharged method results are different from those obtained by EXTRAN 5.1.013. This could be explained by how the MNSA is handled by these versions. An area always available at a node, as version 5.1.012 uses this parameter, could dampen the wave's fronts. Also, the SLOT pressurization algorithm generated peaks that were not produced by EXTRAN surcharge methods.

Example 15 consists of 134 pipes which have mostly circular or egg-shaped cross sections. In this example, the discretized models produced many numerical spikes (Fig. 2.13 (A)). So, a reduction of two decimals places of the head convergence tolerance was performed and these spikes were, in general, diminished as can be seen in Fig. 2.13 (B). However, at links near outfalls, numerical spikes were still present. Ignoring the inertial terms of the Saint-Venant equations also did not bring improvements in this case. Considering the current results, there are differences in the system dewatering (Fig. 2.13 (B) and (C)). As this system also has many nodes, the reason for these differences can be the same explained at Example 14.

2.3.3 Computational time

The computational time spent for each simulation was analyzed and Table 2.3 shows the results. As expected, the computational time spent to perform the simulations using discretized layouts

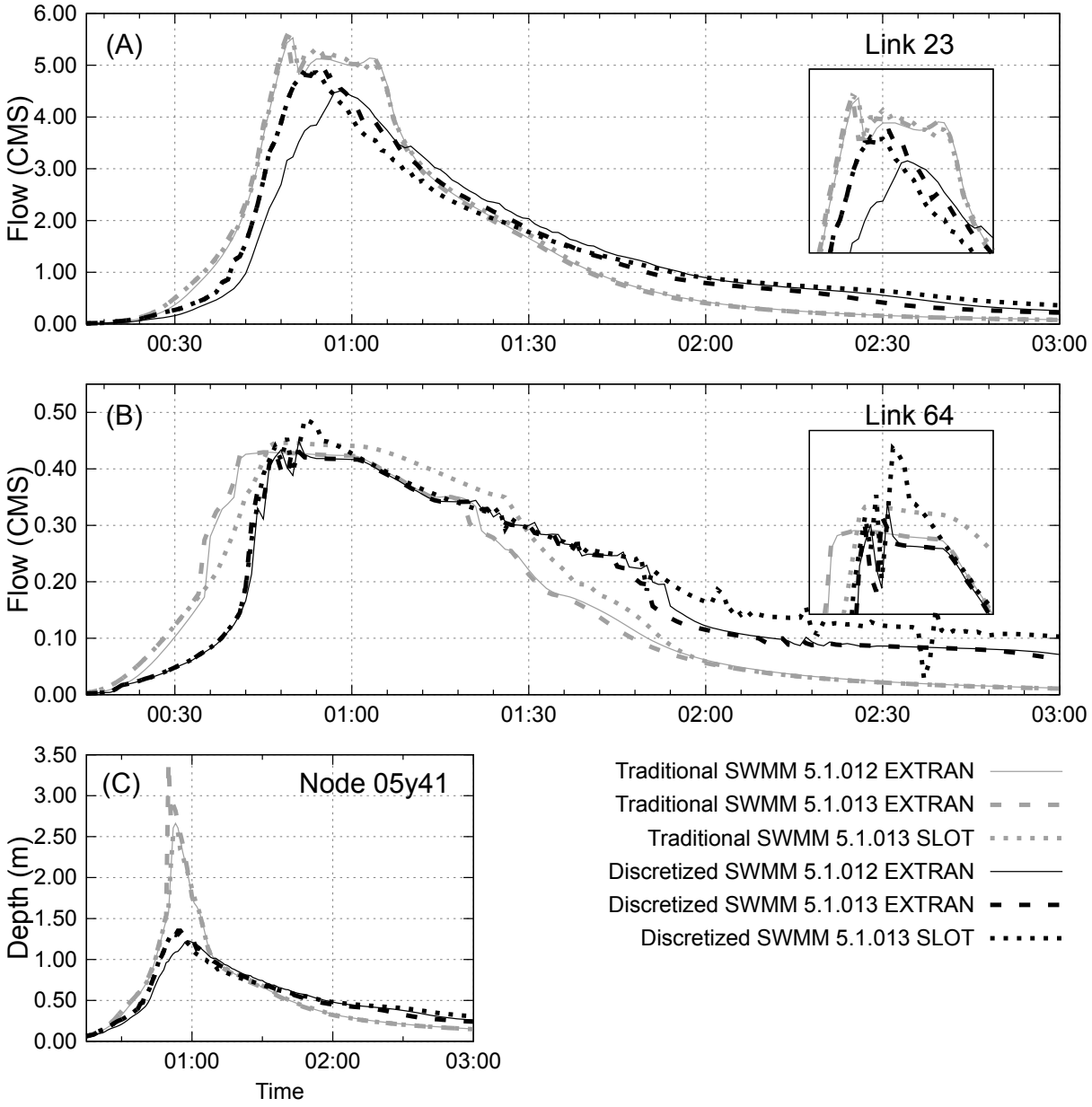

Figure 2.12: Example 14 results.

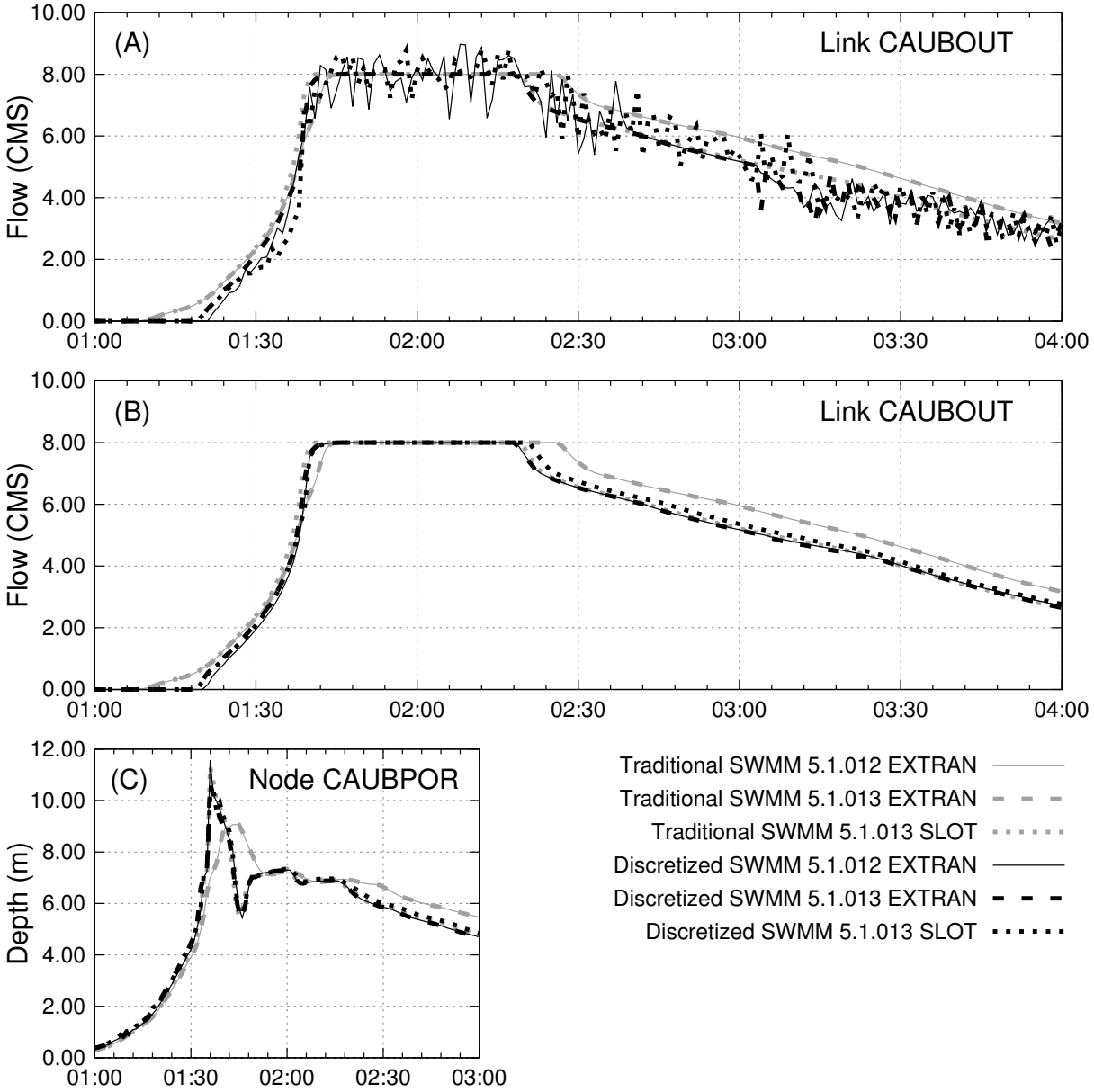

Figure 2.13: Example 15 results keeping the original head convergence tolerance (A), reducing the head convergence tolerance by two decimal places (B), and the water depth in a node (C).

Table 2.3: Computational time spent summary (hr:min:sec).

Example	Traditional Layout			Spatial Discretized Layout		
	EXTRAN (5.1.012)	**EXTRAN (5.1.013)**	**SLOT (5.1.013)**	**EXTRAN (5.1.012)**	**EXTRAN (5.1.013)**	**SLOT (5.1.013)**
1	<1*	<1*	<1*	0:00:33	0:00:22	0:00:22
2	<1*	<1*	<1*	0:00:30	0:00:23	0:00:22
3	0:00:01	<1*	<1*	0:00:35	0:00:28	0:00:28
4	<1*	<1*	<1*	0:00:33	0:00:29	0:00:28
5	<1*	<1*	<1*	0:00:38	0:00:27	0:00:26
6	0:00:01	<1*	<1*	0:00:31	0:00:27	0:00:25
7	<1*	<1*	<1*	0:00:29	0:00:24	0:00:26
8	<1*	<1*	<1*	0:00:01	0:00:01	0:00:01
9	<1*	<1*	<1*	<1*	<1*	0:00:01
10	<1*	<1*	<1*	0:00:04	0:00:02	0:00:03
11	<1*	<1*	<1*	0:00:07	0:00:04	0:00:05
12	<1*	<1*	<1*	0:00:01	<1*	0:00:01
13	<1*	0:00:01	<1*	0:00:01	0:00:01	0:00:01
14	0:00:02	0:00:01	0:00:01	0:04:40	0:03:33	0:03:45
15	0:00:11	0:00:08	0:00:08	0:05:18	0:03:45	0:03:11
16	00:00:07	0:00:07	0:00:06	2:29:56	1:37:57	1:38:04

* Less than 1 second.

is higher when compared to traditional layouts. When analyzing the discretized layouts, it is possible to assert that EXTRAN 5.1.0.12 surcharge method requires more time to perform a simulation than the others. Also, the SLOT surcharge method has a slight reduction of the computation time spent when compared to the EXTRAN 5.1.013 pressurization algorithm.

The computational time spent to perform a single simulation was more relevant in the cases that have higher number of elements (Table 2.1: Example 14, 15, and 16). Examples 14 and 15, using ASD, required a computational time in the order of minutes while the traditional layout required only 1 to 2 seconds to perform the simulation. In the Example 16 it was more remarkable, moving from a computational time in the order of minutes to hours. This example already had a considerable amount of nodes in the non-discretized model (208) and it was increased to 1520 with ASD, exposing the large number of calculations required to be performed at each routing time-step. However, in this set of cases the SLOT, surcharge method does not seem to reduce the computational time when compared to the EXTRAN surcharge method.

2.4 Conclusions

This work presented simulation results of using ASD in SWMM links instead of the traditional link-node approach. Examples presented in Rossman (2006) were used with the purpose of analyzing the improvements achieved in terms of flow continuity error and numerical stability. A total of 96 simulations were performed, including the old surcharged method presented in SWMM version 5.1.012 and the new ones (EXTRAN and SLOT) presented in SWMM version 5.1.013.

The results demonstrated that the Vasconcelos et al. (2018) recommended routing time-step generates small flow continuity error for discretized models, showing less than ± 1% in all simulations. However, even though it improves significantly the SWMM modeling, when many intermediate nodes are added or when there are many source terms such as steep slopes, this recommendation may not be enough to maintain stability. The head convergence tolerance reduction appeared to be a solution for diminishing numerical spikes without altering the inertial terms of the Saint-Venant equations. However, in this work this criteria was not systematically studied and a deeper analysis ought to be performed in order to estimate a more precise value.

There were considerable differences when using ASD in SWMM. Some oscillations or fluctuations that may be due to numerical instabilities were reduced when using the ASD. In some simulations, significant results differences were present between the surcharge method presented in SWMM versions (5.1.012 & 5.1.013) and the SLOT method. The latter reduced significantly the oscillations when compared to the EXTRAN surcharged method. Moreover, significant computational time differences occurred when analyzing both traditional and discretized layouts. As expected, the discretized layouts required more computational time to perform a simulation due to additional nodes but comparable to more robust and accurate models. Also, in some cases the SLOT surcharge method reduced the computational time when compared to the others surcharged methods. It is important to point out that only comparisons between different simulation conditions were evaluated in this work because no field data was available for the selected models. Therefore, there is no guarantee on which simulation condition best represented

the flow propagation. Field data of stormwater systems suitable for model comparisons are necessary but they are often limited.

Finally, based on the results presented in this work and in earlier contributions on unsteady flow SWMM modeling using artificial discretization, an appropriate selection of routing time step and ASD will result in significant improvements in hydraulic modeling. Furthermore, it appears that some instabilities that are intrinsic to the switching of the solution equations in EXTRAN when pressurization happens did not occur when SLOT was used. Therefore, the choice of ASD, adequate time step and SLOT would be the most robust option to simulate situations where mixed flow, pressurization, rapid inflows conditions, and other challenging flows are anticipated. Also, it is believed that the additional computational effort associated with ASD can be justified with the gain in terms of the model accuracy, particularly in highly dynamic conditions. In such cases, much care is needed in modeling setup, with the modeler encouraged to evaluate the effect of parameters such as head convergence tolerance and how inertial terms are accounted for in SWMM. Future research is being developed to understand the impact of the slot width in SWMM simulations, and how to setup models to represent closed conduits as well fast transients.

2.5 Data availability

Some or all data, models, or code generated or used during the study are available in a repository online in accordance with funder data retention policies. The data that support the findings of this study are openly available in:

ReSWMM (Pachaly et al., 2019) executable and manual:

https://github.com/ecotecnologias/ReSWMM

SWMM (EPA, 2018) & Quality Assurance Report (Rossman, 2006):

https://www.epa.gov/water-research/storm-water-management-model-swmm

Chapter 3

Evaluating SWMM capabilities to simulate closed pipe transients[†]

Abstract - One of the most used 1D tools to model collection systems is the Storm Water Management Model (SWMM). Solving the full form of the Saint Venant equations, this model represents typical unsteady flow conditions in sewer systems. However, it may be insufficient to address fast transient flow conditions that can be present during extreme events or unscheduled operational conditions. SWMM version 5.1.013 implemented the Preissmann slot as an alternative method to handle pressurization. To date, no studies were found analysing the applicability of SWMM to represent closed-pipe fast transient flows applying the Preissmann slot pressurization algorithm. Therefore, the present work investigates the ability to model different fast transients conditions in SWMM under various spatial and temporal discretizations along with variations in the Preissmann slot algorithm. Using an alternative implementation of the SLOT pressurization algorithm, along with artificial spatial discretization and routing time-steps estimated by the Courant stability condition, it is shown that SWMM is capable to perform satisfactory certain types of closed pipe transient simulations.

3.1 Introduction and objectives

The Stormwater Management Model (SWMM) is a dynamic hydrologic-hydraulic model (EPA, 2018), result of a long-term development that included many researchers, users, and collaborators (Huber & Roesner, 2012). The model is often used for planning, analysis, and design related

[†]**Published in**: Pachaly, R. L., Vasconcelos, J. G., Allasia, D. G., & Bocchi, J. P. P. (2021). Evaluating SWMM capabilities to simulate closed pipe transients. *Journal of Hydraulic Research*, DOI: https://doi.org/10.1080/00221686.2020.1866695

to collection systems in urban areas (Rossman, 2015b). Many studies have been performed using SWMM, such as runoff quality modelling (Di Modugno et al., 2015; Tsihrintzis & Hamid, 1998), runoff quantification (Abdul-Aziz & Al-Amin, 2016; Meierdiercks et al., 2010), and, more recently, analysis of green infrastructure practices (Campisano et al., 2017; Zahmatkesh et al., 2015). Due to this variety of applications, SWMM is considered by researchers one of the most popular and successful urban water models worldwide (Niazi et al., 2017; Vasconcelos et al., 2018).

The SWMM formulation allows for the representation of unsteady free surface flow in channels and pipes. SWMM uses a link-node approach based on finite differences that solves the head in each node and the flow in each link (Roesner et al., 1988; Rossman, 2006, 2017a). This solution technique does not use spatial discretization within conduits as more contemporary flow solvers; yet SWMM is suitable for the great majority of stormwater flow applications because it can properly simulate most filling processes of collection systems.

Transient flows are commonly observed in collection systems (Chaudhry, 2013). Significant changes in pressure and velocity, vibrations, reverse flows, and other situations can occur in transient flows (Thorley, 1991). In some cases, such as a pump start-up or a pipeline filling, these situations are expected and the system is designed to withstand such conditions. However, in other cases, where this situation is not planned, such as a pump failure, it may lead to unacceptable operational conditions, and even significant damage to systems.

To date, it is unknown the accuracy of SWMM to represent certain closed-pipe transient flow conditions. Furthermore, there are some limitations posed by the current lack of boundary conditions in SWMM that could represent conditions such as one-way tank, hydropneumatic tanks, pressure-relief valves, and other junctions that are present in other systems that are subject to fast transients. However, it is believed that there is a possibility of improving SWMM by adding a wider range of junctions that represent transient protective devices within SWMM.

In this context, the present work aims to evaluate the accuracy and potential limitations of SWMM 5.1.013 to represent cases of transient flows through a comparison with available

analytical solutions and a benchmark model. The first case analysed is a fast transient corresponding to a sudden closure of a downstream valve presented in Wylie and Streeter (1993) and the second case is a type of fast transient resulting from a sudden pipeline flow start-up.

3.2 Methods

3.2.1 SWMM formulation

SWMM uses the Saint Venant equations to solve the unsteady free surface flow through a network of links and nodes (EPA, 2018). These equations form a system of partial differential equations which represent the unsteady open-channel flows (Sturm, 2001) based on the conservation of mass (Eq. 3.1a) and linear momentum (Eq. 3.1b). By default, SWMM solves these equations using a link-node approach, computing the flow at each link and the head in each node (Roesner et al., 1988; Rossman, 2006).

$$\frac{\partial A}{\partial t} + \frac{\partial Q}{\partial x} = 0 \tag{3.1a}$$

$$\frac{\partial Q}{\partial t} + \frac{\partial (Q^2/A)}{\partial x} + gA\frac{\partial H}{\partial x} + gAS_f + gAh_L = 0 \tag{3.1b}$$

where A denotes cross-sectional area; t denotes time; Q denotes flow rate; x denotes distance; H denotes the hydraulic head of water in the conduit; g denotes gravity; h_L denotes the local energy loss per unit length of conduit; and S_f denotes the friction slope, which is implemented with the Manning equation (Rossman, 2006).

This default modelling approach in SWMM does not employ discretization within conduits. In some highly dynamic situations, such as pressurization of conduits, pressure surges, and pipe-filling bores, artificial spatial discretization along the full form of the Saint Venant equations brings significant improvements in SWMM results (Pachaly et al., 2019; Pachaly et al., 2020b; Ridgway & Kumpula, 2007; Vasconcelos et al., 2018). Artificial spatial discretization is implemented by placing dummy nodes between actual nodes, forcing SWMM to solve the Saint Venant equations at various locations within a conduit. Adding more nodes may have a significant impact in the computational time to perform a single simulation since there are

more nodes and links to be solved at each time-step (Pachaly et al., 2019; Pachaly et al., 2020b) and a smaller routing time-step may be required to maintain the stability and flow continuity (Vasconcelos et al., 2018).

When the water level at a node exceeds the crown of the highest conduit connected to a SWMM junction, pressurization occurs (Rossman, 2006, 2017a). The latest version of SWMM introduced a pressurization algorithm based on the Preissmann slot (EPA, 2018). This technique uses a narrow and vertical slot over each pipe, eliminating the need to switch equations and allowing the use of the Saint Venant equations throughout the entire simulation (Cunge, 1980). SWMM uses a formula based on the Sjöberg slot correction (EPA, 2018) to gradually change the slot width when the flow depth is greater than 98.5% of link diameter. For the ratio of hydraulic head and pipe diameter (H/D) greater than 1.78, the slot width in SWMM 5.1.013 is equal to 1% of conduit diameter, which results in an acoustic wavespeed of approximately 27.8 m s^{-1} for a unitary diameter.

The Preissmann slot method has two main deficiencies: it cannot sustain negative pressures and, for certain numerical schemes, spurious numerical oscillations are present when the flow switches to pressurized flow (Malekpour & Karney, 2015; Vasconcelos et al., 2009). In SWMM 5.1.013, due to the approach used to implement the Preissmann slot, the acoustic wavespeed is too low to represent pressure propagation in closed pipe transients. A wider slot creates unrealistic storage that may have considerable consequences in the simulation (Malekpour & Karney, 2015), delaying the propagation of pressure pulses in closed pipe transients.

In this work, the SWMM source code was changed in order to assess the performance of the model after removing the Sjöberg slot correction and decreasing the slot width with a method based on celerity. Since the SLOT method maintains the open-channel flow condition, Eq. 3.2 gives the free surface or slot width (B) based on a specific celerity (c) for a known link cross-sectional area:

$$B = g\frac{A}{c^2}. \tag{3.2}$$

In addition to the original SWMM implementation, three values of celerity were used to set the slot width: 250 m s^{-1}, 500 m s^{-1}, and 1000 m s^{-1}, none of these with Sjöberg slot correction. The selected celerity values represent a range of wavespeeds that could potentially occur in closed pipe transients in collection systems. If there is no gas phase inside a pipe (air, H_2S), the celerity may be close to 1000 m s^{-1}. However, usually there is some gas in collection systems, therefore, celerity values of 250 m s^{-1} or 500 m s^{-1} are feasible in such scenarios (Wylie & Streeter, 1993). To date, there is no design guidelines on how to estimate celerity values in stormwater systems because the celerity values are influenced by air that might be entrained or entrapped during the filling process.

The equation used to estimate the routing time-step was based on the Courant-Friedrich-Lewy (CFL) stability condition (Courant et al., 1928). This condition (Eq. 3) states that the routing time-step (Δt) depends upon the spatial discretization (Δx) and celerity to maintain the stability in a finite-difference scheme (Chaudhry, 2008):

$$\Delta t = C_r \frac{\Delta x}{c}, \tag{3.3}$$

where the C_r term is called the Courant number. The choice of Δx and Δt should ensure that C_r does not depart much from unity to provide good results. Explicit solvers also require that $C_r \leq 1$ at all locations of the solution domain. However, SWMM solver is semi-implicit, so $C_r > 1$ should not crash the model.

Other modelling options in this study were adjusted as follows: the dynamic wave was selected as routing model keeping all inertial terms under all conditions and the normal flow criteria chosen was the slope and Froude number. Also, SWMM solution method uses a convergence tolerance and a maximum number of trials to verify if the solution converged. These values were changed, respectively, from 5×10^{-3} to 5×10^{-6} and from 8 to 20 because artificial spatial discretization was used. Reducing the calculation tolerance leads to more stringent convergence requirement, which is important to avoid numerical instabilities in the solution, and increasing the maximum number of trials will allow for more iterations to achieve this requirement.

3.3 Results and discussion

3.3.1 Case 1: Instantaneous vale closure transient

Figure 3.1 shows a typical case of a transient caused by an instantaneous closure at a downstream end of a closed conduit. This situation may occur when there is a sudden vale gate maneuver, such as the damming of a check valve. Neglecting friction, minor losses and considering an instantaneous closing movement, when the valve is closed, velocity (V) is 0, a pressure wave of magnitude (ΔH) will be created at the downstream end of the pipe and it will travel upstream with the acoustic wavespeed (Chaudhry, 2013; Wylie & Streeter, 1993).

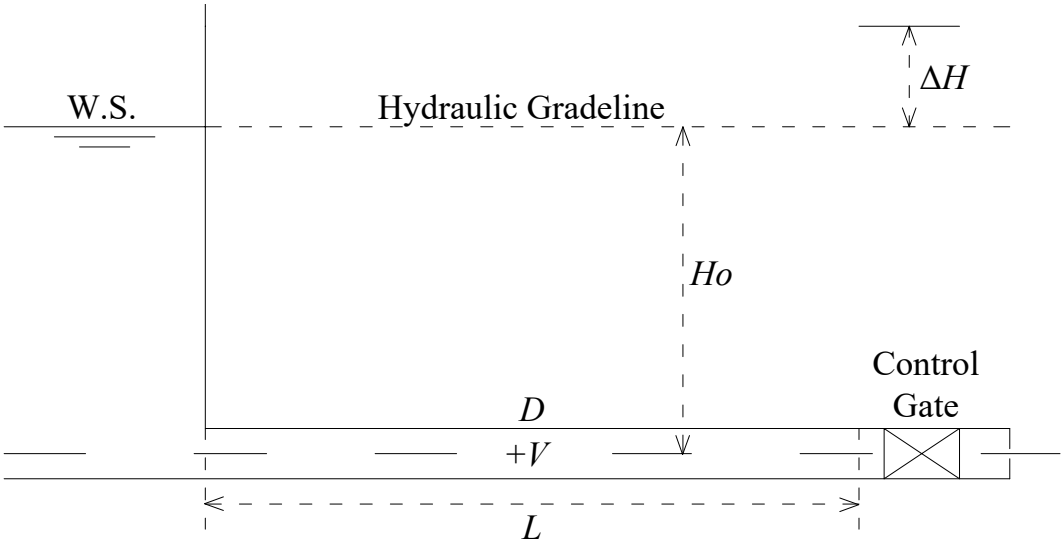

Figure 3.1: Instantaneous valve closure. Adapted from Wylie and Streeter (1993).

The Joukowski Eq. (Eq. 3.4), proposed in 1904, describes the change in pressure related to a change in flow velocity (Ghidaoui et al., 2005; Wylie & Streeter, 1993):

$$\Delta H_{anl} = \pm \frac{c}{g} \Delta V, \tag{3.4}$$

where ΔH_{anl} denotes instantaneous head change and ΔV denotes the instantaneous change of flow velocity. This equation states that the magnitude of the pressure wave is proportional to the change in the water velocity and the speed of propagation of the pressure wave (Parmakian,

1963). The analytical solution yields the maximum upsurge and this value is directly related to celerity.

In order to represent this idealized situation in SWMM, two storage units with a large area ($1 \times 10^6\ m^2$) were used. The first had a static water level (H_o) of 20 m and the second was empty. Between them, a 1000 m long, 1 m diameter pipe followed by a side circular orifice of 0.1 m height and discharge coefficient of 0.505 was set. This orifice was used to limit the flow velocity to 0.1 m s^{-1}. After the flow becomes steady, a control rule was used to rapidly close the orifice (closure time equal to Δt), representing the instantaneous valve closure.

Since changing the celerity values in SWMM will produce different head changes, the data was normalized using Eq. 3.5:

$$\Delta H^*_{sim} = \frac{H_{sim} - H_o}{\Delta H_{anl}} \tag{3.5}$$

where ΔH^*_{sim} denotes the normalized simulated head change and H_{sim} denotes the simulated head from SWMM results. The metric selected to evaluate the model accuracy in this case is the $L2$. For discrete results, this metric measures the distance between two points on variable vectors. In this work, it evaluates the distance between the normalized SWMM values and the normalized analytical values. Eq. 6 describes the L2 norm:

$$L^2 = \sqrt{\sum (\Delta H^*_{sim} - \Delta H^*_{anl})}, \tag{3.6}$$

where ΔH^*_{anl} denotes the corresponding normalized analytical solution. Values closer to 0 indicate better agreement between the data analysed.

Figure 3.2 shows the simulation results for all pressurization algorithms. The simulations shown in these graphs were performed using a C_r of 1. The simulations using a C_r of 0.5 and 2 follow the same pattern and, for the sake of brevity, they are not shown in this work. The SWMM original implementation of the Preissmann slot was not able to represent the analytical solution, as shown in the SLOT graph. For the modified versions of the Preissmann slot algorithm (c250, c500, and c1000), the results show that the models without spatial discretization (Δx = 1000 m) were not able to generate satisfactory results. However, when spatial discretization is adopted,

the modified versions of the Preissmann slot provide results closer to the analytical solution, with finer discretization (Δx = 1 m) resulting in less numerical diffusion, which is in accordance with the literature (Chaudhry, 2013; Popescu, 2014). The difference between changing the celerity's values is the head change, with higher values for higher celerities, and the oscillation's periods, with longer oscillations for smaller celerities. Results in Figure 2 are not normalized; if, however, time was normalized by (L/c), and pressure head was normalized by ($c\ DV/g$), the results would coincide across the different c values for a given Δx.

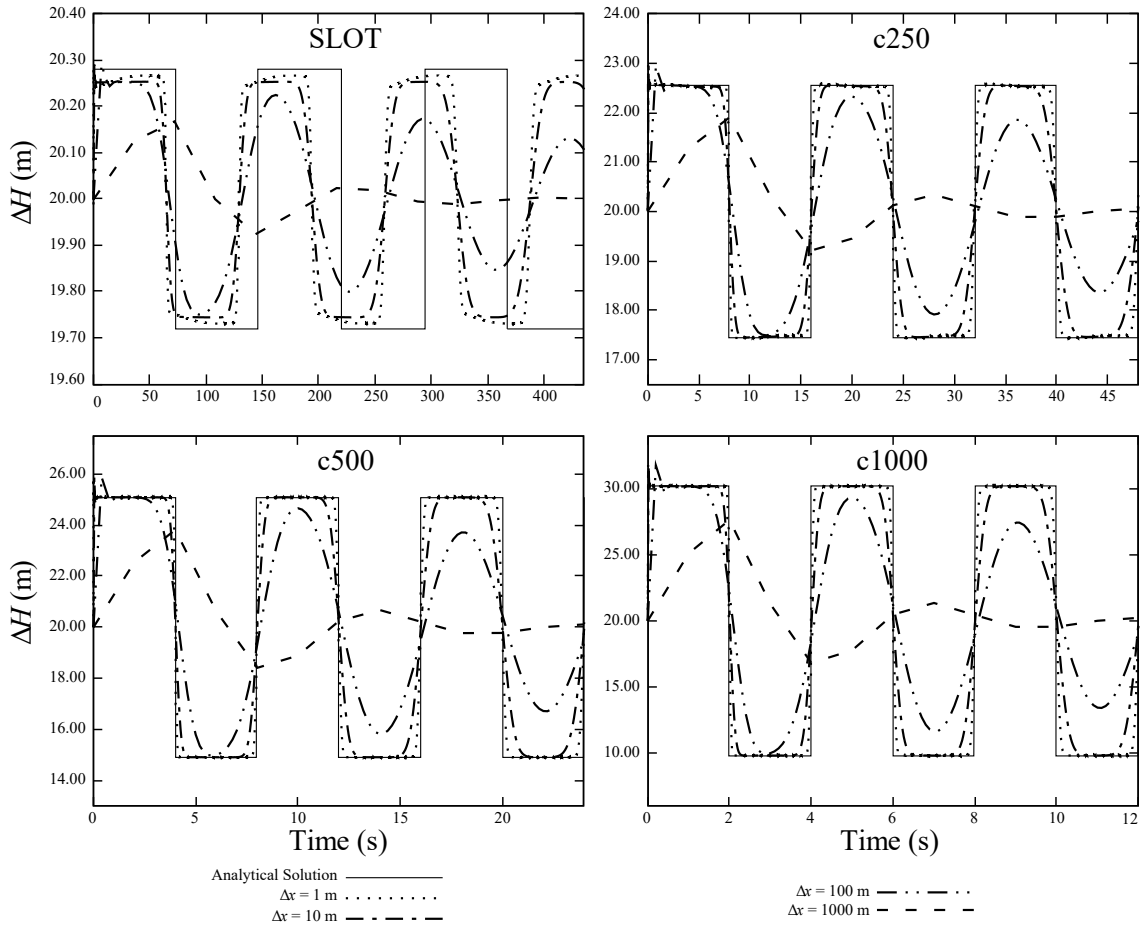

Figure 3.2: Simulation results for all pressurization algorithms showing the head change at the valve after the closure.

Figure 3.3 shows the $L2$ norm results. These results are consistent with the previous ones. The SLOT pressurization algorithm shows values of $L2$ norm in the order of 10 or greater for all discretizations. The modified versions of the Preissmann slot (c250, c500, and c1000) reduced the $L2$ norm values significantly when spatial discretization is adopted. The discretization of

Δx = 1 m showed values lower than 2 for the modified versions of the Preissmann slot. Based on these results, it is possible to state that finer discretizations reduced almost exponentially the $L2$ norm values.

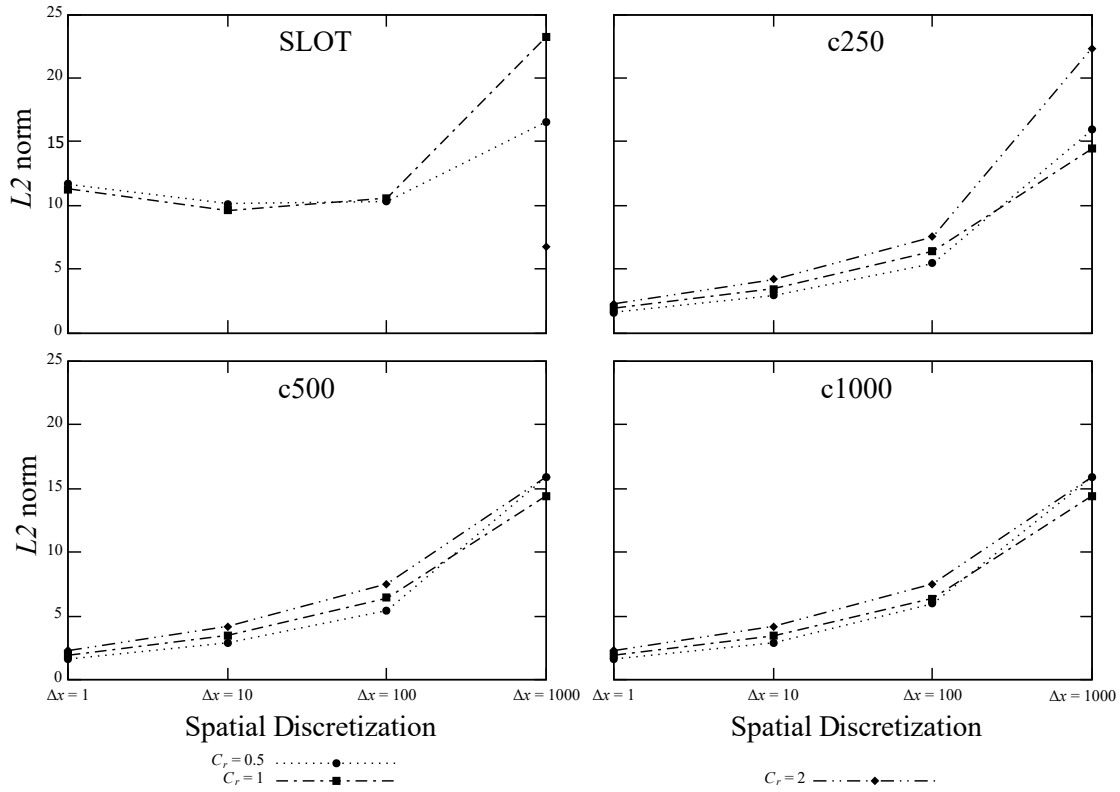

Figure 3.3: Simulation results for $L2$ norm for all spatial discretization adopted and celerity values.

3.3.2 Case 2: Pipeline start-up

The second case considered in this work represents a pipeline with features that are typical of real-world situations. Fig. 3.4 shows the pipeline layout, the piezometric line prior to the valve opening, and the steady state piezometric line after the transient. The valve opening will cause a transient in the system that will propagate from upstream to downstream in cycles that will be dampened by the system's losses.

This pipeline was simulated using an industry-grade transient flow model that uses the Method of Characteristics (MOC) to solve the governing equations for fast transients in closed pipes. The MOC is one of the most popular methods for solving unsteady flows due to its

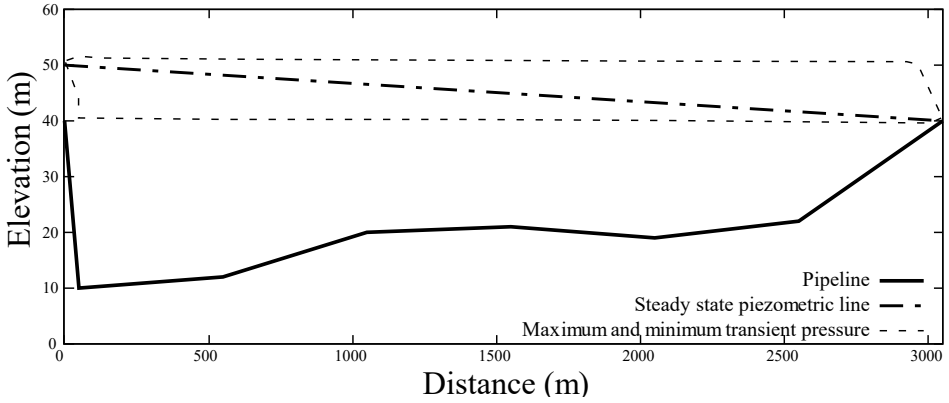

Figure 3.4: Pipeline schematics.

accuracy, numerical efficiency, and programming simplicity (Chaudhry, 2013; Ghidaoui et al., 2005; Wylie & Streeter, 1993). Unlike SWMM, this MOC model is not able to represent transition between flow regimes. The results obtained by this MOC model were compared to SWMM modeling results. Both models were set up with a celerity of 500 m s^{-1} and a C_r of 1 was used to estimate the routing time-step. Spatial discretization of Δx = 0.5 m was adopted in SWMM. The results using the other modified celerities, C_r, and spatial discretizations produced similar results but they were omitted from this work for the sake of brevity. Data were retrieved on specific locations of the pipeline for comparison. Fig. 3.5 shows the results of flow and head at these locations for the first 60 seconds of simulation.

Based on the results, it is possible to state that SWMM is capable of representing the flow rate and the head at those locations with satisfactory accuracy when using the modified Preissmann slot along with spatial discretization. For the first 20 seconds of simulation, when the transient generates the highest head and, consequently, the most critical period, SWMM represents well the transient. However, when simulation time increases, SWMM presents some diffusion that deviates the solution from the MOC model. This situation may be caused by the numerical method implemented in SWMM that uses a method of successive approximations with under relaxation and a convergence tolerance.

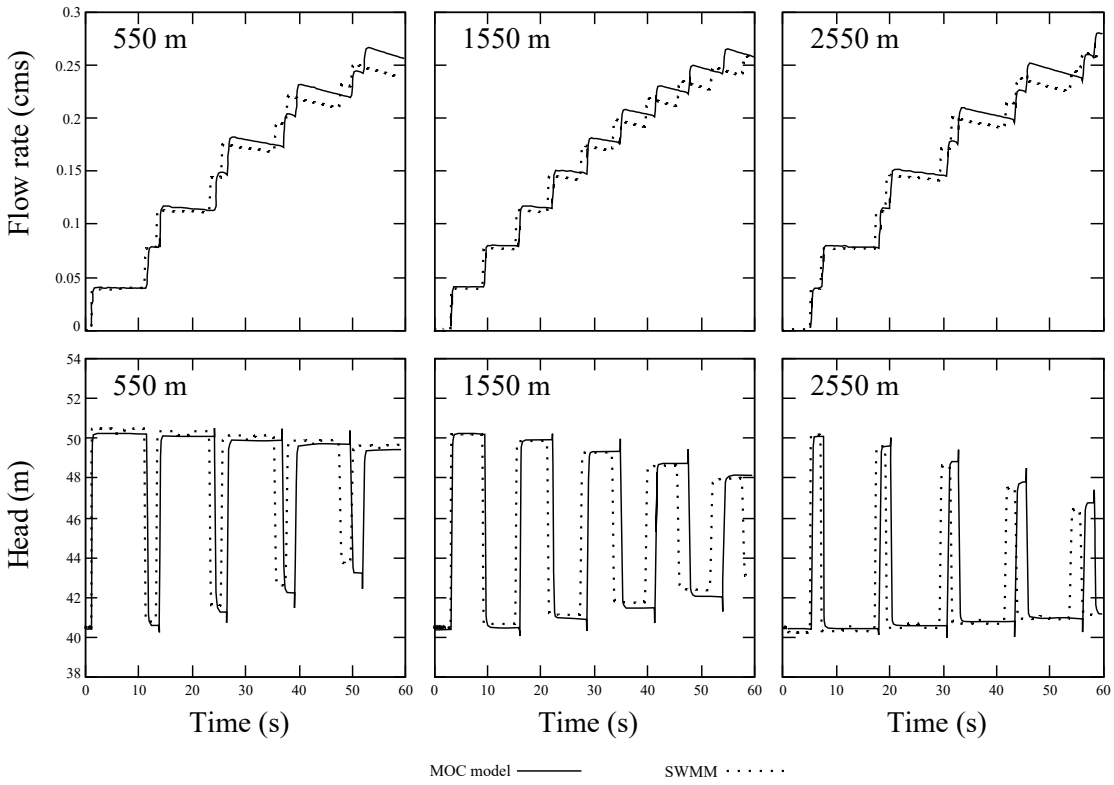

Figure 3.5: Simulation results for different regions of the pipeline.

3.3.3 Conclusions

This work assessed the SWMM capability to simulate certain types of closed pipe transients. It was found that, if SWMM is set up carefully - with additional spatial discretization, a modified version of the Preissmann slot based on expected celerity, and time-step estimated following the CFL stability condition -, SWMM can represent fast transients and certain flows conditions that the model was not originally conceived for.

The results obtained in this work showed that the original implementation of the Preissmann slot method in SWMM 5.1.0.13 is not able to represent closed pipe fast transients since the slot adopted is too wide, creating unrealistic transient storage and delaying the propagation of transient pressures. Furthermore, without spatial discretization, none of the cases analyzed in this work yielded results consistent with theory. This confirms the findings of earlier works by Pachaly et al. (2019), Pachaly et al. (2020b), Ridgway and Kumpula (2008), and Vasconcelos et al. (2018) in the context of mixed flows (i.e., pressurized and free surface flows). These studies also showed spatial discretization as a factor to improve the SWMM accuracy when representing unsteady flows.

The modified versions of the Preissmann slot algorithm based on predefined values of celerity along spatial discretization represented well the closed pipe transients. The results showed that finer spatial discretization produced results with smaller numerical diffusion and, as consequence, smaller values of the $L2$ norm. The relation between spatial discretization and $L2$ norm is almost exponential: when adopting a finer discretization, the $L2$ norm decreases almost exponentially.

In order to represent a more realistic case, a comparison was made between this modified approach implemented within SWMM and a benchmark model. SWMM was able to estimate values of flow and head similar to those obtained by the benchmark model. One limitation found is that as simulation goes on diffusion appears and the results start to differentiate from those generated by the benchmark model. However, the maximum value of head was accurately represented and the flow at the beginning of the simulation was also well estimated by SWMM. It is believed that representing these phenomena with this degree of accuracy in an established

model such as SWMM may aid engineers and modelers in the first stages of designing different types of collection systems.

Chapter 4

Surge predictions in a large stormwater tunnel system using SWMM[†]

Abstract - Stormwater tunnels often have massive geometries, with conduits lengths of several kilometers and a wide range of diameter sizes. Modeling rapid filling of these systems is a complex task and needs adequate methodology. One model used in hydraulic analysis of stormwater tunnels is the EPA's Storm Water Management Model. However, model setup conditions related to pressurization algorithm can significantly impact SWMM's accuracy in surge prediction. This work evaluates SWMM 5.1 accuracy in simulating rapid filling of tunnels, particularly surging conditions. This evaluation is done using a real-world tunnel geometry, the Upper Des Plaines Tunnel (UDP), which is a part of Chicago's TARP tunnel system. Variables considered in SWMM model setup included discretization strategy, pressurization algorithm, and its results are compared with HAST predictions, a model specifically designed to represent surges in tunnels. This work shows that, with adequate setup, SWMM can represent surging in stormwater tunnels much more precisely.

4.1 Introduction

Stormwater management in urbanized areas is a complex task, with goals of minimizing environmental impacts created by runoff discharges to receiving water bodies (Wanielista & Yousef, 1992). These impacts are intensified in the case of combined sewer systems, when the collection systems carry simultaneously stormwater and wastewater. With dense urbanization, the availability of grade-level storage to mitigate these impacts to receiving water bodies is

[†]**Published in**: Pachaly, R. L., Vasconcelos, J. G., & Allasia, D. G. (2021). Surge predictions in a large stormwater tunnel system using SWMM. *Urban Water Journal*, DOI: https://doi.org/10.1080/1573062X.2021.1916828

limited. Below-grade stormwater tunnels, sometimes spanning many kilometers, are an option being adopted in many areas (Wright et al., 2003). In addition to controlling environmental discharges of runoff to the environment, such systems also provide relief to the collection system, preventing episodes of local flooding. However, hydraulic transients are subject to occur within these systems and they may cause structural damages to the system (Li & McCorquodale, 1999). Geysering, pressure surges, mixed flows, and blow-off of manhole covers are examples of the possible effects that could be caused by air entrapment or discontinuities in the conduit network (Cataño-Lopera et al., 2014).

Along these objectives, the Tunnel and Reservoir Plan (TARP) was created to protect Lake Michigan from pollution caused by combined stormwater and sewer overflows in Chicago area (MWRD, 2020). According to the Metropolitan Water Reclamation of the District of the Greater Chicago (2020), the TARP sytem includes four tunnel systems named Upper Des Plaines, Des Plaines, Mainstream, and Calumet. These systems are located 45 to 90 m underground that result in 175 km of constructed tunnels, ranging from 2.5 to 10 m in diameter. Transient analysis involving 1-D and/or 3-D simulations were performed in the Calumet system (Leon et al., 2010) and in the North Branch of the Mainstream system (Cataño-Lopera et al., 2014). These studies evaluated different modeling efforts to represent the complex interaction of air and water in the tunnels. Those complex flows are also anticipated on the Upper Des Plaines (UDP) system. Accurate modeling of inflows within this system is needed to estimate surging processes within vertical structures.

A potential tool to perform this analysis is the EPA's Storm Water Management Model (SWMM 5.1), capable of a wide range of hydrologic and hydraulic analysis. Recent investigations have demonstrated improvements in SWMM 5.1 hydraulic accuracy with the addition of spatial discretization (Pachaly et al., 2019; Ridgway & Kumpula, 2008; Vasconcelos et al., 2018) and the effects of using different pressurization algorithms and time steps (Pachaly et al., 2020a; Pachaly et al., 2020b). Yet, these studies were performed in relatively simple geometries, not accounting for complex and multiple time-varying inflow hydrographs. Moreover, these studies did not involve comparing the accuracy of SWMM with models that were specifically built to represent surging in stormwater tunnels.

This work addresses this limitation by applying SWMM in the context of rapid filling of the TARP-UDP system during a realistic rapid filling scenario. A range of alternative setups to represent pressurized flows is considered, including a comparison between EXTRAN and the Preissmann slot, and different pressurized flow celerity values. Rapid filling and surging results from SWMM were compared to the Hydraulic Analysis of Sewers and Tunnels (HAST) model (Vasconcelos & Wright, 2006), which has a robust hydraulic solver and was previously calibrated in portions of the TARP system.

4.2 Methods

4.2.1 SWMM formulation

The SWMM flow routing is solved using the Saint Venant equations (EPA, 2020b). These equations represent the 1-D unsteady free surface flows based on the conservation of mass (Eq. 4.1a) and linear momentum (Eq. 4.1b) (Sturm, 2001). SWMM uses a network of links and nodes to compute the flow at each link and the head in each node (Roesner et al., 1988; Rossman, 2006).

$$\frac{\partial A}{\partial t} + \frac{\partial Q}{\partial x} = 0 \tag{4.1a}$$

$$\frac{\partial Q}{\partial t} + \frac{\partial (Q^2/A)}{\partial x} + gA\frac{\partial H}{\partial x} + gAS_f + gAh_L = 0 \tag{4.1b}$$

where A denotes cross-sectional area; t denotes time; Q denotes flow rate; x denotes distance; H denotes the hydraulic head of water in the conduit; g denotes gravity; h_L denotes the local energy loss per unit length of the conduit; and S_f denotes the friction slope, which is implemented with the Manning equation (Rossman, 2006). More information on SWMM unsteady flow formulation, including its pressurization algorithms, can be found in Rossman (2006).

4.2.2 HAST formulation

The HAST model also uses the Saint Venant equations for solving pressurized and free surface flows. The model was used because its formulation was tested in a wide range of applications

involving rapid inflows in closed conduits including large-scale stormwater systems (Vasconcelos & Wright, 2007, 2017). The model uses the Two-component Pressure Approach (TPA) (Vasconcelos & Wright, 2006). The TPA represents the effects of pressurization in a single set of equations, starting from the set of mass and momentum equations in traditional pressurized pipe flows and assuming an elastic behavior to the pipe wall while neglecting water compressibility. This leads to the following set of equations:

$$\frac{\partial \overrightarrow{U}}{\partial t} + \frac{\partial \overrightarrow{F}}{\partial x} = S(\overrightarrow{U}) \tag{4.2a}$$

$$\overrightarrow{U} = \begin{bmatrix} A \\ Q \end{bmatrix} \quad F(\overrightarrow{U}) = \begin{bmatrix} Q \\ \frac{Q^2}{A} + gAh_c + gAh_s \end{bmatrix} \quad S(\overrightarrow{U}) = \begin{bmatrix} 0 \\ gA(S_o - S_f) \end{bmatrix} \tag{4.2b}$$

where h_c denotes the depth of the centroid of the cross-sectional flow area; and h_s denotes the pressure head associated with pressurized flows (positive or negative).

Equations 4.2a and 4.2b differ from the traditional Saint-Venant formulation because a surcharge head h_s is included. This term is zero if the pipeline flows in a free surface flow regime, and relates to the cross-sectional flow area A, the original pipe wall A_{pipe} and the acoustic wave speed a when the flow regime is pressurized. An advantage of HAST is that it was implemented using Roe's non-linear numerical scheme, as presented in Macchione and Morelli (2003), and shows little numerical diffusion for low Courant numbers. This is an important feature when modeling flow regime transition given that pressure wave celerity values can differ by up to 2 orders of magnitude.

4.2.3 Geometry of TARP Upper Des Plaines

The TARP Upper Des Plaines (UDP) system includes various dropshafts and tunnel reaches with diameters ranging from 1.5 m to 6.1 m, comprising a total length of approximately 13 km. Figure 4.1 presents a diagram of the UDP and some of its geometric features, including its junctions.

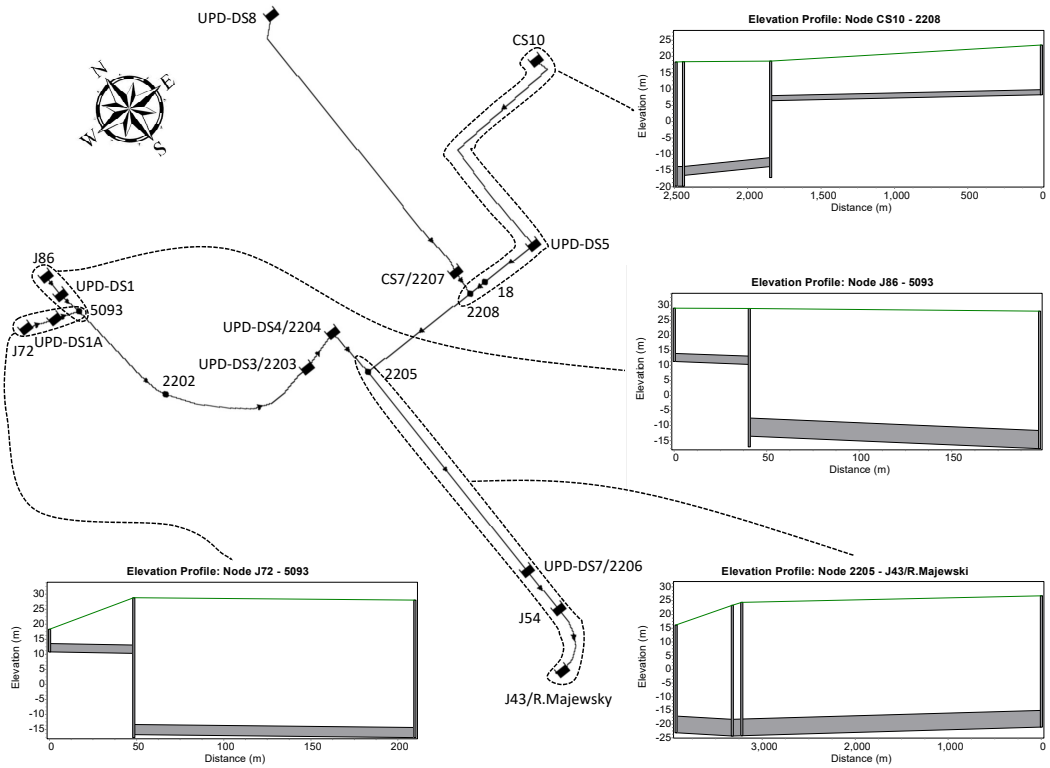

Figure 4.1: TARP Upper Des Plaines System schematic. Details in the figure show specific characteristics of the system: adverse slopes and drop shafts.

Typically when surging analysis is performed, it is desirable to account for a range of inflow hydrographs that are deemed representative for rapid inflow scenarios. However, this work focuses on a comparative analysis of SWMM 5.1 solution approaches to represent surges, thus a single inflow hydrograph was used for all tested conditions. This inflow hydrograph is shown in Figure 4.2, presenting its characteristics in different UDP dropshafts that were used in the SWMM and HAST simulations.

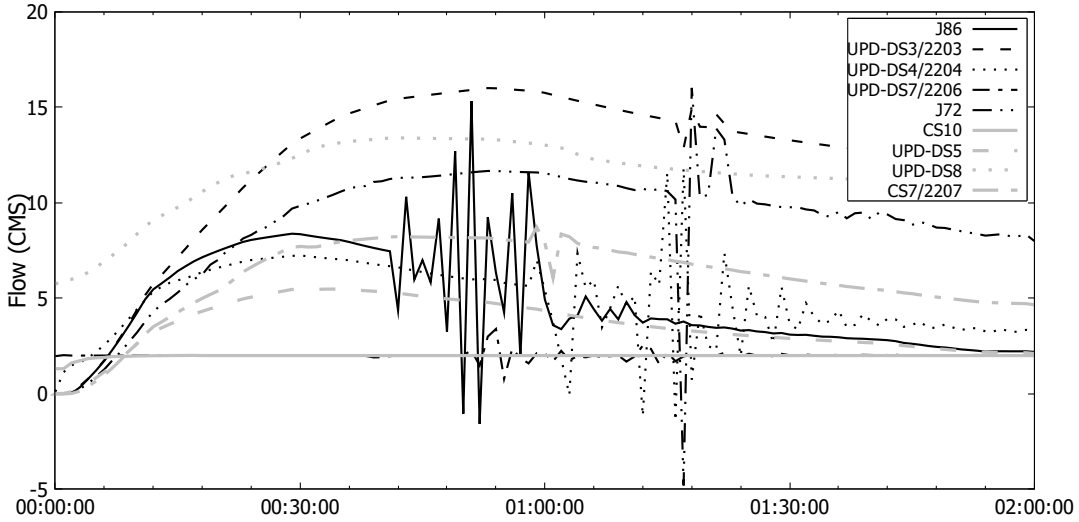

Figure 4.2: Inflow hydrographs in different UDP dropshafts.

Numerical modeling variables

Recent investigations have indicated that SWMM modeling results are influenced by the choice of pressurization algorithm (Pachaly et al., 2020a; Pachaly et al., 2020b), by using spatial discretization (Pachaly et al., 2019; Ridgway & Kumpula, 2008; Vasconcelos et al., 2018) and also by the size of the time step (Pachaly et al., 2020b). These modeling setup variables were also selected in the present study in order to assess the accuracy of surge modeling accuracy in the context of stormwater tunnels.

One setup variable in this analysis is alternatives for SWMM flow pressurization algorithm. This work considered both the EXTRAN algorithm and four different alternatives of the SLOT algorithm. The first alternative was the SLOT as implemented in SWMM 5.1, is 1% of the pipe diameter and results in a pressure wave celerity in the range of 30 m/s for an unitary diameter. The SLOT implementation in SWMM includes the a modification proposed by Sjöberg (1982) whereby a gradual slot width change result in a smoother transition between free surface and pressurized celerity values. The second SLOT algorithm also has the 1% pipe diameter with but did not considered this gradual transition. The third and fourth SLOT algorithms applied a narrower slot developed by the authors that yielded a celerity of 250 m/s, either with or without the gradual slot transition. The rationale is that these larger wave celerity values are in the

range of celerity values in pressurized flows with a small fraction of air. Altogether, 5 distinct pressurization algorithms were considered.

The second variable considered in this comparative study was the spatial discretizaton, and this was done by increasing the number of computational nodes in-between two consecutive structures (Ridgway & Kumpula, 2008; Vasconcelos et al., 2018). As this option is not native in SWMM, the ReSWMM (Pachaly et al., 2018) tool was used. In addition to the traditional link-node approach, three discretization strategies were used splitting conduit reaches into smaller reaches of 20 (20 DxD), 10 (10 DxD), and 5 (5 DxD) times its own diameter.

Finally, the effect of time discretization was also considered. For the SLOT pressurization algorithm, it was used a range of values for Δt based on the Courant Condition (Eq. 4.3a). When the EXTRAN pressurization algorithm was used, the range of values for Δt followed the recommended routing time step proposed by Roesner et al. (1988), presented in equation Eq. 4.3b.

$$\Delta t = Cr\frac{L}{c} \qquad (4.3a) \qquad\qquad \Delta t \leq \frac{L}{\sqrt{gD}} \qquad (4.3b)$$

where Δt is the routing time-step; Cr is the Courant number; L is the smallest link length of the system; c is the wave celerity; and D is the link diameter. Figure 4.3 shows the simulations' summary that can be used as guide for readers. With a systematic variation of these parameters a total of 100 unique SWMM modeling setups are compared in the simulation of the TARP-UDP system, as is shown in Figure 4.3.

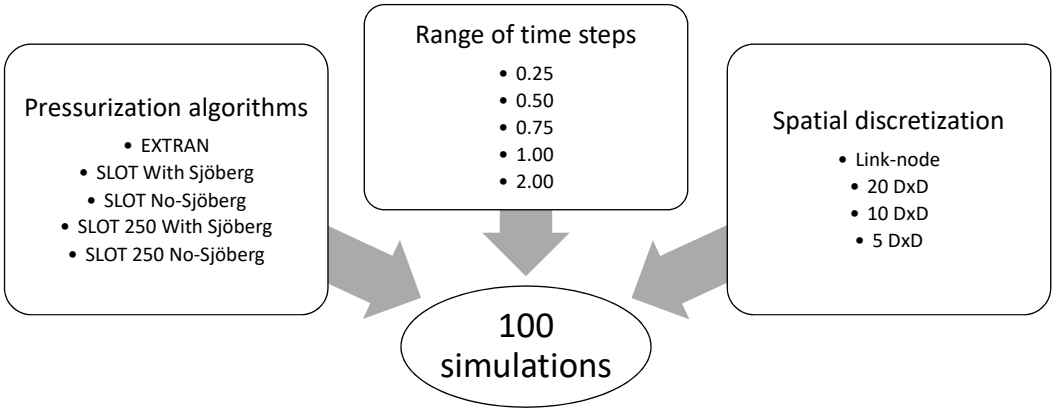

Figure 4.3: Simulations' summary

The TARP-UDP simulation performed with HAST used an acoustic wavespeed of 250 m/s, a discretization strategy where $\Delta x = D$, and a Courant number of 0.9. Facing the lack of observed field data and since the HAST modeling had as a key objective to understand possible causes and locations for observed geysering events, the calibration of HAST model was considered successful as it predicted the formation of large of large air pockets at the exact locations where it occurred within the TARP-UDP.

4.3 Results and discussion

4.3.1 Numerical modeling continuity errors

One of the most relevant outcome in a hydraulic simulation is to ensure small continuity error, at maximum in the order of few percent. With a high absolute continuity error, the model is not representing the flow as there is an incorrect storage or loss of water. We have postulated for the sake of comparison that results with continuity errors under than 1% as good, between 1% and 5% as acceptable, and larger than 5% as unacceptable. In comparison, continuity errors in HAST were under 0.2%. A summary of the continuity errors for all 100 SWMM simulations are presented in Table 4.1.

The vast majority of simulations had an absolute continuity error in the acceptable range of 1% and 5%. The worst continuity errors results were associated with the pressurization algorithms using the SLOT with 250 m/s and not using the gradual celerity transition by

Table 4.1: Flow continuity error

Time Step Ratio	**0.25**	**0.5**	**0.75**	**1**	**2**
Spatial Discretization	**EXTRAN**				
Link-node	28.82	28.75	22.61	28.20	28.72
20 DxD	6.21	6.07	6.01	7.12	9.63
10 DxD	-0.02	3.24	4.99	6.74	16.03
5 DxD	-5.05	-4.08	3.41	5.69	15.46
	SLOT with Sjöberg				
Link-node	4.16	4.47	3.53	3.41	-7.20
20 DxD	2.12	1.78	1.38	2.18	2.76
10 DxD	1.80	2.12	2.28	2.03	-2.28
5 DxD	2.04	1.99	2.49	1.01	2.38
	SLOT No-Sjöberg				
Link-node	4.57	4.26	3.93	4.05	3.15
20 DxD	3.62	3.30	3.10	3.22	2.16
10 DxD	2.59	2.58	2.12	2.59	2.66
5 DxD	2.38	2.52	2.67	2.20	2.45
	SLOT 250 with Sjöberg				
Link-node	1.51	2.28	-1.42	3.40	2.96
20 DxD	4.22	3.96	3.78	3.81	3.62
10 DxD	3.55	3.38	3.13	2.86	2.48
5 DxD	3.10	2.70	2.92	3.02	3.17
	SLOT 250 No-Sjöberg				
Link-node	-1.00	0.24	4.04	-8.03	32.44
20 DxD	49.23	54.55	56.37	57.51	56.12
10 DxD	52.80	56.63	58.15	59.76	59.82
5 DxD	53.94	57.07	56.15	59.93	55.07

Sjöberg (1982). This was explained because in the simulations a hydraulic bore formed at the downstream end of the system junctions 2205 and J43/R.Majewski and pressurized the flow. Pressure oscillations at the pressurized side of the bore influenced the results negatively, consistently creating large continuity errors. Figure 4.4 illustrates this issue by presenting the water elevation profile predicted by HAST and different SWMM pressurization algorithms. The amplitude of pressure oscillations for the 250 $m.s^{-1}$ SLOT without gradual transition was the highest of the tested cases, including presenting unexpected large negative pressures. The representation by EXTRAN and the original SWMM slot algorithms, on the other hand, yielded hydraulic bore fronts with pronounced numerical diffusion, which in turn had an effect on surge prediction, as is discussed below.

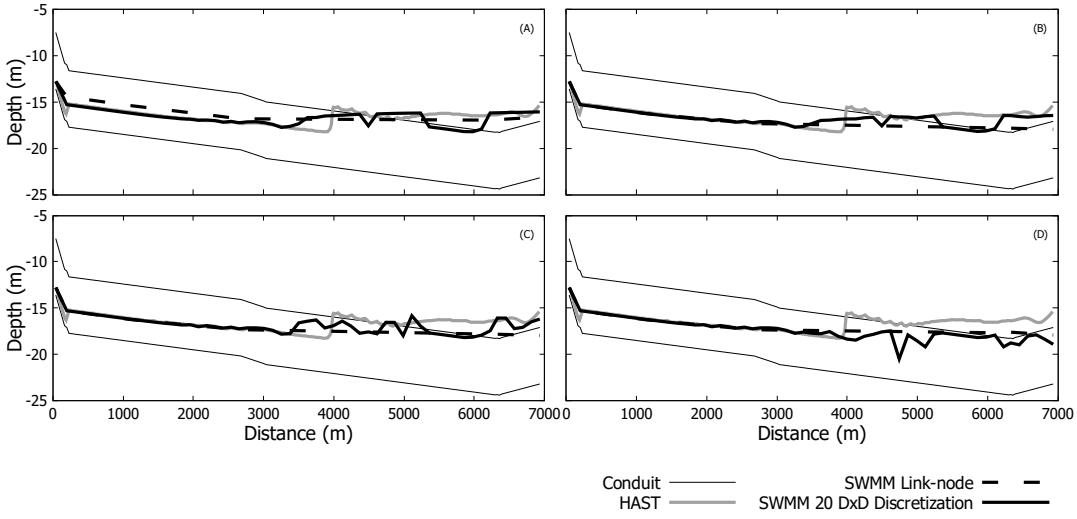

Figure 4.4: Profile at 3222s of simulation (Cr = 1) between UPD-DS1 and J43/R.Majewski: (A) EXTRAN; (B) SLOT; (C) SLOT 250m/s with Sjöberg transition; and (D) SLOT 250m/s without Sjöberg (1982) transition.

4.3.2 Surge results

Given the large number of tested conditions only the most relevant results are presented for the sake of brevity. Junction 2205 was selected to be evaluated because it is located in a key UDP location where different UDP reaches merge. Moreover, these results are representative of the surging predicted in other UDP junctions. Results with large continuity errors were not considered in the surge comparison as these are not representative of the flows. Therefore, solutions using the narrower SLOT with 250 m/s without gradual transition are omitted.

Comparing the SWMM results with the ones from the HAST model, EXTRAN pressurization algorithm was not able to properly capture the mass oscillations associated with surging after the pressurization of UDP reaches, as is shown in Figure 4.5. Peak surge was underestimated by more than 5 meters, and the oscillation period of surges was much larger. Spatial discretization improved results slightly, but in general these results are not representative of the anticipated surges. It is speculated that numerical diffusion of pressurization bores could be linked with this modeling outcome.

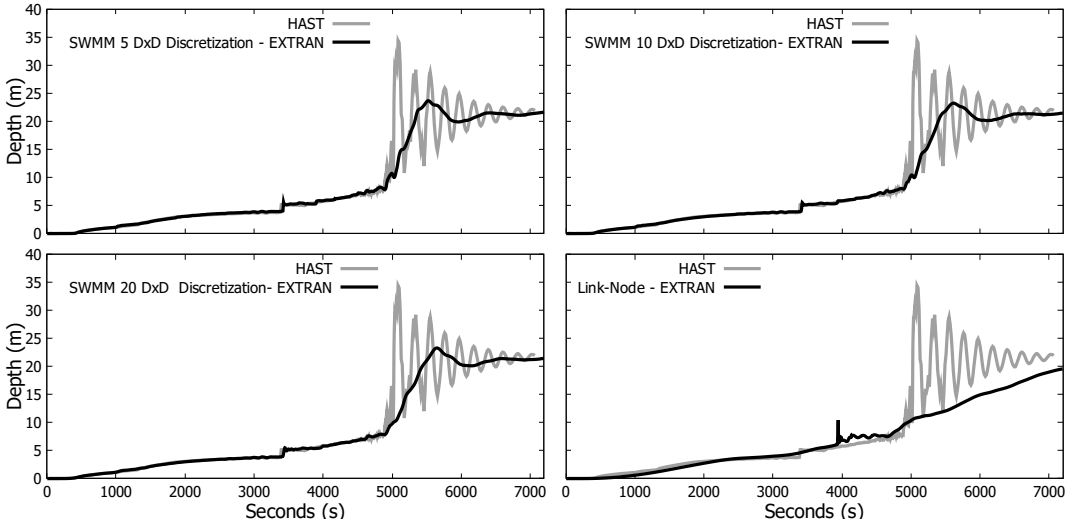

Figure 4.5: Surges predicted at Junction 2205 with EXTRAN algorithm using time step $\Delta t = L/\sqrt{gD}$

Results with the SLOT pressurization algorithm had a slight improvement in surging prediction when compared to the EXTRAN results as shown in Figure 4.6. However, the comparison with HAST results indicate that the peak surge is still underestimated and the frequency of surging is also not well represented. Similarly to the case of EXTRAN results, it is speculated that numerical diffusion and low acoustic wavespeed can be factors in the observed discrepancies in surging predicted by HAST and SWMM.

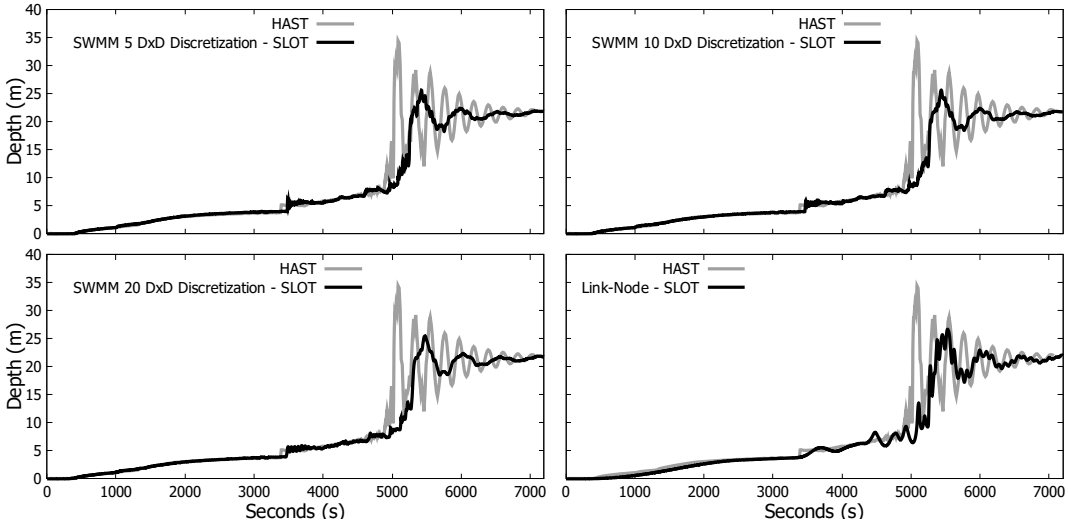

Figure 4.6: Surges predicted at Junction 2205 with SWMM original SLOT algorithm using time step $\Delta t = 1.0(L/c)$

Surge predictions yielded by SWMM improved significantly when the narrower SLOT with 250 m/s celerity and Sjöberg slot transition was used. Although there was a slight delay in the initiation of surges, it can be noticed in the results presented in Figure 4.7 that the amplitude and the period of surges predicted by SWMM matched the results presented by HAST. With link-node discretization, however, spurious high-frequency oscillations were noticed in the surge results.

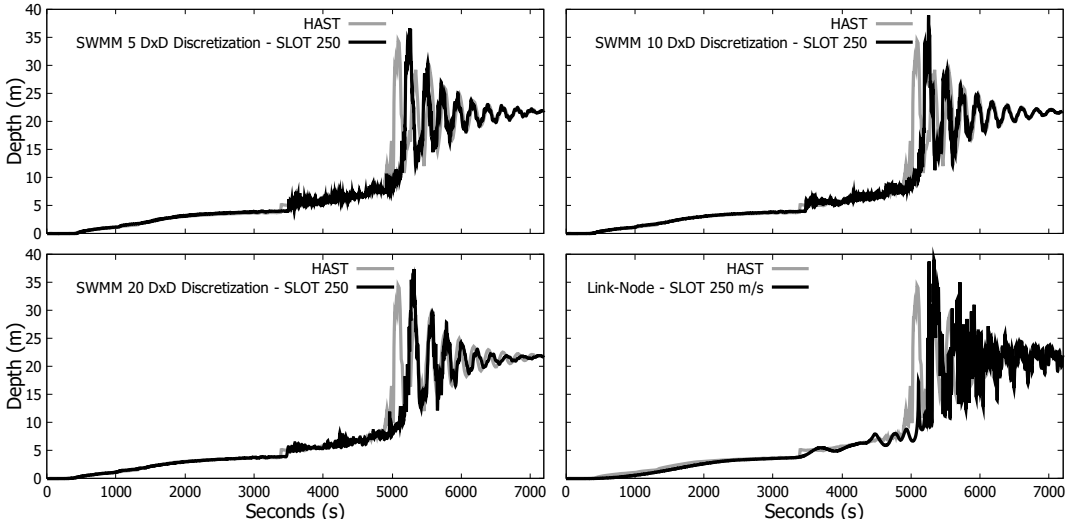

Figure 4.7: Surges predicted at Junction 2205 with the 250 m/s SLOT algorithm, Sjöberg gradual slot transition and time step $\Delta t = 1.0(L/c)$

Modeling runs with the SLOT algorithm and using other values of the Courant number indicated that SWMM can run simulations with Courant numbers exceeding 1. This is due to its iterative implicit procedure to update flows and head (Rossman, 2017a). However, the use of larger values of the Courant number occasionally created numerical instabilities, albeit resulted in smaller simulation times. On the other hand, using low values of the Courant number led to small-amplitude, high-frequency oscillations in surging results, in addition to longer computational times. Therefore, the recommendation for surge simulation using SWMM is to use spatial discretization, narrow SLOT algorithm (with Sjöberg transition) and a Courant number close to 1.0.

4.3.3 Additional remarks in SWMM surging modeling setup

As this investigation was performed, a problem was found in the cases when spatial discretization was used near junctions with discontinuous conduit invert elevations such as dropshafts. This problem was noticed through strong local numerical oscillation, that was also increasing continuity errors. A fix that was found for such issues was to artificially increase the slope of the last discretized reach at the upstream end of the drop. It is speculated that this change created a supercritical flows immediately prior to the drop, which is anticipated in real-world conditions. While in this investigation it was noticed that an offset of one diameter addressed these instabilities, this fix should be evaluated in a case-by-case basis. Figure 4.8 shows one instance where slopes were adjusted in the SWMM modeling of UDP.

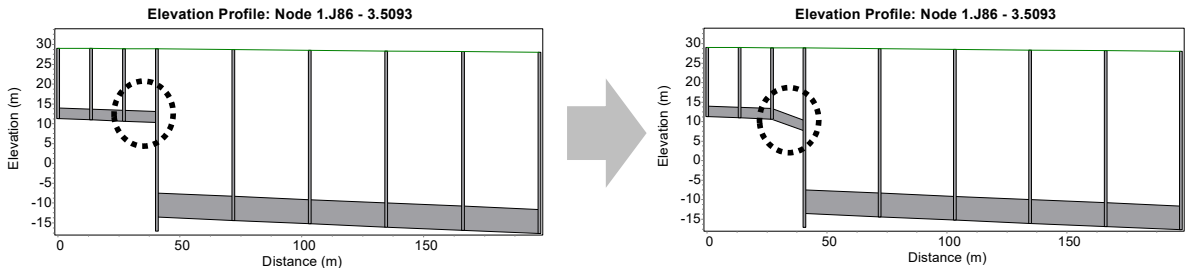

Figure 4.8: Slope adjustment.

Another remark of using SWMM with spatial discretization for such large systems is the computational time spent to perform a single run. A simulation with the narrower SLOT algorithm can take few hours to be performed in a usual personal computer. However, the computational time by SWMM was still smaller than HAST model. This is possibly due to the finer spatial discretization used in HAST model.

A final point to be made is that SWMM is a single-phase (e.g. water) hydraulic model and thus neglect the effects of entrained/entrapped air phase during filling processes. In some cases such phenomenon is of fundamental importance to evaluate the likelihood of other relevant phenomena such as stormwater geysers, air-water surging and manhole cover displacements. If hydraulic modeling goals include represent air-water interactions during rapid filling in tunnels, other tools should be considered instead of SWMM.

4.4 Conclusions and recommendations

This work evaluated the applicability of SWMM to model surges in stormwater tunnels by comparing its results to another model that was specifically constructed to represent such flow conditions. Through the use of the narrow SLOT algorithm with gradual transition, spatial discretization, and Courant number of 1 it was noticed that predicted surges were very close in magnitude and frequency than the ones yielded by HAST model. This may indicate an interesting possibility to practitioners interested in hydraulic simulation of stormwater tunnels. In other conditions, SWMM predictions could yield significant continuity errors, misrepresentation of pressurization bores and surges of incorrect magnitude and frequency.

In the context of the rapid filling of the TARP UDP system, both pressurization algorithms originally implemented in SWMM underestimated the water peak level in the shafts and yielded much larger surge oscillation periods. Another finding of this work was the importance of the Sjöberg (1982) slot transition in improving the stability of bore propagation predictions. Particularly for the narrow slot alternative, the gradual slot transition enabled the decrease of continuity errors during the simulation of hydraulic jump propagation. Other sources of instabilities linked to the discontinuity of conduit inverts were also noticed in the study; a fix based on increasing the conduit slope immediately upstream from the drop addressed this issue. A final observation was that SWMM simulations using pressurization algorithms based on the Preissmann slot can have the time step decision based on the Courant condition. While SWMM could handle simulations with Courant number deviating from unity, best results were achieved with Courant number close to unity.

It is hoped that this finding will help practitioners in setting up SWMM models to represent with better accuracy the surging processes in stormwater tunnels. Since SWMM is one of the most popular stormwater models worldwide that has many different boundary conditions and it is an open-source software, increasing its applicability to surge prediction can facilitate the modeling of stormwater systems by avoiding the usage of other models for surge prediction that are often not free-to-use software. However, one disadvantage is the inability of SWMM to consider air phase effects in the simulation of rapid filling tunnels and related surging. Tools

that incorporate this aspect should be used if these interactions are anticipated in stormwater systems undergoing rapid filling.

Chapter 5

Numerical modeling study of flooding in Brighton and Midfield

Abstract - Two urban communities, Brighton and Midfield, AL, are experiencing recurrent flooding events. Significant portions of their watershed have impervious areas and high slopes, leading to intense and short-duration peak flows. A modeling framework that combined a 1D PCSWMM model for simulating the surface hydrology and a 2D HEC RAS model for representing the flooding areas was proposed. Also, field data was collected for calibration purposes and different conceptual design approaches were suggested upstream the flooded areas with the intention of mitigating the flooding events. The proposed modeling framework predicted the flooded areas according to the reported flooding events and the conceptual design approaches reduced the flooding extent, depth, and duration significantly.

5.1 Introduction and objectives

There are strong indications that the number of heavy precipitation events will increase in the next years (Kundzewicz et al., 2014). Urban areas are more likely to experience social and economical damages caused by these intense rain events than rural areas. Flooding is one of these problems, occurring when the collection system cannot properly convey the water that it is receiving (Wanielista & Yousef, 1992). This can be caused by a poor design that did not anticipate these heavy rain events or by an aged system with detritus in its pipes (Yen, 1986). Communities in urban developed areas may experience flooding events, and suffer the impacts of such occurrences. This is the case of two residential areas located in Jefferson County, AL where flooding events are being frequently reported in the communities of Brighton and Midfield.

Their watersheds include large tracts of impervious areas as well as high slopes, resulting in fast overland flow time, small times of concentration, and intense peak flows.

Recent studies showed that coupling 1D and 2D models can be used as a modeling framework for effective flooding simulation (e.g. David and Schmalz (2020), Leandro et al. (2009), Nguyen et al. (2015), Papaioannou et al. (2016), and Rai et al. (2018)). This combination is often performed by using a 1D model to represent the hydrology and/or the river channels and a 2D model for representing the floodplains. The great majority of these studies are related to river flooding, such as the cases where HEC HMS and HEC RAS were coupled (David & Schmalz, 2020), HEC RAS and MIKE 11 (Papaioannou et al., 2016), SWMM and HEC RAS (Vemula et al., 2020), and others. In the context of urban flooding, studies were performed coupling SWAT and SWMM model with iRIC (Rai et al., 2018), DHI with FULLSWOF_2D (Salvan et al., 2016), SWMM with HDM-2D (Kim et al., 2018), and SWMM with HEC RAS (Akter et al., 2020; Khalaj et al., 2021). Moreover, there are studies that considered only a 1D model (Kim et al., 2019; Lyu et al., 2019) or a 2D model (Yalcin, 2019) to analyse urban stormwater flooding.

The methodology proposed in this study combined a 1D PCSWMM model to represent the surface hydrological aspects of the study area and a 2D HEC RAS model to represent the flooding extent. PCSWMM is third party software developed by the Computational Hydraulics International (CHI) that uses SWMM engine (Rossman, 2015b) together with calibration tools and the capability to perform 1D-2D and quasi-2D modeling procedures (Beck, 2016). HEC RAS 6.0 is a model capable of performing many hydrological, hydraulic, and water quality modeling. HEC RAS is developed at the Hydrological Engineering Center (HEC) by the U.S. Army Corps of Engineers (Brunner, 2021a). Employing a 1D hydrological model to indicate regions where flooding may occur and to predict expected flow rates combined with a 2D hydraulic model to represent the flooding extent would enable a better understanding of the issues associated with the observed flooding in the context of urban water systems. Also, once these models are calibrated, and able to predict flooded areas, conceptual approaches to alleviate flooding could be calculated and compared using these models.

Therefore, this chapter presents the results of a hydrological and hydraulic study performed in watersheds subject to flooding in Brighton and Midfield. The goal of this study is to obtain insights of the flooding processes occurring within these areas, and evaluate possible alternatives to mitigate the flooding. Different modeling approaches and conceptual designs that could mitigate the extent of flooding are presented and discussed in this chapter.

5.2 Methodology

5.2.1 Hydrological modeling

The subcatchments and the 1D links' network were developed based on the Digital Elevation Model (DEM). The LiDAR Elevation Dataset, which has a 1 meter resolution, was retrieved from the USDA/NRCS Geospatial Data Gateway. The subcathments' slopes, links' length, elevations, and transects were all obtained directly from the DEM. Some underground geometries, such as bridges, pipes, and culverts, were field-measured. Figure 5.1 shows the 1D drainage channels and subcatchments generated by PCSWMM for both study areas as well as their Curve Number (CN) values. The CN for each subcatchment was estimated based on the land cover, retrieved from National Land Cover Database (NLCD), and soil information, retrived from Soil Survey Geographic Database (SSURGO).

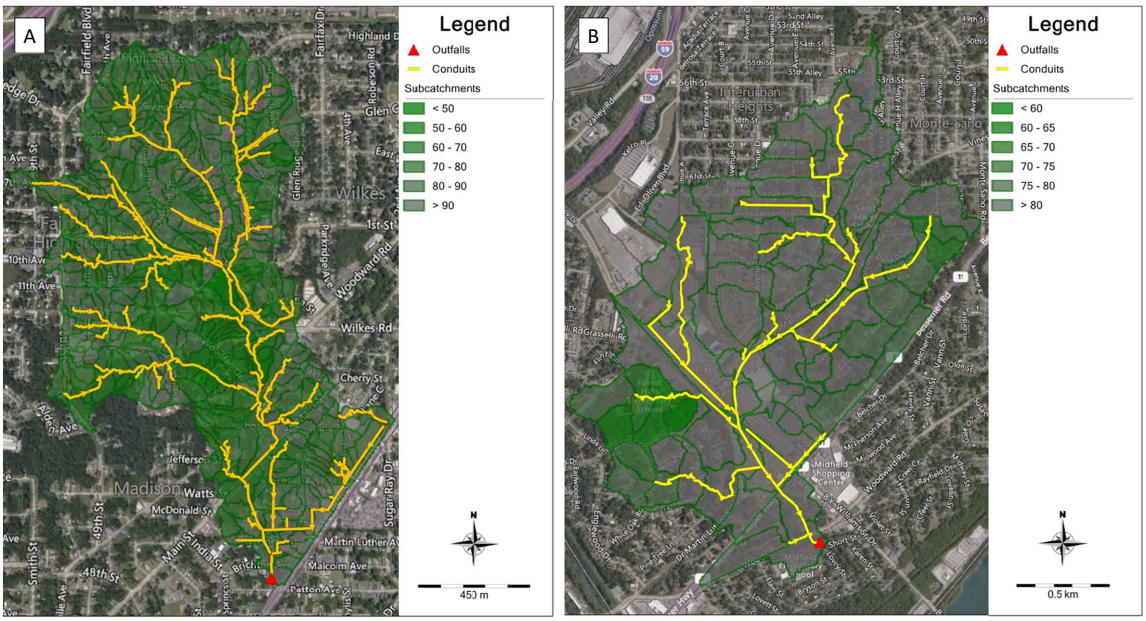

Figure 5.1: Brighton (A) and Midfield (B) PCSWMM drainage channels & subcatchments.

The rainfall data was obtained through two data sources: USGS Water Data (USGS, 2021) and NOAA Global Hourly (NOAA, 2021). The first data source was used for calibration purposes since it has 15 minutes recording interval and the rain gauge (site 02461192) is close to both study areas. The second data source was used for generating the design rainfalls using a software named NetSTORM (Heineman, 2004) since long term rainfall data is available. The selected rainfall gauge is located at the Birmingham Airport (NOAA ID 13876) and it comprises a total of 20 years (2001-2021) of measured hourly rainfall. The monthly statistics are shown in Table 5.1.

The flooding in Brighton and Midfield was evaluated using design rainfalls. These design rainfalls were developed following the SCS procedure. The total rainfall for each return period was estimated based on NetSTORM frequency estimates (Heineman, 2004), the storm pattern is Type II, the storm duration was set as 6 hours, and the rain interval was set as 6 minutes. The selected return periods were 1, 5, and 10-years. The duration of the design rainfalls was set as 6 hours because the flooding effects of the 12 and 24 hours design rainfalls were less intense. This results in a total of 3 rainfall scenarios for both areas. Figure 5.2 shows the selected design rainfalls.

Table 5.1: Average monthly rainfall and duration.

Month	Rainfall (in)	Duration (hrs)
Jan	4.65	18.16
Feb	5.44	18.39
Mar	5.89	16.49
Apr	5.44	12.22
May	5.10	13.11
Jun	4.76	14.60
Jul	5.16	9.08
Aug	4.88	8.81
Sep	3.80	17.49
Oct	3.06	18.20
Nov	4.02	15.42
Dec	5.24	18.56

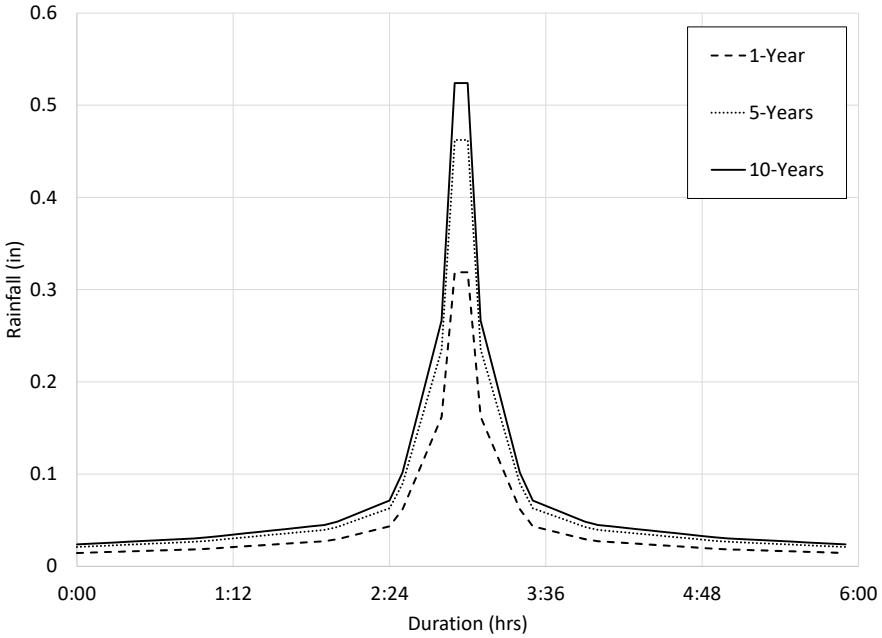

Figure 5.2: Selected design rainfalls.

In order to calibrate the models, three pressure sensors were deployed at specific locations (Figure 5.3). One sensor was used for monitoring the atmospheric pressure, and the other two were used to measure water depth. The sensors were deployed in 07/30/2021 and retrieved on 09/06/2021, recording total absolute pressure at every 15 minutes. However, the sensor located in Brighton was lost along with the obtained data. Therefore, Midfield was calibrated using the available data and, since Midfield is close to Brighton, the same parameters calibrated in Midfield were assumed to be valid for Brighton. The obtained data does not have a long record

period but it is still valuable for calibration purposes, and were the feasible option given the duration of this project.

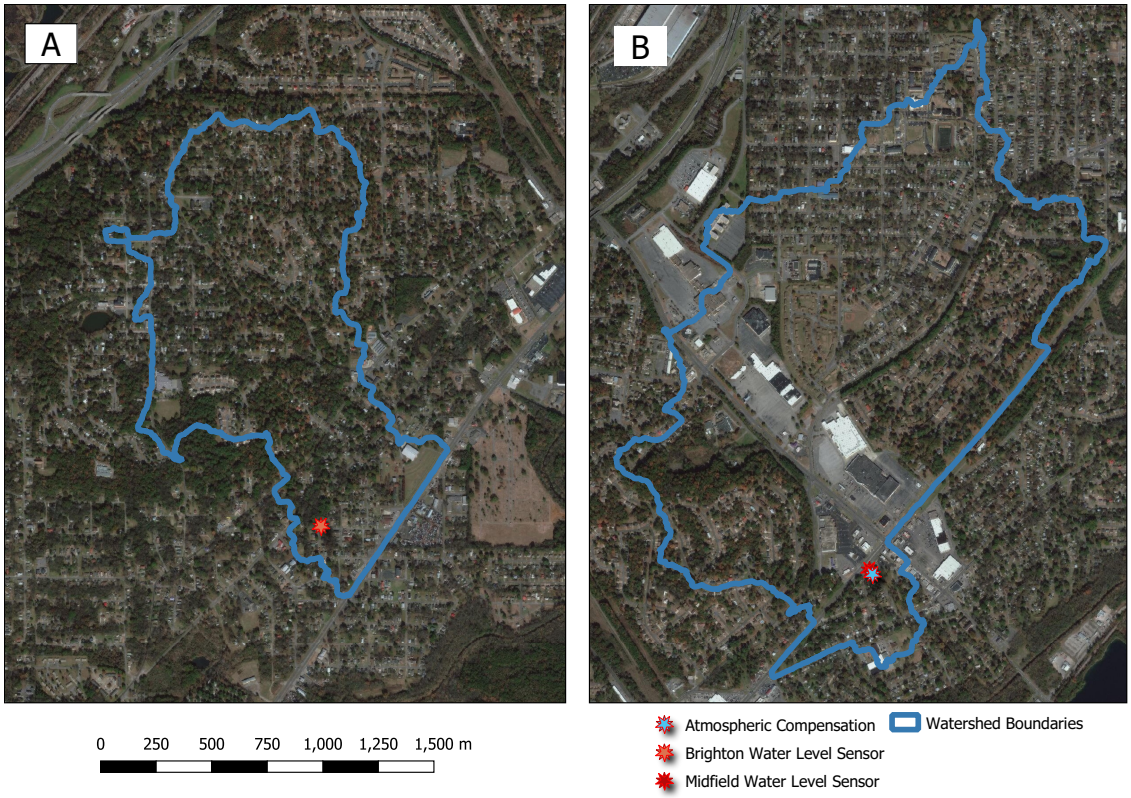

Figure 5.3: Brighton and Midfield sensors locations.

The calibration process used the PCSWMM's Sensitivity-based Radio Tunning Calibration (SRTC) tool. This tool changes the modeling parameters following an user's predefined range. Then, it linearly interpolates between these different simulation results based on the parameter's extreme value. Once the model is assumed calibrated, a last simulation is performed considering the modified parameters.

5.2.2 Hydraulic modeling

The flooded areas were modeled using HEC RAS 2D Diffusion Wave Equation (DWE) (Brunner, 2021a) since no significant changes were noticed when modeled using the SWE. This equation can be used instead of the full momentum equation when the velocity is determined by a balance between barotropic pressure gradient and bottom friction, simplifying to an one equation model and resulting in Equation 5.1 (Brunner, 2021b):

$$\frac{\partial h}{\partial t} = \bigtriangledown \cdot (\frac{R^{2/3}h}{n|\bigtriangledown z_s|^{1/2}} \bigtriangledown z_s) + q \tag{5.1}$$

where h is water depth, t is time, R is hydraulic radius, $\bigtriangledown z_s$ is water surface elevation gradient, n is Manning's roughness coefficient, and q is a source/sink flux term. Differently from the SWE, the DWE runs faster for many flooding applications, such as the one investigated in this study, and it is inherently more stable (Brunner, 2021b). The SWE is recommended for situations such as dam breaks, hydraulic jumps, critical flows, and others because it can account for Coriolis effects and turbulence. However, this results in more computational efforts and longer run times.

The HEC RAS model was developed based on the DEM and in the geometric data obtained on the field, as in the hydrological modeling portion of this study. However, the inflow into the model was the PCSWMM results of the design rainfall events. Since the area modeled by HEC RAS is significantly smaller than the area modelled by PCSWMM, rainfall was not added to HEC RAS modeling efforts.

In Midfield, 6.5x6.5 ft rectangular cells were employed, resulting in a total of 41,034 cells in the 2D flow area. The Manning's number was assumed as 0.06, recommended for open spaces with low development (Brunner, 2021b). Also, the time step for this modeling was set as a fixed value of 10 seconds. In Brighton, a total of 7,372 cells with 16x16 ft were used. Also in this case, the Manning's was assumed as 0.06. The time step was set as 2 seconds but variable to 0.01 of the Courant condition for faster computational calculations. Due to the number of bridges and culverts being modelled, a lower time-step is required for keeping the model stable in this area. Therefore, a higher cell size was employed to compensate for excessive computational efforts caused by the lower time-step.

5.2.3 Conceptual approaches to mitigate flooding

One hydraulic structure upstream the flooding area and two hydraulic structures at the flooding area were proposed for mitigating the flooding extent in Midfield area. Three different areas of 2.5 acres, 5 acres, and 6.2 acres were proposed for the upstream storage unit, located on a parking lot, and the two downstream detention ponds had areas of 1,75 acres and 0.9 acres,

close to the flooded areas and referred as park. All upstream conceptual approaches for Midfield block the main underground channel for diverging the excessive flow but a rectangular orifice (10'4" x 1') is kept at the bottom for low flow situations and to avoid trash accumulation. The downstream detention ponds have connections to the channel that is experiencing flooding.

The next three figures show the upstream storage units locations as well as the conceptual design schematics implemented in each one of these conceptual approaches. The first upstream storage unit location and schematics is shown in Figure 5.4. This storage unit uses half of the parking lot area. The second upstream storage unit occupies all south portion of the parking lot. Its location and schematics is shown in Figure 5.5. The last upstream storage unit uses the whole south portion of the parking lot as well as an extra portion on the north. The schematics and location for this storage unit are shown in Figure 5.6. Finally, Figure 5.7 shows the detention ponds at the flooding areas in a 3D representation with an elevation exaggeration.

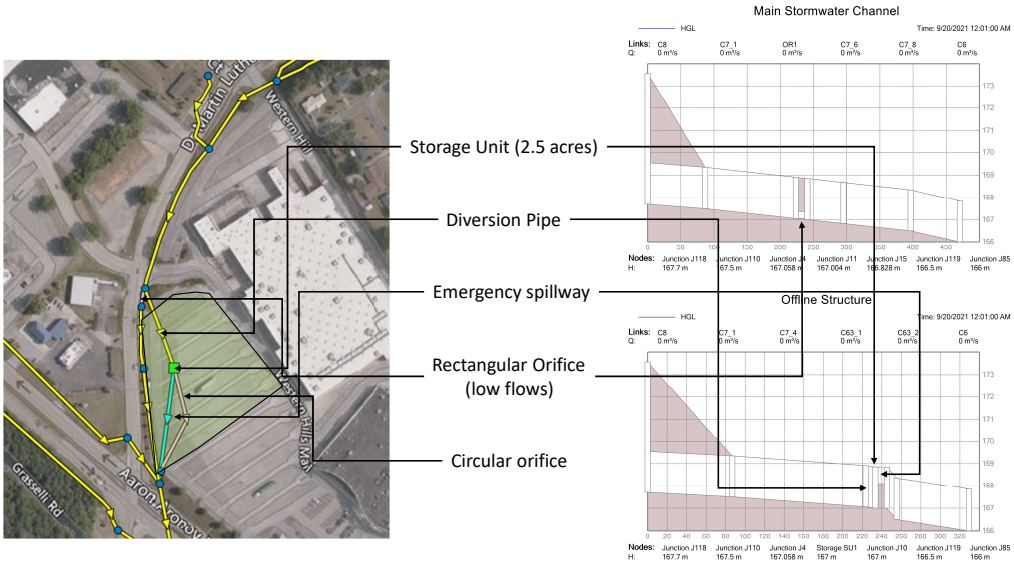

Figure 5.4: Midfield storage unit with 2.5 acres location and schematics.

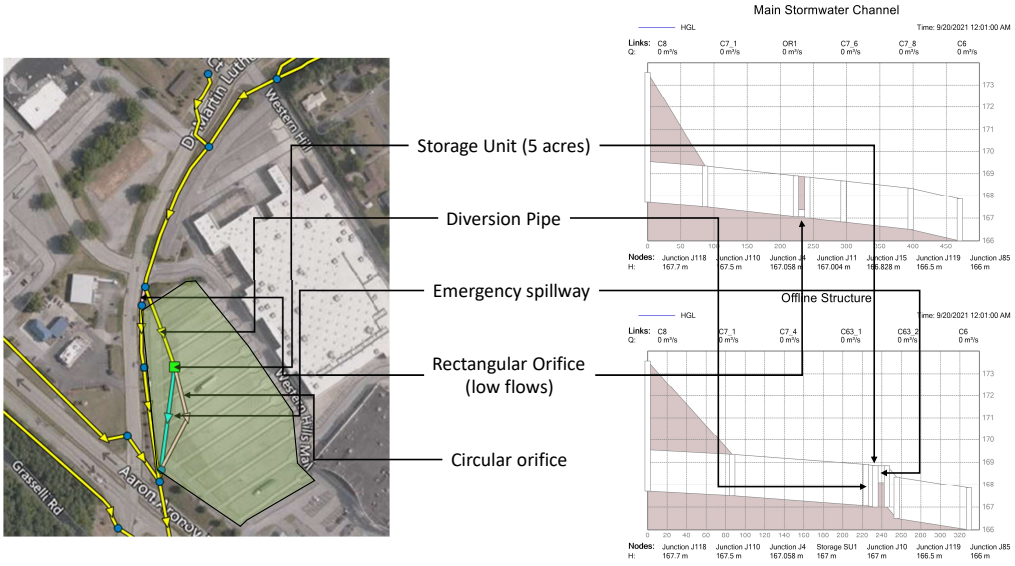

Figure 5.5: Midfield storage unit with 5 acres location and schematics.

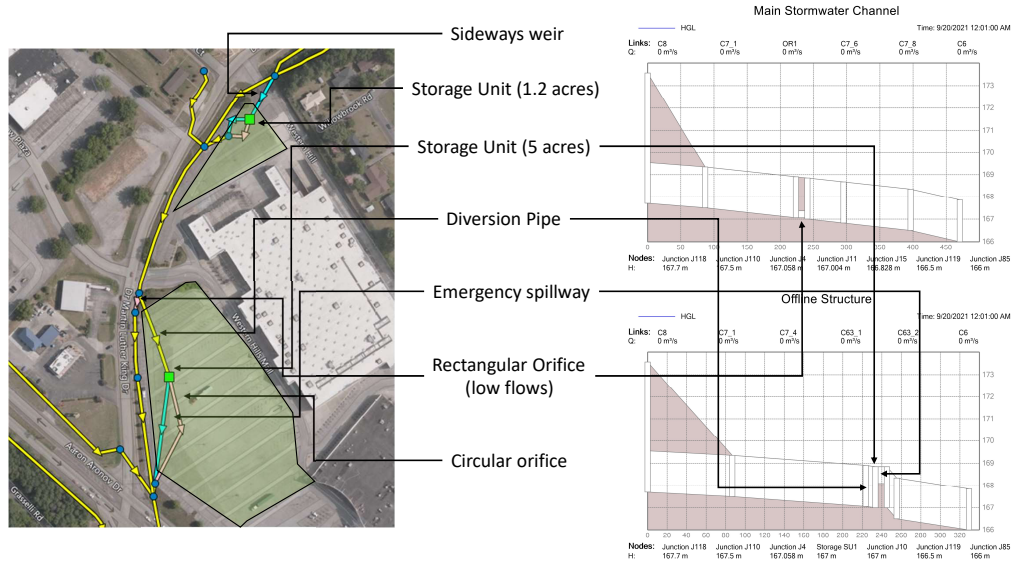

Figure 5.6: Midfield storage unit with 6.2 acres location and schematics.

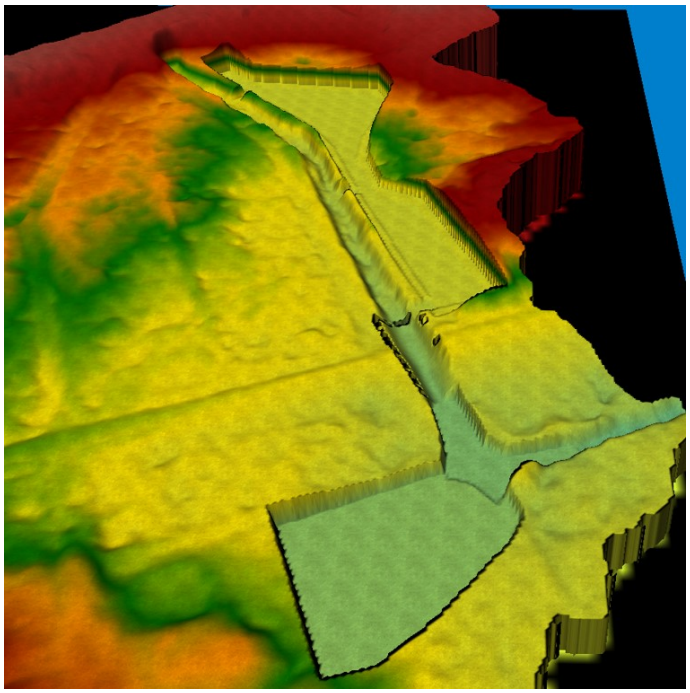

Figure 5.7: Midfield detention ponds location and schematics.

Four conceptual approaches were proposed for mitigating the flooding in Brighton area. First, three storage units, referred as Up, Mid, and Down, upstream the flooding area were suggested, all of those not located in private properties. Figure 5.8 shows the locations of these storage units at the upstream regions of the watershed as well as an example of the storage unit conceptual schematics. All three storage units had the same area but different areas were evaluated: 2.5 acres, 1.85 acres, and 1.25 acres. Then, a last approach was proposed with two storage units upstream, one with an area of 5 acres, at the same location of the Mid storage unit, and other with an area of 1 acre, between Down and Mid storage units (not shown in Figure 5.8).

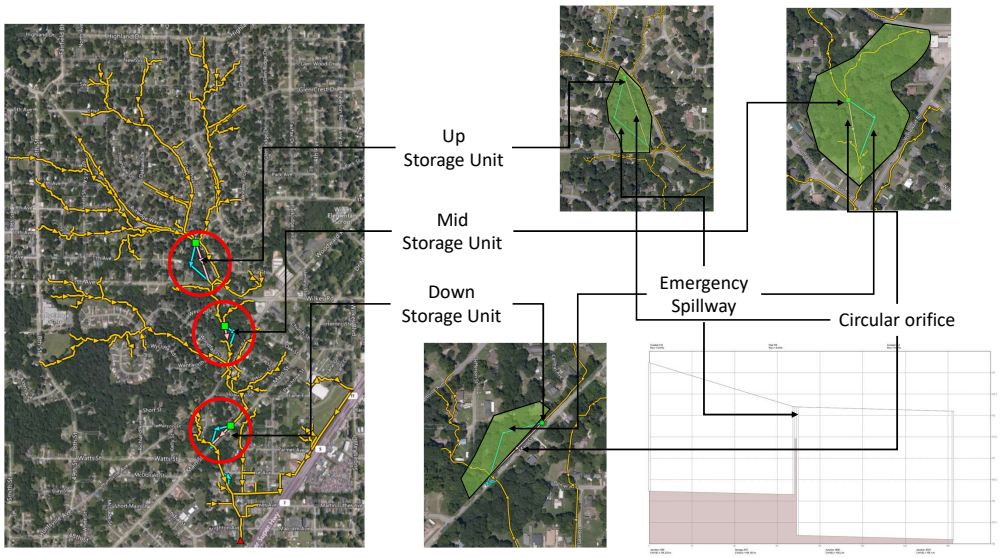

Figure 5.8: Brighton storage units locations schematics.

5.3 Results

5.3.1 Hydrological modeling

Figure 5.9 shows the calibration performed at Midfield. The upper portion of the figure shows the rainfall data over the period of data collection and the lower portion of the figure shows the observed water depth versus the simulated water depth at the bridge where the sensor was deployed. Nash–Sutcliff efficiency and R^2 were, respectively, 0.3 and 0.5. It is important to highlight that the peak levels were very close but the recession limb had a significant disagreement between the simulated and observed data. It is hypothesized that this disagreement comes from the groundwater contribution to the channel. However, since the peaks are more relevant for a flooding analysis than the recession limb, and given the lack of available information and the short period of data collection, the results can be considered adequate with the goal of studying peak flows and flooding.

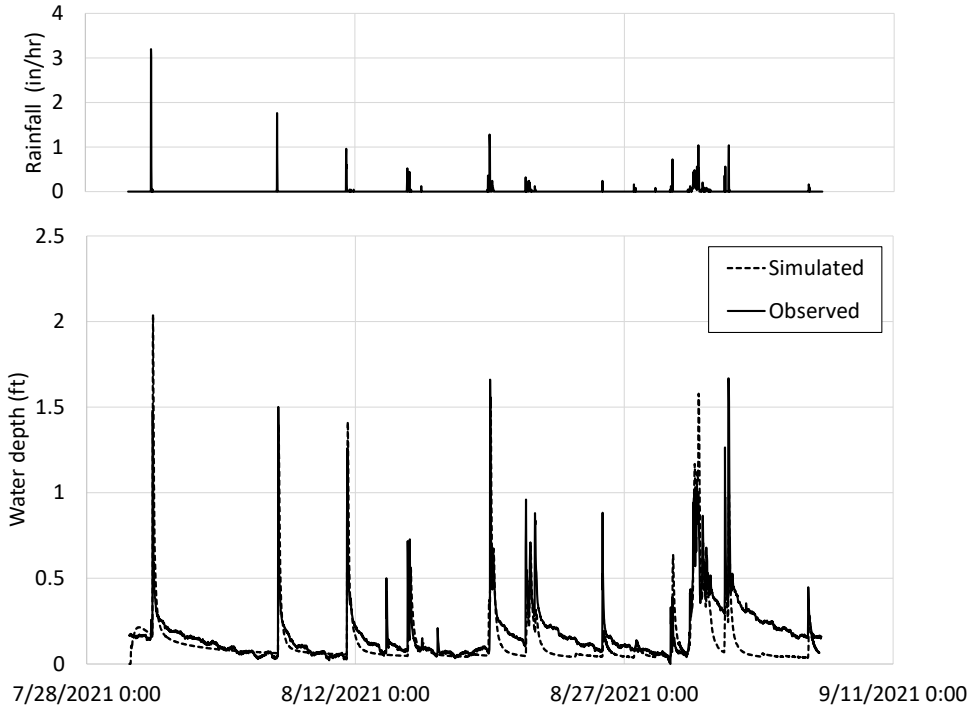

Figure 5.9: Midfield calibration results.

The selected rain events were simulated using the calibrated PCSWMM model and their results are shown in Figure 5.10. This figure shows the flow rate that is being discharged on the unpstream area where the flooding is being reported, considering all rainfall scenarios. Graph A present results for the 10-years, graph B presents results for the 5-years, and graph C presents results for the 1-year rain events. In these graphs, it is possible to notice that the peak level was significant reduced when the proposed conceptual approaches were employed, specially the 6.2 and 5 acres storage units. Moreover, the rising limb is basically the same for the three rain events because of the online rectangular orifice. When the water starts to diverge to the storage unit, the differences become noticeable.

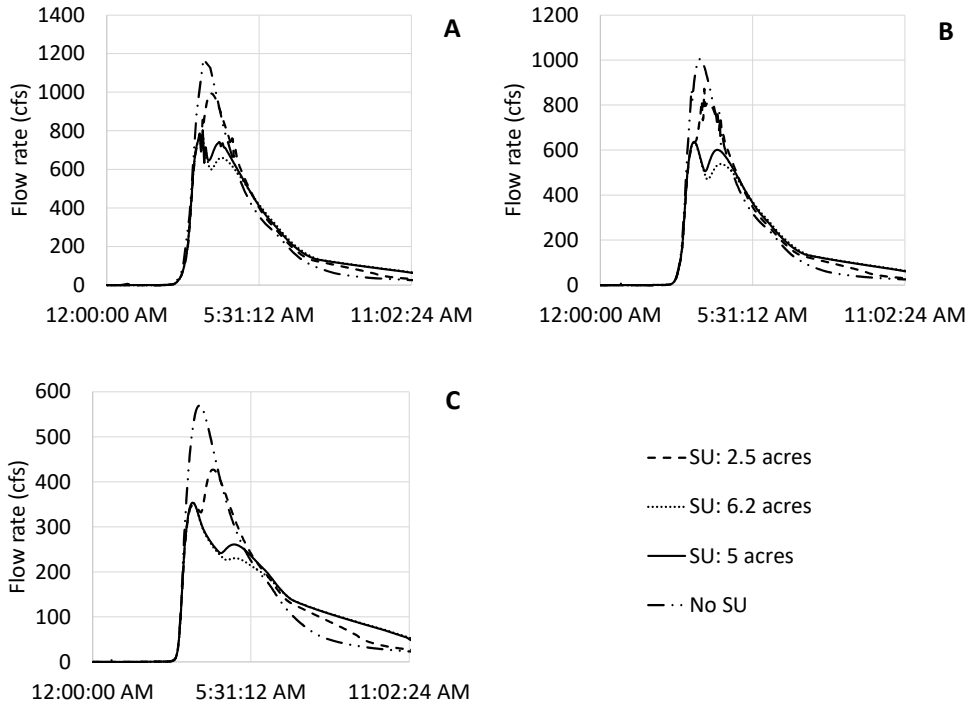

Figure 5.10: Midfield inflows considering all rainfall scenarios along with the proposed conceptual approaches: (A) is the 10-years, (B) is the 5-years, and (C) is the 1-year.

Since the pressure sensor was lost in Brighton, it was not possible to perform a local calibration for the watershed. However, Midfield and Brighton watersheds are close and their general characteristics are assumed to be similar. Therefore, the same Midfield calibration parameters were assumed in Brighton. Figure 5.11 shows the flow rate that is being discharged upstream the area where the flooding is being reported. As in the previous figure, the rain events are shown in the graphs A, B, and C. The proposed conceptual approaches not only reduced the peak levels but also delayed the rising limb since the storage units are located online.

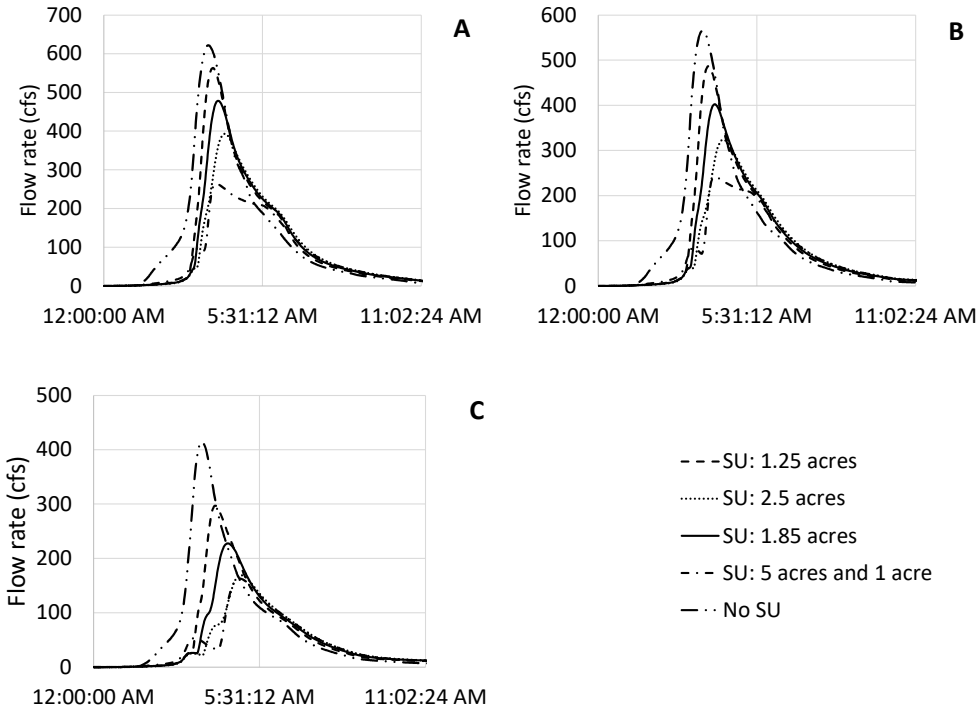

Figure 5.11: Brighton inflows considering all rainfall scenarios along with the proposed conceptual approaches: (A) is the 10-years, (B) is the 5-years, and (C) is the 1-year.

5.3.2 Flooding extent mapping

In Midfield, the flooding results were being reported between the two bridges on the downstream region of the watershed. The upstream bridge is where the pressure sensor was deployed and the downstream bridge is located around 885 ft downstream. The flooding starts at the bridge located downstream and Figure 5.12 shows the results for all scenarios and all proposed conceptual approaches at this specific location. Park is when the two detention ponds downstream are employed. The bridge high chord is located 4.45 ft measured from the bottom of the channel. For the 1-year rain event, only the two scenarios without any upstream hydraulic structure overtops the bridge high chord. For the 5 and 10-years rain events, considering all scenarios, there is overtopping but the water depth is significantly reduced when the hydraulic structures are employed, both upstream and at the flooding areas.

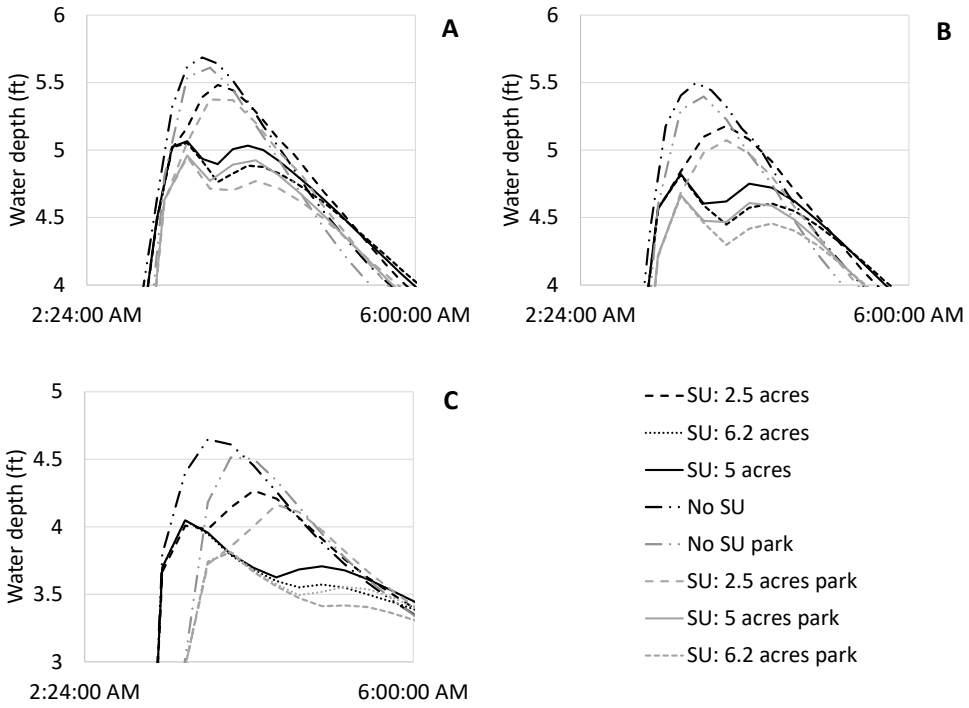

Figure 5.12: Midfield water depth at downstream bridge considering all rainfall scenarios along with the proposed conceptual approaches: (A) is the 10-years, (B) is the 5-years, and (C) is the 1-year.

Figure 5.13 shows the simulated flooding considering each scenario analyzed for the 1-year rainfall event. Based on this figure, the following results were obtained:

- The flooded area was reduced by 43% when the 5 acres and 6.2 acres storage units were employed and by 24% when the smaller storage unit is employed.
- When the two detention ponds (park) are employed at the downstream, the flood extent reduction is estimated at 54% for the 5 acres and 6.2 acres, and 47% for the 2.5 acres
- When no upstream hydraulic structure is adopted and only the two detention ponds (park) are employed at the downstream, the flood extent reduction is estimated at 29%.

Figure 5.14 shows the simulated flooding extent considering each scenario analyzed for the 5-year rainfall event. In this case, the flooded area is not so significantly reduced as the 1-year rain event, but the following results were obtained:

- The 5 acres and 6.2 acres storage units reduced the flooded area by around 31% while the 2.5 acres storage unit reduced the flooded area by only 13%
- When the two detention ponds (park) are employed at the downstream, the reduction is around 51.5% for the 5 acres and 6.2 acres storage units and 40% for the 2.5 acres storage unit.
- When no upstream hydraulic structure is adopted and only the two detention ponds (park) are employed at the downstream, the flood extent reduction is estimated at 29%.

Figure 5.15 shows the simulated flooding considering each scenario analyzed for the 10-year rainfall event. As in the 5-years rain event, the two largest storage units reduced more the flooded area when compared to the smallest storage unit. The following results were obtained:

- The flooded area reduction was 25% for the 5 acres and 6.2 acres storage units and only 10% for the 2.5 acres storage unit.
- When the two detention ponds (park) are employed at the downstream, the reduction was 48.5% for the two largest storage units and 36% for the 2.5 acres.
- When no upstream hydraulic structure is adopted and only the two detention ponds (park) are employed at the downstream, the flood extent reduction is estimated at 28%.

The flooded area in Brighton was not so significantly reduced when the storage units at the upstream areas were employed. This is noticeable in Figures 5.16, 5.17, and 5.18. Figure 5.16 indicates that the flooded area for 1-year, Figure 5.17 for 5-years, and Figure 5.18 for 10-years rain events. However, significant changes were noticed in the flooded depth in the impacted areas as well as the duration of the flooding event. It is important to highlight that Figures 5.16, 5.17, and 5.18 show the moment of the maximum flooding extent.

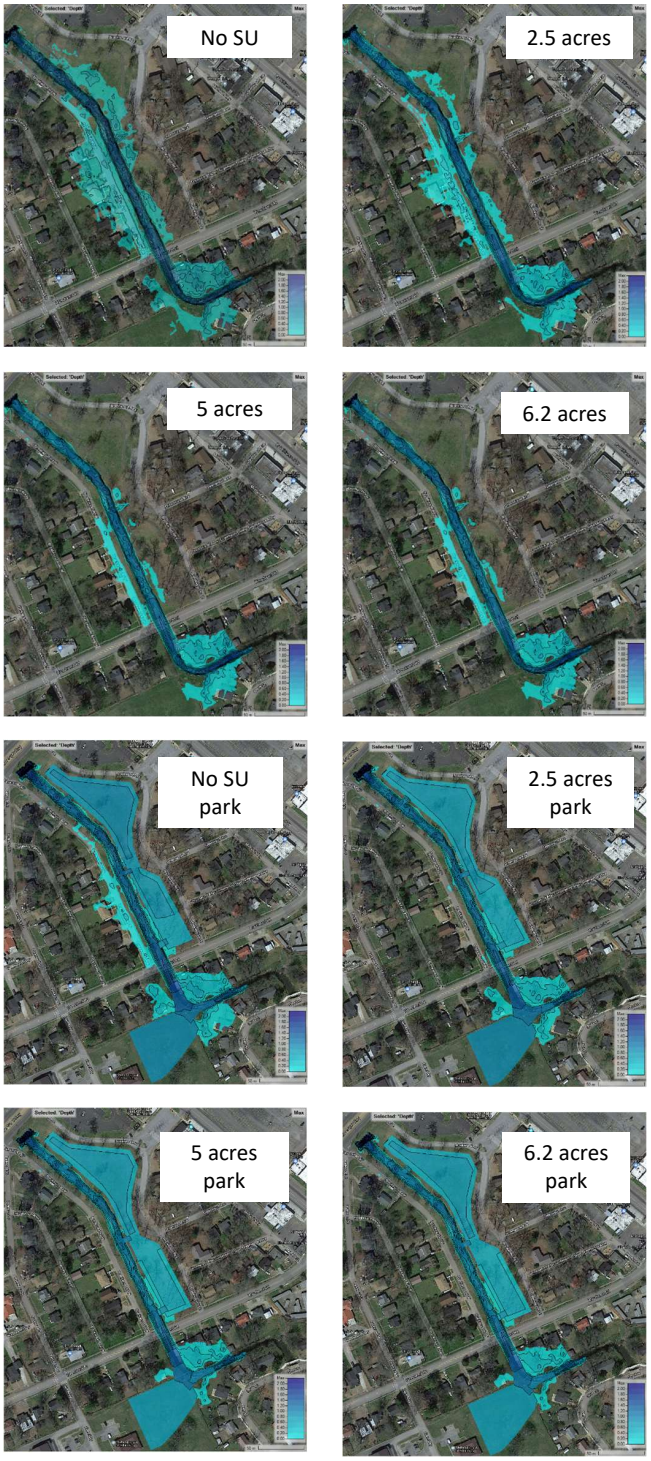

Figure 5.13: Midfield flood 1-year flood with proposed conceptual approaches.

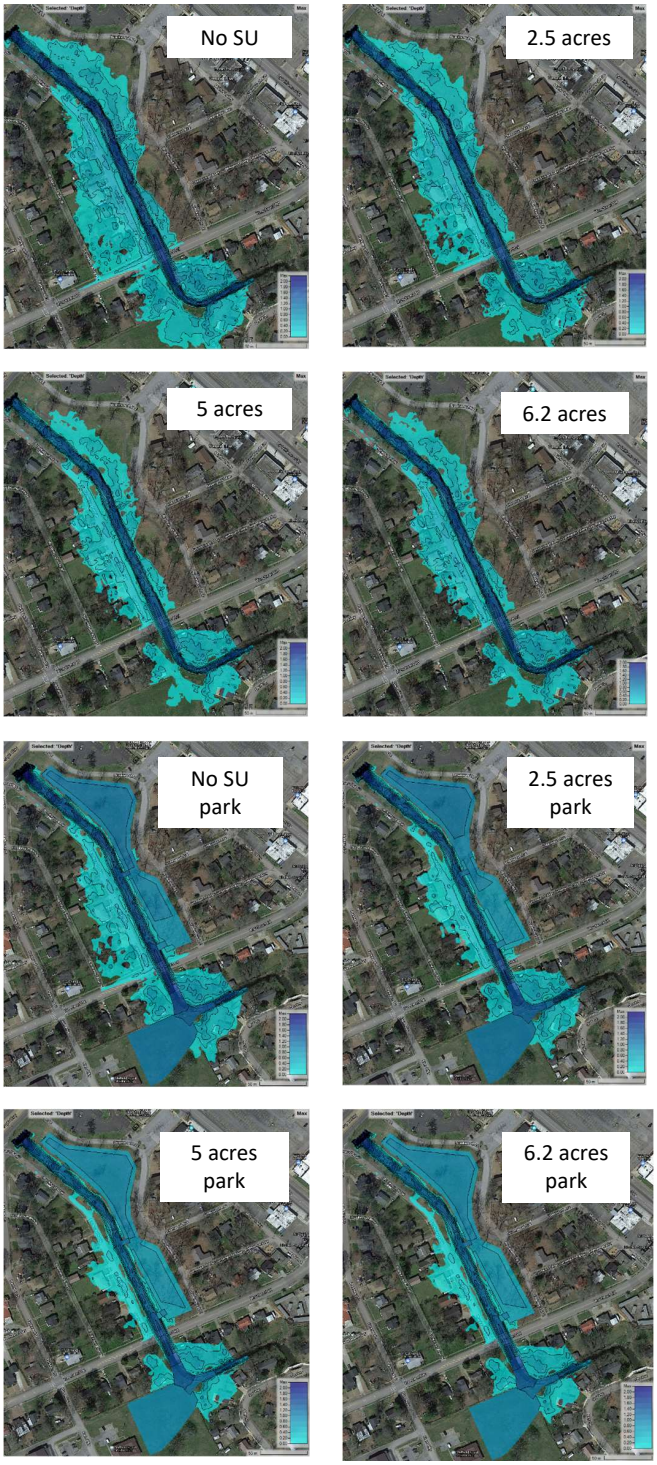

Figure 5.14: Midfield 5-year flooding with proposed conceptual approaches.

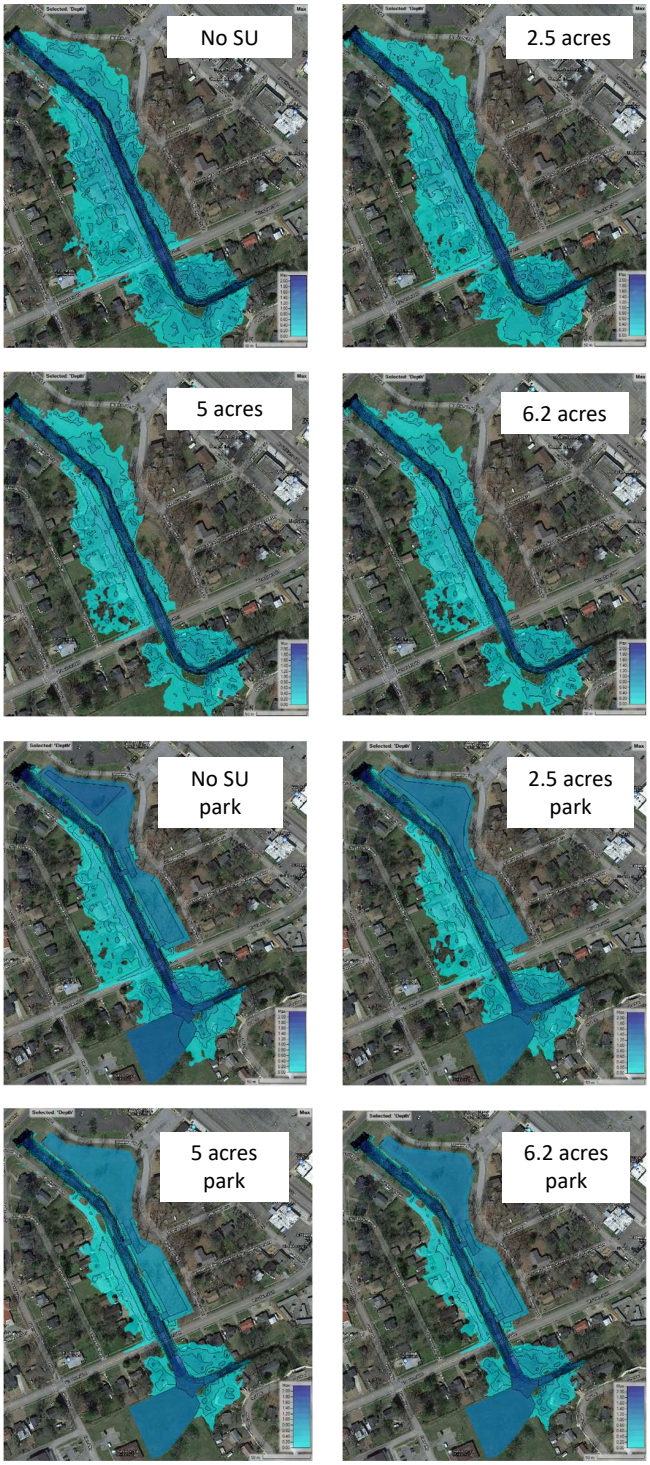

Figure 5.15: Midfield 10-year flooding with proposed conceptual approaches.

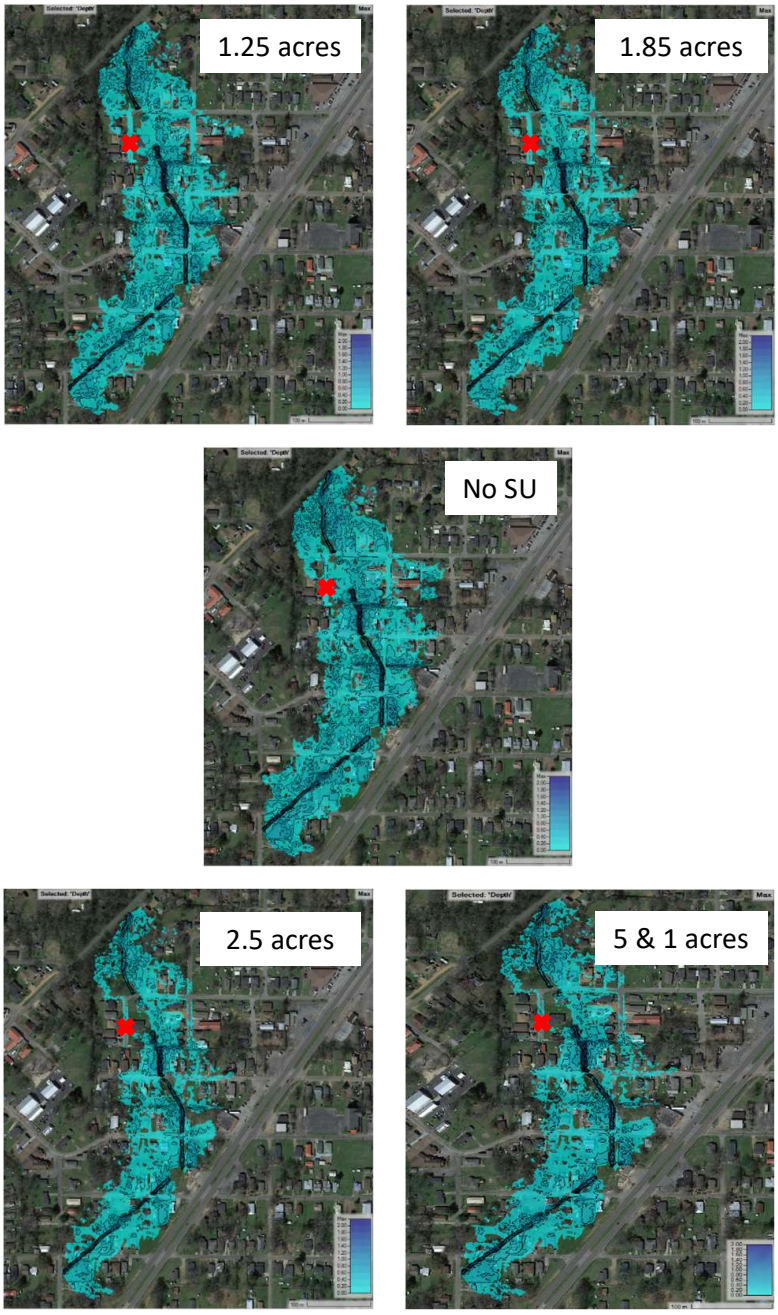

Figure 5.16: Brighton 1-year flooding with proposed conceptual approaches.

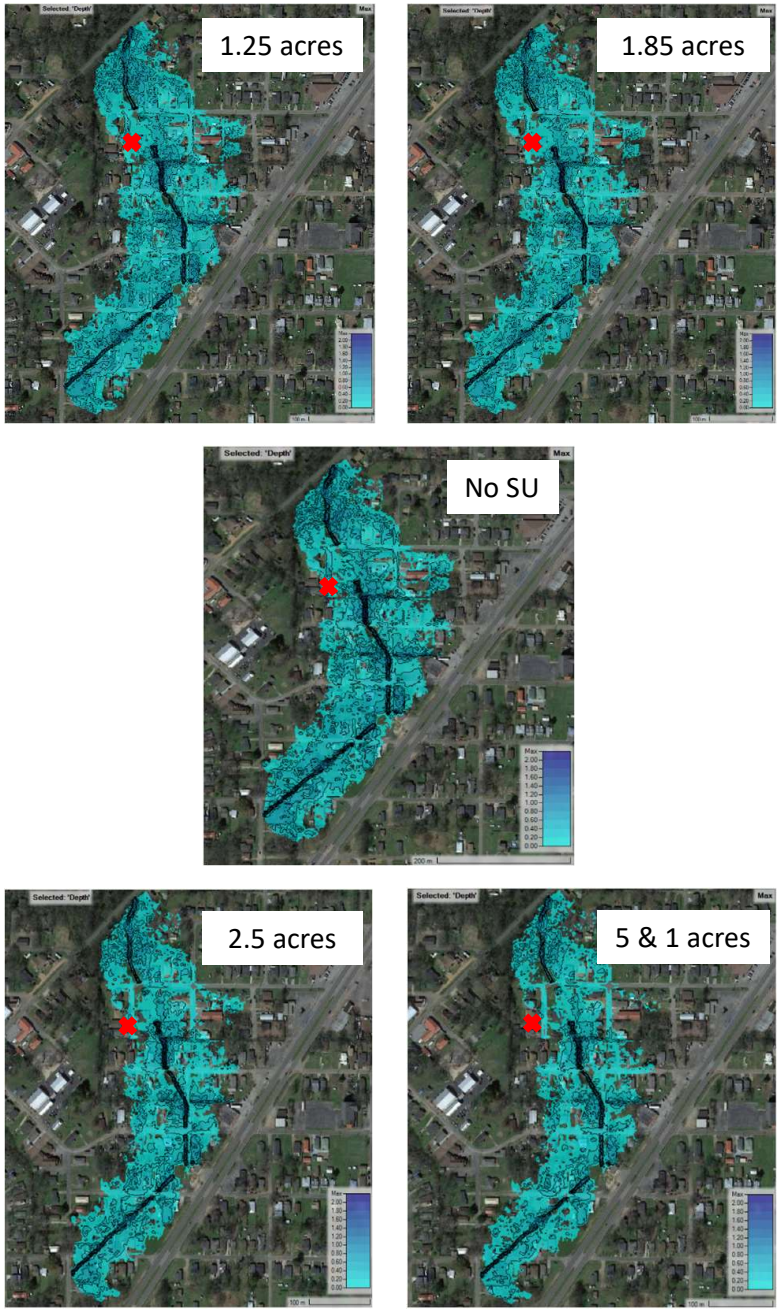

Figure 5.17: Brighton 5-year flooding with proposed conceptual approaches.

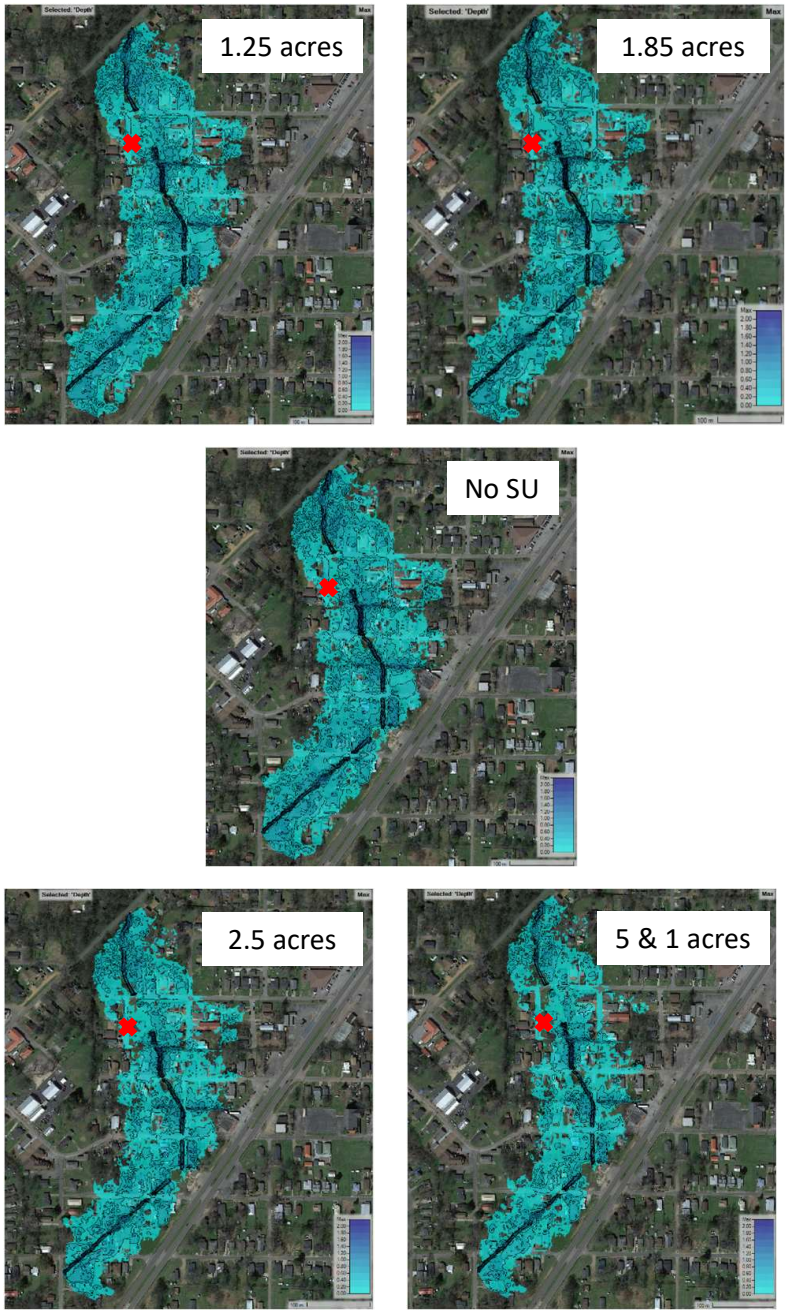

Figure 5.18: Brighton 10-year flooding with proposed conceptual approaches.

Figure 5.19 presents the water depth variation over time at the locations marked with a red cross in Figures 5.16, 5.17, and 5.18. Graph A shows the 10-years, graph B shows the 5-years, and graph C shows the 1-year rain events. It is possible to notice that employing the

three storage units as well as only the two storage units upstream not only decreased the water depth but also reduced the duration of the flooding. Also, employing the three 2.5 acres storage units reduced the flooding effects of a 10-years rain event to a 1-year rain event and the two storage units upstream decreased even more the flooding effects.

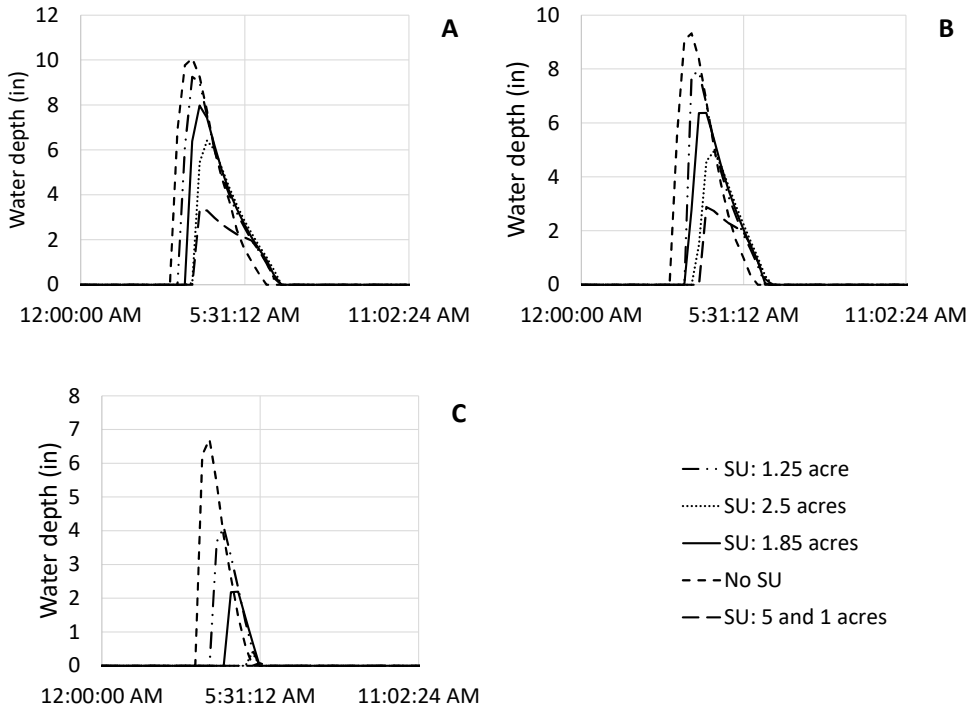

Figure 5.19: Brighton water depth at the street considering all rainfall scenarios along with the proposed conceptual approaches: (A) is the 10-years, (B) is the 5-years, and (C) is the 1-year.

5.4 Conclusions

Two urban communities, Midfield and Brighton, AL, have been experiencing events of flooding at selected locations. This chapter explored the causes for these flooding events and also proposed conceptual alternatives to mitigate this problem. The methodology employed considered a 1D modeling strategy to estimate the flow rate at the upstream regions of the reported flooding events and a 2D modeling strategy to estimate the flooded areas where flooding events were reported.

The hydrological calibration was performed using 1D PCSWMM model in Midfield. The calibration was successful to represent peak flows but was less successful in representing the recession limbs. However, this is not considered critical for the representation of flooding processes. The same calibrated parameters used in Midfield were assumed in Brighton. 1-year, 5-years, and 10-years design rainfalls were employed to evaluate the flooding extent. Extensive inundation areas were indicated by the 2D model for the design rainfalls, but most with flooding depths within a few inches.

In Midfield, three conceptual approaches at upstream regions of the watershed as well as two detention ponds at the flooding areas were evaluated using three design rainfalls, for a total of 24 simulation scenarios. First, it was considered a storage unit with an area of 2.5 acres, then a storage unit with an area of 5 acres, and finally two storage units with an area of 5 acres and 1.25 acres. Additionally to these conceptual approaches, two detention ponds with a total area of 2.6 acres were evaluated. Based on the results obtained by modeling efforts, the two largest storage units reduced the flooded area by the same amount and the detention ponds aided in flooding reduction as well. Therefore, it might be more attractive to employ the storage unit in the range of 5 acres and the two downstream detention ponds.

In Brighton, four scenarios were also studied, resulting in a total of 15 simulations. The first three scenarios considered three storage units at upstream regions of the watershed with varying areas and the fourth scenario considered two storage units also in the upstream regions of the watershed. The first scenario considered an area of 1.25 acres, the second scenario considered an area of 1.85 acres, the third scenario considered an area of 2.5 acres, and the fourth scenario considered one storage unit with an area of 5 acres and other storage unit with an area of 1 acre. Based on the obtained results, the fourth scenario was the most effective in reducing flooding depth and duration. Therefore, this alternative might be the most suitable to mitigate the flooding issues that were studied here for Brighton.

In summary, these simulation results were supported by a relative short calibration effort, but nevertheless it is hoped that they can help in future actions to support flooding control in the studied areas.

Chapter 6

Multiphase rapid filling conditions of tunnel system in Columbus, Ohio[†]

Abstract - The City of Columbus, Ohio is implementing a tunnel system to reduce the number of episodes of combined sewer overflows into the Scioto River. The tunnel systems provide relief to the existing Olentangy Scioto Interceptor Sewer. Two new tunnels being implemented are the OSIS Augmentation and Relief Sewer (OARS), in service since July 2017, and the Lower Olentangy Tunnel (LOT) that is planned to be in service in 2025. The performance of these tunnels in respect to high inflow conditions was investigated with the use of the HAST mixed flow model and the OpenFOAM CFD model to determine the magnitude of surges, the possibility of air pocket entrapment, air–water surging, and the consequences of uncontrolled air pocket releases through shafts. Inflows into the systems were obtained from a calibrated collection system SWMM model. Modeling results quantified surging in the tunnel dropshafts and their mitigation from built-in surge control chambers. HAST simulations also pointed to locations where air pockets could form. These results were used in OpenFOAM to determine the effects of uncontrolled air release through the shaft that links the two tunnels. It was shown that proper ventilation at the shaft will mitigate the growth of air phase pressure to damaging levels.

6.1 Introduction and objectives

Stormwater management is a very complex task in highly urbanized areas and involves a combination of draining excess runoff efficiently while minimizing environmental impacts to the

[†]**Accepted for publication in**: Vasconcelos, J. G., Gheith, H., Pachaly, R. L., Abdel-Latif, M., & Herr, R. (2021) Multiphase Rapid Filling Conditions of Tunnel System in Columbus, Ohio. *Journal of Water Management Modeling*

receiving water bodies. Such a task is more complex when storm sewers and wastewater sewers are combined in the same system. Around 860 municipalities in the United States have combined systems (EPA, 2020a), and during intense rain events episodes of discharge of combined sewage in waterbodies occur that increase the severity of the environmental impacts.

The City of Columbus, Ohio is one municipality that operates combined sewer systems, and it is implementing a long term control plan to reduce the frequency of CSO discharges into the Scioto River. A key component of Columbus infrastructure is the Olentangy sewer interceptor system (OSIS). Given the limited availability of storage at grade level, OSIS storage is augmented using the OSIS augmentation and relief system (OARS) and the Lower Olentangy tunnel (LOT) to reduce the frequency of CSO episodes. With these tunnels systems, the City of Columbus aims to prevent two billion gallons (910 ha m) of combined sewage from reaching the Scioto River without treatment (Pratt, 2019).

While deep tunnel systems are a technically sound approach to manage large flows in highly urbanized areas, there are some design concerns over their implementation. Since the implementation of these tunnels in the late 1970s and 1980s, researchers have pointed to potential problems linked to surging in these systems (Guo & Song, 1990; Song et al., 1983). More recent research has also recognized the important role of the entrapped air phase within conduits, such as in air–water surging (Vasconcelos & Leite, 2012; Zhou et al., 2002).

Much is still unknown with regards to air–water interactions in stormwater systems. There are various uncertainties with regards to the mechanisms for air pocket formation in closed conduits (Schulz et al., 2020; Vasconcelos & Wright, 2006). Once entrapped, the fate of air pockets is still largely unknown. One hypothesis has been to assume that entrapped air pockets move in closed conduits as discrete gravity currents (Chosie et al., 2014; Hatcher & Vasconcelos, 2014). Upon reaching vertical shafts and other ventilation points, air will be released in an uncontrolled fashion, potentially leading to structural damage (Zhou et al., 2002), geysering episodes (Muller et al., 2017; Vasconcelos & Wright, 2011; Wright et al., 2011) and slab or access cover displacement (Wang & Vasconcelos, 2020).

Few numerical models able to simulate rapid filling in stormwater tunnel systems have explicitly incorporated air–water interactions, and this has significantly affected overall model

accuracy (Vasconcelos et al., 2015). Considering all these aspects, the simulation of the rapid filling conditions in the OSIS–OARS–LOT system, which is summarized in this paper, used state-of-the-art methodology. First, a 1D model able to track air pocket motion was used to predict the potential regions of air pockets formations within the system. Then, facing the insufficient capability of these models to simulate multiphase air pockets discharge through vertical structures, a 3D model was used for predicting the pressure variations within these structures. The reason for a limited usage of 3D model is that, to date, it is computationally infeasible to use a 3D model in system-wide applications. Therefore, this sequential application of 1D and 3D models combines a reasonable approach to identify pocket formation and anticipating potential issues associated with the uncontrolled air release in complex structures.

6.2 Methodology

6.2.1 Geometry of OSIS-OARS-LOT tunnel system

The connections between OSIS and OARS and LOT are through several dropshaft structures as the tunnels are deep underground. In 2020, the connection between OARS and OSIS was made through three dropshafts at locations referred to as shafts 4, 5 and 6. A future drop shaft connection (shaft 3) is scheduled to be in service by the year 2025. When LOT is in service, by 2025, OSIS will connect with LOT at three dropshafts known as the Tuttle, Gowdy and Vine shafts. Vine shaft is also connected with OARS at the shaft 6 dropshaft through a 3.66 m diameter connector. The schematics of these tunnels are presented in Figure 6.1.

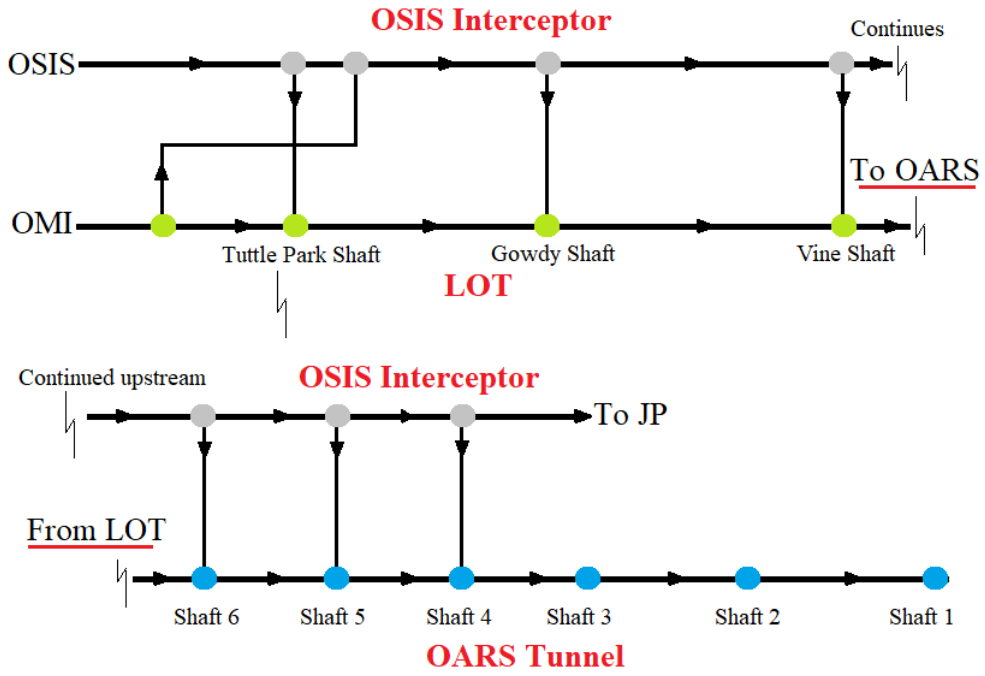

Figure 6.1: Schematic of OARS and LOT tunnel systems and their points of connection with OSIS.

Most of OSIS is of circular cross section that varies from 3.1 m to 3.6 m in diameter, transiting to a 3.2 m × 4.2 m rectangular cross section toward the downstream end of the combined flow portion. The cross section of OARS is also circular, with a much larger diameter of 6.10 m through the entire extension of 7.05 km. The LOT cross section is circular, with a diameter of 3.66 m and length of 5.12 km. Detailed geometry of OARS shaft 6 and the LOT Vine shaft are presented here as it is relevant to the CFD modeling component of this study. Geometry from remaining junctions are not included here for brevity.

Shaft 6, shown in Figure 6.2, is a large structure with 18.4 m diameter located at the upstream end of OARS. It serves four different purposes: inflow admission through an approaching channel and a 4.9 m diameter vortex structure; air ventilation through a 6.10 m diameter vertical shaft; surge relief through a built-in overflow chamber with area 270 m^2; and a near-future connection with the LOT system.

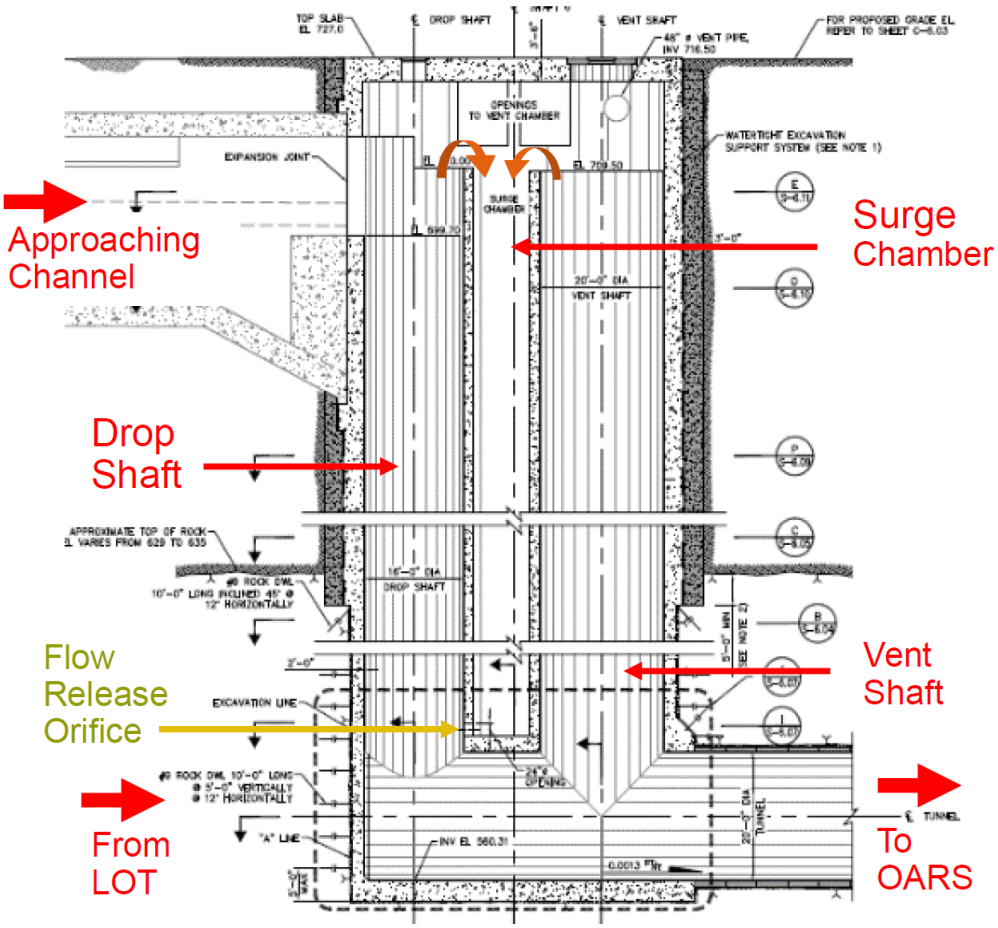

Figure 6.2: Schematic of OARS shaft 6, including the dropshaft, surge chamber, ventilation shaft and future connection to LOT.

Vine shaft, presented in Figure 6.3, has a 33.5 m deep lower shaft with a diameter of 7.6 m, which is divided between a baffled shaft to dissipate inflow energy and a ventilation shaft for air discharge. The upper portion of Vine shaft is 21.3 m high and has a 15.2 m diameter. It is fitted with control gates to regulate inflows from LOT into OARS, and a flap gate to prevent backflow from OARS into LOT.

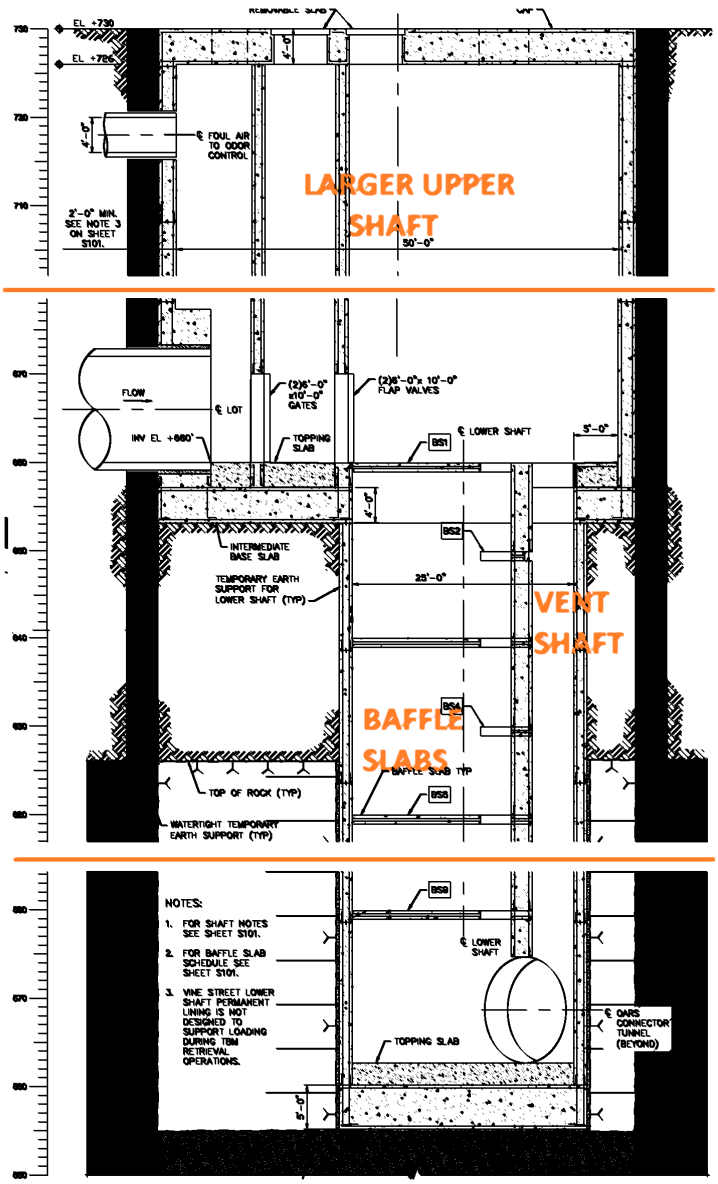

Figure 6.3: Schematic of Vine shaft in the downstream end of LOT and its downstream connection to OARS.

Numerical simulation

OSIS–OARS–LOT performance was evaluated using 1D system-wide modeling and 3D computational fluid dynamics (CFD) modeling of Vine shaft. The former used the Hydraulic Analysis of Stormwater Tunnels (HAST) model, which is based on the solution of the Saint-Venant equations. The main features of the numerical solution used in HAST are:

1. The use of a nonlinear numerical scheme based on the Roe scheme, as presented in Macchione and Morelli (2003), renders a robust and accurate solution even with low local Courant numbers, which is typical for flow regime transition conditions.

2. Enabling the Saint-Venant equations to represent both free surface and pressurized regimes, through application of the two-component pressure approach (Vasconcelos et al., 2006).

3. Explicit treatment of regions where air pockets appear in closed conduits, tracking compression and expansion processes, spreading, motion and release through junctions.

4. Representation of the unique geometric characteristics of junctions in the tunnels through construction of custom boundary conditions in the model as required.

To date, most mixed flow models do not explicitly track the formation and interactions of the air phase in closed conduits. As we show in this work, this feature was very important in determining potential adverse air–water interactions within the tunnels. The mathematical implementation of the model can be found in Vasconcelos et al. (2015). For OSIS–OARS–LOT modeling, 59 junctions were represented in the model, with 63 reaches, totaling 26.5 km of conduits. The initial conditions of the simulation considered the tunnel initially empty, and inflow hydrographs were admitted at selected locations according to the results of surface hydrological modeling. Each junction in the system was represented through specific boundary conditions. These boundary conditions apply equations that include mass and energy balance, characteristic equations, and empirically-derived rating curves. An in-depth discussion of these boundary conditions is outside of the scope of this work. After discretization, 4,127 computational cells were used in the model, with time steps in the order of few milliseconds once the pressurization conditions developed.

A CFD tool was used to describe the effects of a potential air pocket release through Vine shaft from OARS into LOT. Since the work of Choi et al. (2014), there have been many subsequent studies using relatively simple geometries, such as Muller et al. (2017) and Qian et al. (2020). However, results in these more fundamental studies are difficult to generalize for physical shaft geometries such as Vine shaft. This motivated the development of a CFD model to assess the effects of air release through that structure.

The CFD model was developed using OpenFOAM, an open source C++ object-oriented library that can perform multiphase flow simulation. In this application, Navier–Stokes equations were solved, tracking the free surface in using the volume of fluid (VOF) method (Hirt & Nichols, 1981). There are various multiphase flow solvers within OpenFOAM, and here the continuity, momentum, and energy equations were solved using the *compressibleInterFoam* solver (Svenungsson, 2016). Equations 6.1a, 6.1b and 6.1c present the two-phase continuity, momentum, and energy expressions solved in OpenFOAM. Equation 6.1d is used to track the free surface and is modified to reduce issues associated with the convection of a step function.

$$\frac{\partial \rho}{\partial t} = \bigtriangledown \cdot (\rho U) = 0 \tag{6.1a}$$

$$\frac{\partial (\rho U)}{\partial t} + \bigtriangledown \cdot (\rho U U) = - \bigtriangledown p + \bigtriangledown \cdot (\mu \bigtriangledown U) + S_U \tag{6.1b}$$

$$\frac{\partial (\rho C_p T)}{\partial t} + \bigtriangledown \cdot (\rho U C_p T) = \bigtriangledown \cdot (k \bigtriangledown T) + S_T \tag{6.1c}$$

$$\frac{\partial \alpha}{\partial t} + \bigtriangledown \cdot (\alpha U) + \bigtriangledown \cdot ((1 - \alpha) \alpha U r) = 0 \tag{6.1d}$$

where:

r = fluid density,

t = time,

U = 3D velocity vector,

p = pressure,

μ = dynamic viscosity,

S_U = momentum source term,

C_p = specific heat,

T = temperature,

S_T = energy source term,

α = volume fraction ($0 \leq \alpha \leq 1$), and

U_r = velocity field to compress the interface.

In the CFD formulation, the values of α represent the liquid fraction within a cell, with unity representing pure water and zero pure air. The velocity field U_r is included to counter a

disadvantage of VOF in solving for the free surface that is related to interface smearing near the free surface, as described by Rusche (2003). Turbulence was represented initially in this research using a $k - \epsilon$ model but subsequently a $k - \omega$ SST model was used.

Mesh generation was completed using the *snappyHexMesh* utility supplied by OpenFOAM. This tool generates 3D meshes that are in the stereolithography (STL) or wavefront object (OBJ) format from triangular surface geometries (Greenshields et al., 2015). Since different geometries were evaluated, mesh details will be further discussed in section 4, OpenFOAM modeling results. CFD modeling was performed in different stages, which varied according to the volume of air released in the tunnel–shaft system, initial water volume, or ventilation. These values were selected with the intention of representing different scenarios ranging from less critical (e.g. 12.5 m of water level and 209 m^3 of air volume) to highly critical (e.g. 35 m of water level and 576 m^3 of air volume) in regions where the HAST model predicted a tendency for formation of air pockets. A total of 14 simulation conditions were tested, and these are presented in Table 6.1.

Table 6.1: CFD study variables and ranges of variation.

Variable	**Range of variation considered in the modeling**
Initial water level (m)	12.5, 25.0 and 35.0
Ventilation conditions	Ideal ventilation, fully blocked, 2 ports 2.4 m × 2.4 m
Initial air volume in system	Various, ranging from 209 m^3 to 576 m^3
Turbulence model	$k - \epsilon$ model but subsequently the $k - \omega$ SST model
Number of computational cells in CFD model	Up to 5.09 million

For various system-wide 1D rapid filling simulations performed with HAST, we noticed a tendency for air pocket formation in the tunnel reaches between shaft 5 and shaft 6. Given the slope of the tunnel and that there is no route for air escape in shaft 6, entrapped air pockets in this region are likely to be discharged through the 6.1 m diameter ventilation shaft of shaft 6. Muller et al. (2017) demonstrated using CFD that it is possible that, even with such large ventilation, there was a residual volume of air that could not be ventilated in the shaft and remained in the system. In the present case, this air could be routed through the connection between OARS and LOT and through Vine shaft, as illustrated in Figure 6.4.

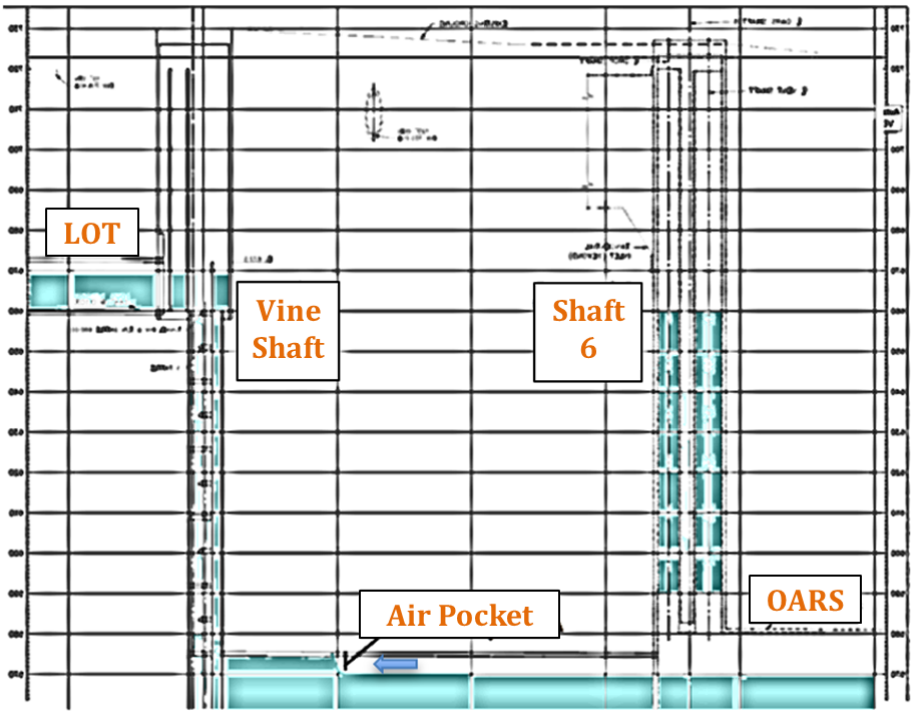

Figure 6.4: Potential air pocket entrapment in OARS and release of a fraction of the air pocket in Vine shaft.

6.3 HAST modeling results

Inflows used in the HAST modeling were obtained through a calibrated SWMM model with a time series spanning 20 years. The City of Columbus model was recently updated using the innovative Model at the Source approach (Gheith, 2014; Herr & Gheith, 2015), which leads to a high quality flow prediction compared to observed data. Inflows from 10 rain events were selected based on the flows that were most likely to generate the strongest surges. According to Vasconcelos and Wright (2017), such conditions are expected when inflows are highest while horizontal storage in tunnels is depleted (i.e. full pressurization of horizontal reaches). Table 6.2 lists the events in a ranked order based on higher to lower inflows that were modeled in HAST based on the summation of inflows at the time when the tunnel reaches were pressurized. The normalized value for the tunnel system diameter of 3.85 m was computed using the diameters DR and lengths LR of each tunnel reach through Equation 6.2:

$$D = \sum(L_R D_R) / \sum L_R \tag{6.2}$$

Table 6.2: Rank of inflow events from OSIS to OARS and LOT when pressurization of the tunnel reaches occurred.

Rank	**Date**	**Q inflow (Qi) at pressurization (m^3/s)**	**Normalized Qi = Qi/(gD^5)$^{0.5}$**
1	2003-08-30	59.8	0.66
2	2009-08-28	56.1	0.62
3	2004-06-11	37.3	0.41
4	2005-01-11	30.1	0.33
5	1997-05-13	25.7	0.28
6	2000-01-03	24.5	0.27
7	1998-12-21	22.6	0.25
8	2004-01-03	18.5	0.20
9	2011-12-05	14.6	0.16
10	1995-01-15	13.6	0.15

In the early stages of a storm event, OSIS begins to fill before flows start to divert into OARS and LOT over relief weirs located upstream of the dropshafts. In normal conditions, as OARS is filling, the reaches between the downstream end and shaft 6 become pressurized. Typically, the upstream end of OARS at shaft 6 is the last portion to undergo pressurization, as illustrated in Figure 6.5.

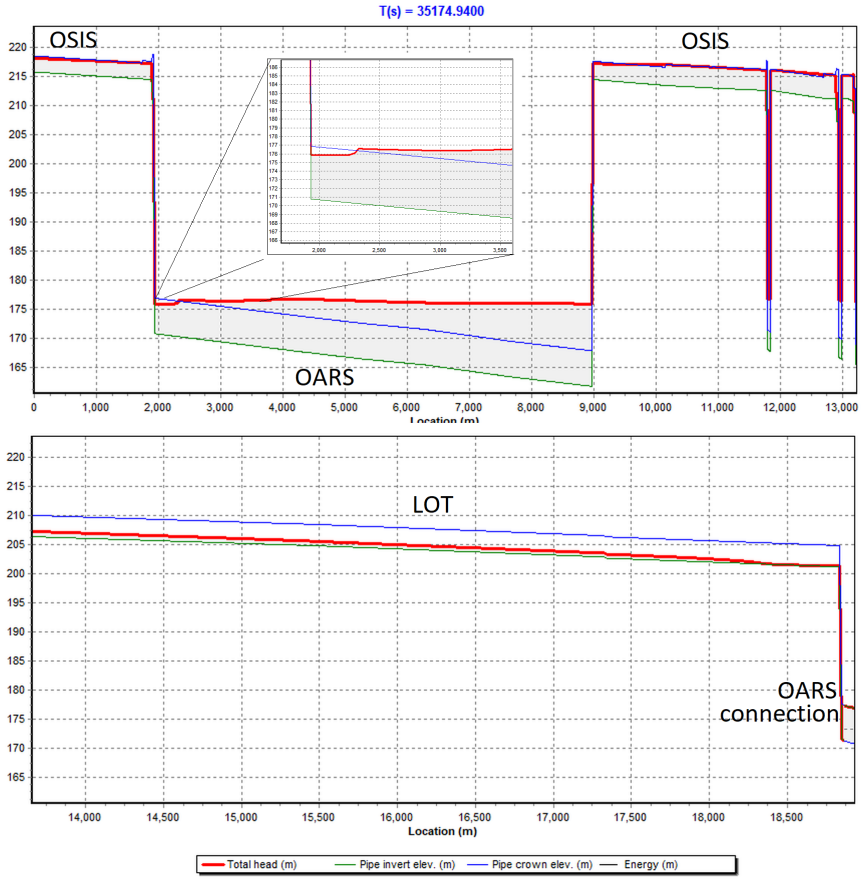

Figure 6.5: HGL in OARS, LOT and a portion of OSIS immediately prior to the full pressurization of OARS (2005-01-11).

Following the rapid filling of the horizontal reaches, deep tunnels begin to experience a rapid rise of water in the vertical structures. If this filling is too fast, surging processes can develop with a risk of water reaching grade if adequate design does not control the formation of surge conditions. The dropshaft structures in OARS shafts 4, 5 and 6 were designed with surge chambers to control the surge propagation. The performance of the surge chamber at shaft 6 during a large storm event is illustrated in Figure 6.6. HAST computed that up to 6.1 m^3/s is diverted from the dropshaft into the surge chamber, causing a significant attenuation in the surge as it propagated up to the surge chamber weir crest.

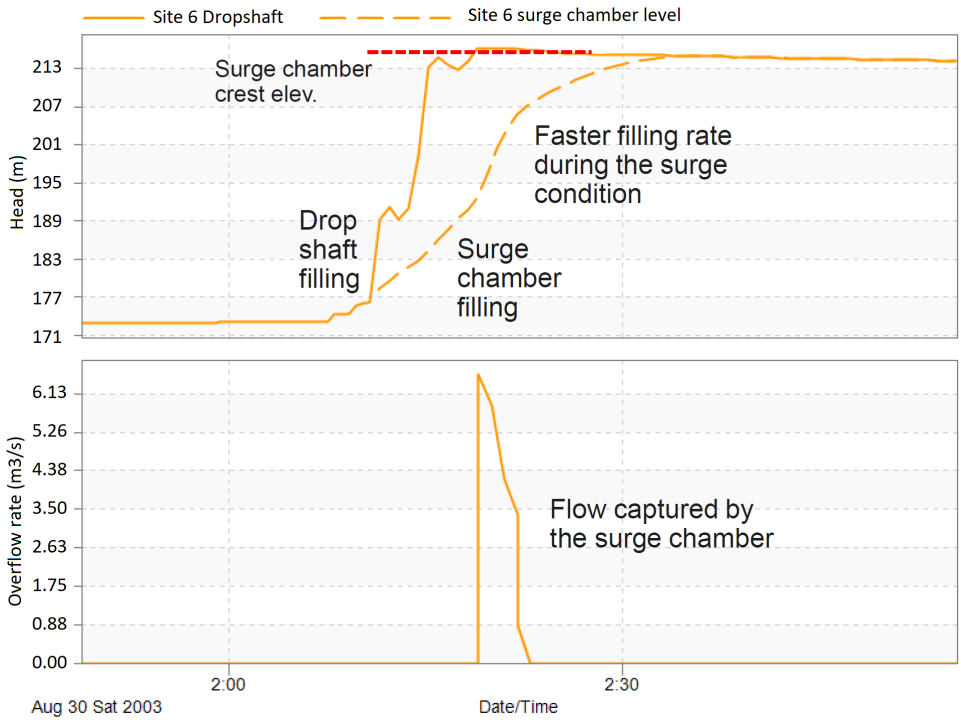

Figure 6.6: Water level at shaft 6 dropshaft and surge chamber, along with flow rate diverted to the surge chamber (2003-08-30 event).

One aspect of LOT design that was evaluated using HAST was the benefits of including a flap gate at Vine shaft to prevent OARS from backing up into LOT. Simulation results from HAST indicated that without flap gates the filling of LOT would occur at least 1.5 h sooner, with potential propagation of surge in OARS into LOT. Alternatively, with flap gates, the two systems are disconnected and filling in LOT would occur due to inflows diverted directly into it. The differences between these two outcomes, computed with HAST, are presented in Figure 6.7.

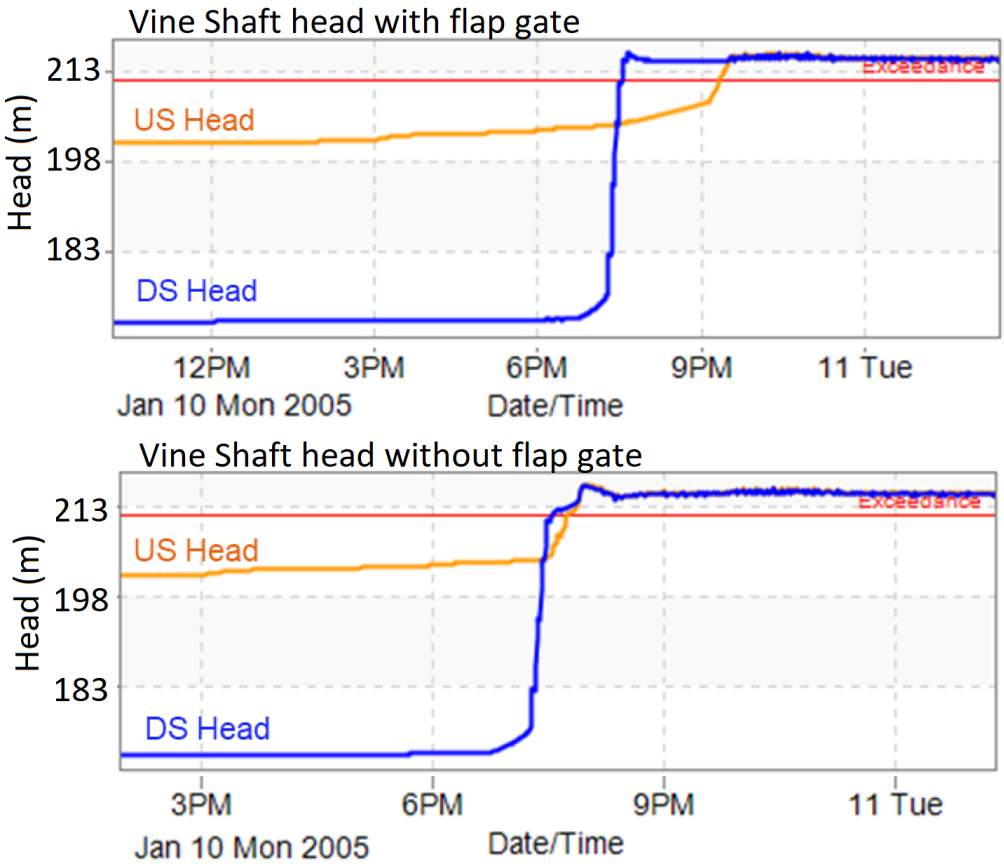

Figure 6.7: Water levels upstream (US) and downstream (DS) of Vine shaft for scenarios with or without flap gates (2005-01-11 event).

As pointed out earlier, in different simulation conditions we noticed a tendency of air pockets to form at particular locations, including near shaft 6. Despite the ventilation in shaft 6, we hypothesized that a large pocket could form in this location and not be fully ventilated. In such an event, the connecting tunnel between shaft 6 and Vine shaft in LOT would be a possible location for air to escape to Vine shaft. The CFD study was performed to assess the effects of an uncontrolled release of a large air pocket through Vine shaft.

6.4 OpenFOAM modeling results

The first step in the OpenFOAM CFD modeling of the uncontrolled release of air pockets through Vine shaft involved the development of a mesh using the tool *snappyHexMesh*. Mesh development was incremental with respect to the ventilation conditions in Vine shaft. At this point it is important to highlight that a systematic mesh convergence analysis was not performed

in this work due to time constraints. However, several meshes were tested in order to guarantee the grid independence. The initial mesh development iterations included perfect ventilation, in which the top slab did not exist. Such simulations were intended to assess whether the release of air could potentially raise the water level within the shaft above grade. As it is shown in Figures 6.8 and 6.9, the release of large air pockets through a water filled Vine shaft did raise the free surface within Vine shaft. However, through all the simulated conditions, the change in the water level was not large enough to reach grade elevation and trigger geysering. This is attributed to the much larger plan area of Vine shaft at elevations that are close to grade.

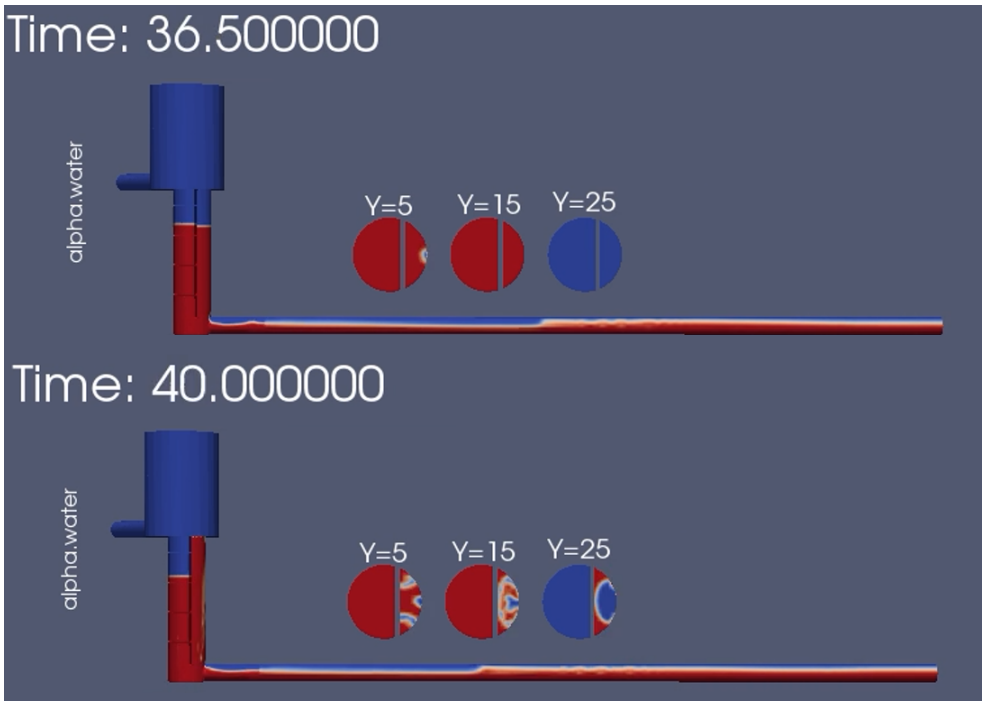

Figure 6.8: Air pocket release impact on water level in Vine shaft for a 25 m initial water level assuming no top slab.

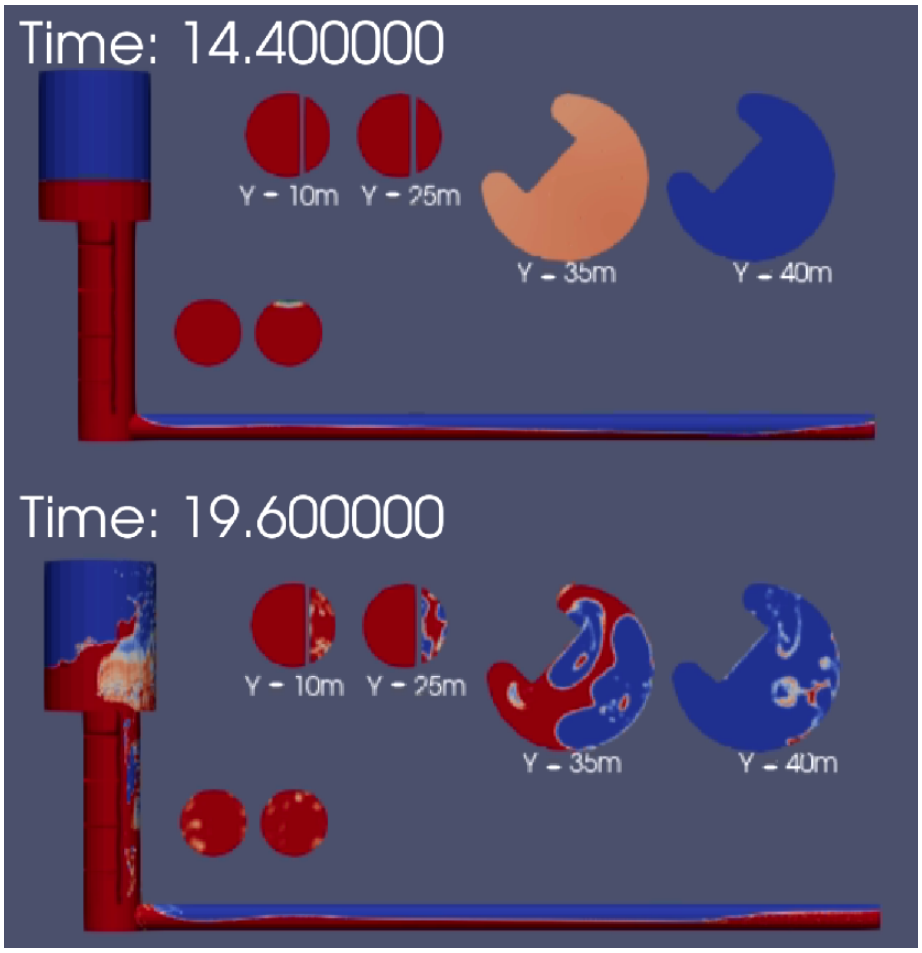

Figure 6.9: Impact of air pocket release on water level in Vine shaft for a 35 m initial water level assuming no top slab.

The second group of CFD simulations assumed zero ventilation conditions in Vine shaft, so vertical water motion created by the air pocket release caused compression of the air in the headspace under the slab. Figure 6.10 shows air pressure at the headspace for different air pocket sizes. Large air pockets were released in separate segments, creating separate air phase growth spurts. Of most importance is that the magnitude of the air phase pressure head, depending on the scenario, can increase to up to 6 m of water in the absence of ventilation, which in turn could create potentially significant forces in the slab of Vine shaft.

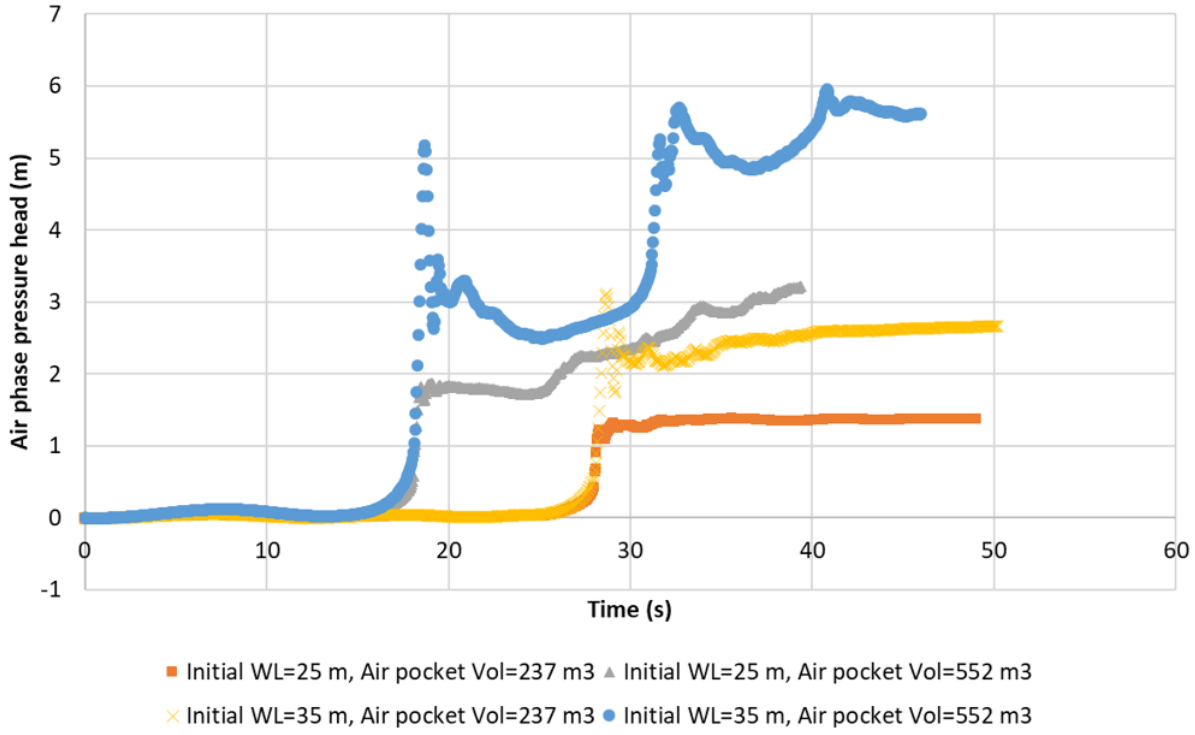

Figure 6.10: Air pressure head under Vine shaft slab in different scenarios of uncontrolled air pocket release if no ventilation is available.

The last CFD simulation considered the most adverse conditions for headspace air pressurization when a proposed ventilation in Vine shaft was added. As shown in Figure 6.11, two ports with dimensions 2.4 m × 2.4 m near the top of Vine shaft were proposed in the LOT design. This modeling is the most representative condition for the uncontrolled release of air in Vine shaft.

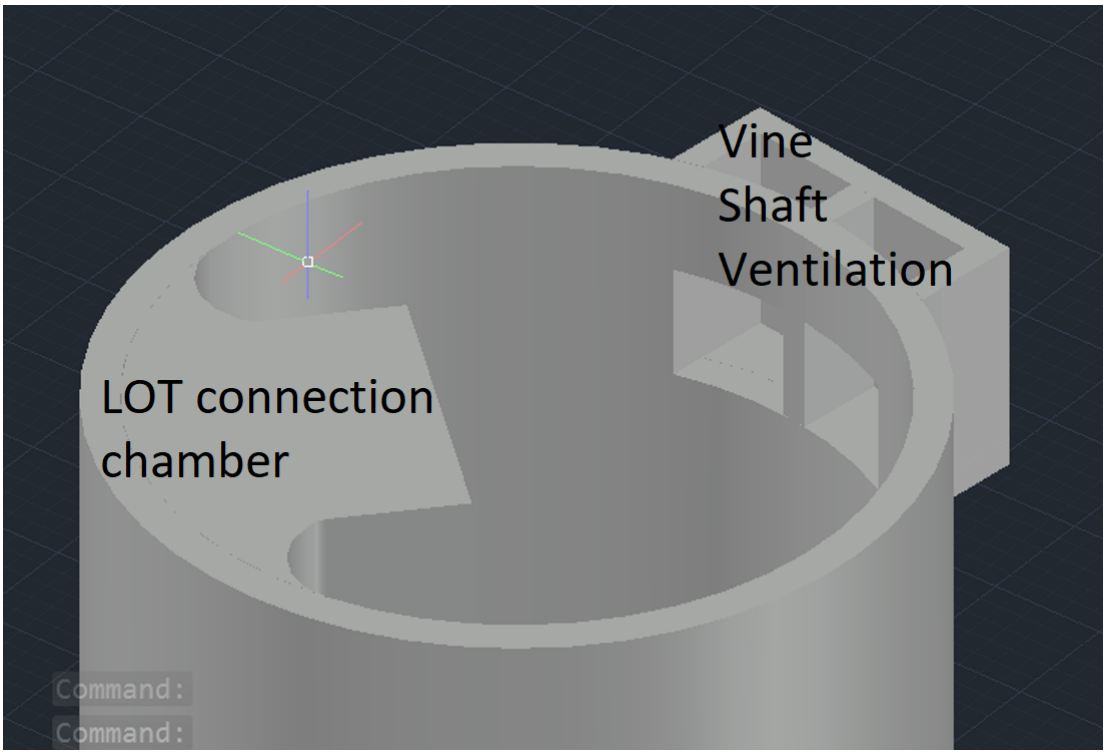

Figure 6.11: Geometric details of the ventilation underneath the top slab at Vine shaft.

Figure 6.12 shows the CFD simulations of the air phase pressure head, expressed in meters of water, underneath the slab and at the two ventilation ports. As can be seen in the figure, the release of the air phase at the bottom of Vine shaft was initiated at time t = 15 s. Within 3 s, the free surface at the top of Vine shaft began to experience additional pressure because of the water displacement created by the air pocket. Pressures increased very rapidly, achieving a peak at t = 18.4 s, after which a sudden drop occurred as the water interface collapsed after the pocket opening. The values of the peak pressures at the three locations varied slightly, with the maximum of 2.3 m under the Vine shaft slab.

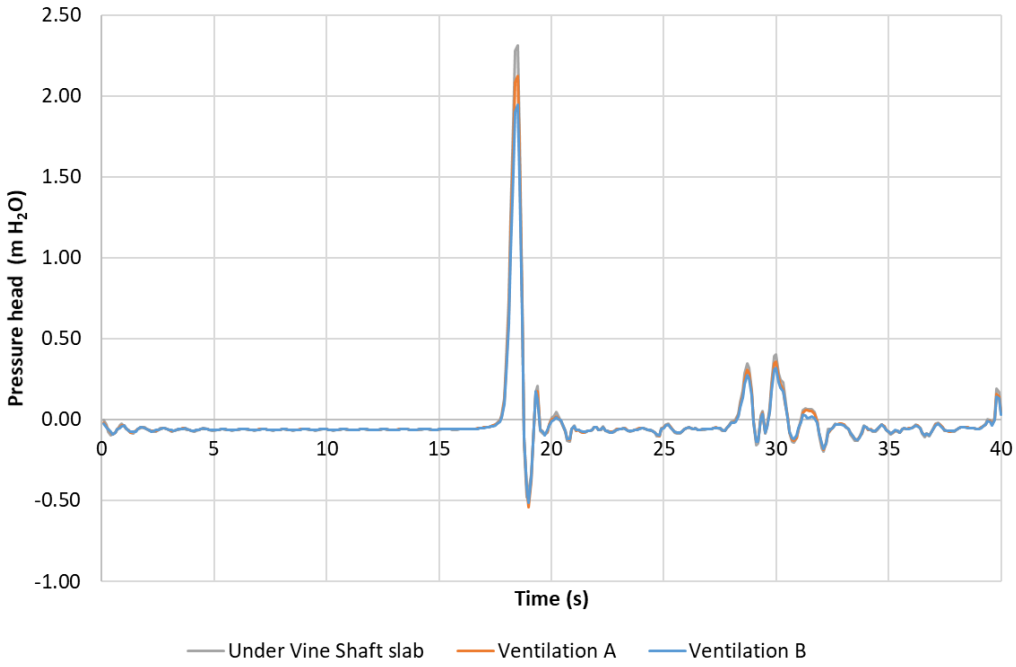

Figure 6.12: Air phase pressure results in Vine shaft with proposed ventilation.

Simulation results of the pressures on the baffles indicated in general an immediate drop as the air pocket started rising in Vine shaft, as shown in Figure 6.13, which is consistent with previous studies (Muller et al., 2017). As the air pocket reached the surface, pressures were minimum, and a series of pressure oscillations caused by mass oscillations in Vine shaft are seen.

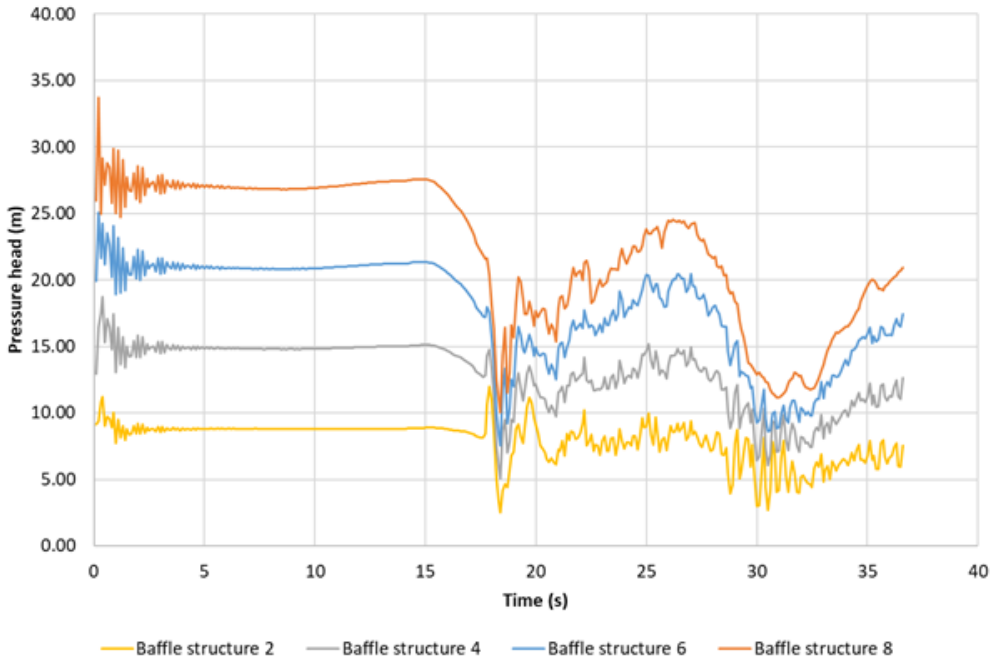

Figure 6.13: Water pressure on different baffle structures in the Vine shaft during air release.

6.5 Final remarks and conclusion

From the development of these studies that involved the numerical simulation of different rapid filling scenarios of the OSIS–OARS–LOT systems, the following conclusion are drawn:

1. Rapid filling conditions underlie the complex interactions between junctions and reaches in these tunnel systems. Adequate modeling using tools such as HAST enable the accurate quantification of surges in the tunnel junctions and dropshafts. The new OARS and LOT systems did not show excessive surging as the structures were adequately designed to mitigate such events.

2. Despite the adequate sizing of junctions and tunnels, numerical simulation of the filling processes indicated possible air pocket formation at specific locations in OARS, LOT and OSIS. In particular, the formation of air pockets near shaft 6 can potentially lead to air release through shaft 6 in OARS and Vine shaft in LOT.

3. The behavior of Vine shaft in scenarios of uncontrolled air pocket release was evaluated using a state-of-the-art OpenFOAM CFD modeling approach. Our work indicated that the

occurrence of geysering is unlikely at that location. However, this study also demonstrated the need for an adequate ventilation structure at that point to avoid potential damage created by air compression underneath the Vine shaft top slab.

We hypothesize that the types of flow conditions and air–water interactions during intense rain events are more widespread than is realized by designers and city officials. However, as monitoring tools and design strategies improve, such adverse air–water interactions will become better recognized. The development of modeling studies such as this offers one possible path for designing future systems or evaluating existing systems. It is expected that with the improvement of this method, stormwater systems will achieve better operational conditions and greater resiliency.

Chapter 7

General conclusions

Stormwater management can be considered as a group of structural and non-structural measures to manage the runoff generated by urban areas, and involve the design, operation and maintenance of urban drainage infrastructure. An important component of these measures is the prediction of flows characteristics of the urban runoff that are generated particularly by intense rain events, which can be destructive and damaging to communities. Such prediction has been one of the main goals of Computational Hydraulics, a discipline that combines fluid mechanics, mathematical and numerical methods, and calibration techniques that are implemented in computers to simulate flows (Popescu, 2014). It is increasingly popular, taking place as an important modeling tool to aid engineers and decision-makers to design and propose more resilient, cost-effective, and safe hydraulic structures. The accuracy of such modeling tools is fundamental for effective predictions of runoff quantity and its routing through urban drainage systems. Therefore, an effective design and operation of urban drainage infrastructure is supported by the successful implementation of modeling tools, which in turn require adequate modeling setup techniques. This is the motivation of this research, which has spanned various applications in the context of Computational Hydraulics in urban drainage applications.

The results of Chapters 2, 3, and 4 presented in this dissertation showed that, in general, employing additional spatial discretization along with appropriate selection of routing time step resulted in significant improvements in SWMM's hydraulic modeling. Also, when these new model set up methodologies are employed along with modifications in its SLOT algorithm by reducing the slot width and, consequently, increasing the wave celerity, SWMM is able to simulate flows conditions that the model was not originally conceived for, such as mixed flows,

pressurization, rapid inflows conditions, closed pipe transients, bore propagation, and surges in collection systems. Additionally, the SLOT's modification allowed for a more precise routing time step estimation based on the CFL stability condition, even though SWMM can generate satisfactory results with Courant number greater than unity due to the implicit nature of its numerical solution.

Combining smaller routing time steps along with additional spatial discretization generated small flow continuity errors, less numerical diffusion, and reductions on oscillations or fluctuations caused by numerical instabilities. However, care is needed when using the proposed modeling set up strategies since some SWMM's numerical scheme intrinsic parameters should be adjusted to maintain the numerical stability, such as the case of head convergence tolerance. Also, some numerical instabilities, linked to the discontinuity of conduit inverts, could arise and minor modifications in the system's geometry must be employed to improve the simulations, this is discussed in more detail in Chapter 4. Furthermore, these new model set up methodologies require more computational time to perform the simulation, but such effort is comparable to other stormwater transient models such as HAST (Vasconcelos et al., 2015). Therefore, with all these improvements achieved, SWMM can be used as an effective tool to analyse more complex flows conditions present in stormwater systems, particularly linked to intense rainfall and rapid filling conditions.

The analysis performed in the first three chapters compared new SWMM set up modeling strategies with analytical solutions and benchmark models but no field water depth or flow rates data of actual stormwater systems was used. Therefore, even though is difficult to obtain these type of data in stormwater systems, specially during intense rain events, data collection of such conditions occurring in stormwater systems is needed for better assessment of SWMM capabilities. Furthermore, at the end of these three chapters, a software named ReSWMM (Pachaly et al., 2018) that automatically discretizes SWMM models was developed, aiding in SWMM model set up for future applications of more precise hydraulic simulations. It can be downloaded along with its manual at: https://github.com/ecotecnologias/ReSWMM.

Chapter 5 presented a study that employed a combination of a 1D-2D methodology to predict flooding events in two urban watersheds located on the Jefferson County, AL as well as

proposed conceptual approaches to mitigate the frequency and intensity of these flooding events. The hydrology was modeled by a 1D PCSWMM rainfall-runoff model and the flooded extent was modeled by a 2D HEC RAS model. Calibration was performed on one watershed and its calibration parameters were assumed on the other watershed. The flooded areas were predicted according to reported high water marks observed during flooding events. Proposed conceptual approaches were evaluated by using design rainfalls and the best solution was selected based on reduction of flooded area, duration of flooding, and economical terms. The results are limited by calibration efforts and data availability but they are valuable in future flooding control efforts. Even though the flooding events were not completely eliminated by the proposed conceptual approaches, the flooding area and duration of flooding extent was significantly reduced, specially for smaller return periods.

This combination of 1D-2D models came out to be a satisfactory solution to model flooded areas in urban areas. When employing a model with more complex formulation, such as the 2D HEC RAS, a higher computational time is expected to perform a single simulation. In urban areas, modeling the whole watershed using a 2D model can be time-consuming, and it is difficult to set up hydraulic structures such as bridges, culverts, and below grade pipes. Also, the flooding may occur only in small portions of the watershed. Thus, employing a 1D rainfall-runoff, such as SWMM, to simulate the surface hydrology and identify the most likely regions where flooding occurs decreases the time spend in modeling set up as well as the computation time to perform the simulation that a 2D model would require. Once these regions are identified, the 2D model must be employed. Therefore, this combination of 1D-2D models reduces model set up time and aids on numerical modeling of flooded areas.

Chapter 6 evaluated the multiphase rapid filling conditions of the tunnel system in Columbus, OH by employing a 1D-3D methodology. The 1D model was used to quantify the surges in the tunnel's junctions and dropshafts since, to date, it is computational unfeasible to use a 3D model in a system-wide application. Air pockets motion as well as the prediction of the potential regions of air pockets formation and air pockets discharges in vertical structures were accurately tracked by the 1D model without excessive computational effort. The 3D model was used to estimate the release of these air pockets within the vertical dropshaft. The 3D modeling efforts

showed that geysering is unlikely to occur due to the long size of the shaft structure. Adequate ventilation at the dropshaft was shown to be required to avoid potential damage created by air compression. Therefore, coupling 1D and 3D simulations aided in the modeling of multiphase simulations in stormwater tunnels. The development of these modeling studies are important for better design of future systems or evaluation of existing systems.

As aforementioned, all fluid flow are 3D by nature, but the currently available technology does not allow for widespread applications of 3D models. The usage of 1D model to represent fluid flows, specially in stormwater systems, has been employed for many years and it is still appropriate in many situations such as backwater, surcharging, gradual filling, and others. However, there are situations where the flow condition being simulated violates the assumptions of 1D flow. At this moment, a 1D model starts to misrepresent the flow and a 3D model should be employed to represent more accurately the flow condition. Nevertheless, 1D models can, with the correct formulation, identify when air pockets may be compressed, and move within pressurized flows. Given that, using a 1D model until the point where flow conditions that could violate its assumptions may arise and then a 3D model to represent more complex conditions is a possible path forward in the simulation of actual stormwater systems that was explored in this dissertation. This approach produced satisfactory results in predicting the air pockets formation, motion and discharge within a vertical shaft in a stormwater tunnel system. Therefore, while the technology still does not allow for a widespread application of 3D models in stormwater systems, this coupled 1D-3D methodology can improve the accuracy of the simulation of complex flow conditions in stormwater systems.

To conclude, this dissertation proposed methodologies to improve the numerical simulation of stormwater systems involving mainly rapid filling conditions. Also, it involved SWMM, a well-known 1D model with widespread applications around the world, and 2 and 3D models with also extensive applications. The methodologies proposed improved the numerical simulation of flows in stormwater systems. Moreover, it is expected that these new modeling strategies and methodologies aid engineers in the modeling of such systems, leading to better operational conditions and greater resiliency.

Chapter 8

Future studies

This dissertation proposed several innovative approaches in the context of numerical modeling of stormwater systems. However, there are many topics that were not considered given the scope of this study, and those should be addressed in future research efforts. This is the case of the wave celerity during the pressurization of flows. Even though there are guidelines for estimating the celerity for open channel flows and for fully pressurized flows (e.g. no air or any gas entrapped within the pipes), the current body of knowledge still lacks the estimation of celerity values for flows where air is entrapped within the pipes, such as the case of a collection system undergoing pressurization. The research done in this dissertation employed a pressurization algorithm that uses celerity values in its formulation, but since there are no current guidelines on how to estimate the celerity values during pressurization of flows, different values were selected for a more detailed study on the impact of this variable in the simulations. Therefore, it is expected that a more precise estimation of celerity values would increase the accuracy of modeling stormwater systems and future research must be conducted in this direction.

References

Abbott, M. B., & Basco, D. R. (1997). *Computational Fluid Dynamics*. Longman.

Abdul-Aziz, O. I., & Al-Amin, S. (2016). Climate, land use and hydrologic sensitivities of stormwater quantity and quality in a complex coastal-urban watershed. *Urban Water Journal*, *13*(3), 302–320. https://doi.org/10.1080/1573062X.2014.991328

Ahiablame, L., & Shakya, R. (2016). Modeling flood reduction effects of low impact development at a watershed scale. *Journal of environmental management*, *171*, 81–91.

Akter, A., Tanim, A. H., & Islam, M. K. (2020). Possibilities of urban flood reduction through distributed-scale rainwater harvesting. *Water Science and Engineering*, *13*(2), 95–105.

Bates, P. D., Lane, S. N., & Ferguson, R. I. (2005). *Computational fluid dynamics: Applications in environmental hydraulics*. John Wiley & Sons.

Beck, J. (2016). Comparison of three methodologies for quasi-2d river flood modeling with swmm5. *Journal of Water Management Modeling*.

Benito, G., Dıez-Herrero, A., & De Villalta, M. F. (2003). Magnitude and frequency of flooding in the tagus basin (central spain) over the last millennium. *Climatic Change*, *58*(1), 171–192.

Bi, E. G., Monette, F., Gachon, P., Gaspéri, J., & Perrodin, Y. (2015). Quantitative and qualitative assessment of the impact of climate change on a combined sewer overflow and its receiving water body. *Environmental Science and Pollution Research*, *22*(15), 11905–11921.

Bousso, S., Daynou, M., & Fuamba, M. (2013). Numerical modeling of mixed flows in storm water systems: Critical review of literature. *Journal of Hydraulic Engineering*, *139*(4), 385–396.

Brunner, G. W. (2021a). *Hec-ras river analysis system. 2d modeling user's manual. version 6.0* (tech. rep.). Hydrologic Engineering Center.

Brunner, G. W. (2021b). *Hec-ras river analysis system. hydraulic reference manual. version 6.0* (tech. rep.). Hydrologic Engineering Center.

Buahin, C. A., & Horsburgh, J. S. (2018). Advancing the Open Modeling Interface (OpenMI) for integrated water resources modeling. *Environmental Modelling and Software*, *108*(April), 133–153. https://doi.org/10.1016/j.envsoft.2018.07.015

Burger, G., Sitzenfrei, R., Kleidorfer, M., & Rauch, W. (2014). Parallel flow routing in SWMM 5. *Environmental Modelling and Software*, *53*, 27–34. https://doi.org/10.1016/j.envsoft.2013.11.002

Butt, M. J., Umar, M., & Qamar, R. (2013). Landslide dam and subsequent dam-break flood estimation using hec-ras model in northern pakistan. *Natural Hazards*, *65*(1), 241–254.

Campisano, A., Catania, F. V., & Modica, C. (2017). Evaluating the SWMM LID Editor rain barrel option for the estimation of retention potential of rainwater harvesting systems. *Urban Water Journal*, *14*(8), 876–881. https://doi.org/10.1080/1573062X.2016.1254259

Campisano, A., Gullotta, A., & Modica, C. (2019). Using EPA-SWMM to simulate intermittent water distribution systems. *Urban Water Journal*, *00*(00), 1–9. https://doi.org/10.1080/1573062X.2019.1597379

Cataño-Lopera, Y. A., Tokyay, T. E., Martin, J. E., Schmidt, A. R., Lanyon, R., Fitzpatrick, K., Scalise, C. F., & Garcıa, M. H. (2014). Modeling of a transient event in the tunnel and reservoir plan system in chicago, illinois. *Journal of Hydraulic Engineering*, *140*(9), 05014005.

Causon, D. M., & Mingham, C. G. (2010). *Introductory Finite Difference Methods for PDEs*. Bookboon.

CD-adapco, S. (2017). Star ccm+ user guide version 12.04. *CD-Adapco: New York, NY, USA*.

Chaudhry, M. H. (2007). *Open-channel flow*. Springer Science & Business Media.

Chaudhry, M. H. (2008). *Open channel flow*. Springer Science & Business Media. https://doi.org/10.1007/978-0-387-68648-6

Chaudhry, M. H. (2013). *Applied hydraulic transients* (Third Edit, Vol. 9781461485). Springer. https://doi.org/10.1007/978-1-4614-8538-4

Cho, J. H., & Seo, H. J. (2007). Parameter optimization of SWMM for runoff quantity and quality calculation in a eutrophic lake watershed using a genetic algorithm. *Water Science and Technology: Water Supply*, *7*(5-6), 35–41. https://doi.org/10.2166/ws.2007.114

Choi, Y. J., Leon, A. S., & Apte, S. V. (2014). Three-dimensional numerical modeling of air-water geyser flows. *World Environmental and Water Resources Congress 2014*, 1535–1548.

Chosie, C. D., Hatcher, T. M., & Vasconcelos, J. G. (2014). Experimental and numerical investigation on the motion of discrete air pockets in pressurized water flows. *Journal of Hydraulic Engineering*, *140*(8), 04014038.

Courant, R., Friedrichs, K., & Lewy, H. (1928). Über die partiellen differenzengleichungen der mathematischen physik. *Mathematische Annalen*, *100*(1), 32–74. https://doi.org/10.1007/BF01448839

Cunge, J., Holly Jr, F., & Verwey, A. (1980). *Practical aspects of computational river hydraulics*. Pitman Advanced Pub. Program. https://doi.org/10.1038/sj.cgt.7700426

Cunge, J. (1980). *Practical aspects of computational river hydraulics*. Pitman publishing.

David, A., & Schmalz, B. (2020). Flood hazard analysis in small catchments: Comparison of hydrological and hydrodynamic approaches by the use of direct rainfall. *Journal of Flood Risk Management*, *13*(4), e12639.

Di Modugno, M., Gioia, A., Gorgoglione, A., Iacobellis, V., la Forgia, G., Piccinni, A. F., & Ranieri, E. (2015). Build-up/wash-off monitoring and assessment for sustainable management of first flush in an urban area. *Sustainability (Switzerland)*, *7*(5), 5050–5070. https://doi.org/10.3390/su7055050

Eldayih, Y., & Vasconcelos, J. G. (2018). Preliminary research on air pocket entrapments caused by shear-flow instabilities in rapid-filling pipes. *World Environmental and Water Resources Congress 2018: Hydraulics and Waterways, Water Distribution Systems Analysis, and Smart Water*, 285–292.

EPA. (2018). Storm water management model (swmm) ver. 5.0.13. https://www.epa.gov/water-research/storm-water-management-model-swmm

EPA. (2020a). Combined sewer overflows (csos). https://www.epa.gov/npdes/combined-sewer-overflows-csos

EPA. (2020b). Storm water management model (swmm) ver. 5.0.13. https://www.epa.gov/water-research/storm-water-management-model-swmm

Gheith, H. (2014). *An innovative approach to quantify rdii sources using swmm groundwater module*.

Ghidaoui, M. S., Zhao, M., McInnis, D. A., & Axworthy, D. H. (2005). A review of water hammer theory and practice. *Applied Mechanics Reviews*, *58*(1), 49. https://doi.org/10.1115/1.1828050

Goncalves, M. L., Zischg, J., Rau, S., Sitzmann, M., Rauch, W., & Kleidorfer, M. (2018). Modeling the effects of introducing low impact development in a tropical city: A case study from joinville, brazil. *Sustainability*, *10*(3), 728.

Greenshields, C. J. et al. (2015). Openfoam user guide. *OpenFOAM Foundation Ltd, version*, *3*(1), 47.

Guo, Q., & Song, C. C. (1990). Surging in urban storm drainage systems. *Journal of hydraulic engineering*, *116*(12), 1523–1537.

Haltas, I., Tayfur, G., & Elci, S. (2016). Two-dimensional numerical modeling of flood wave propagation in an urban area due to ürkmez dam-break, izmir, turkey. *Natural Hazards*, *81*(3), 2103–2119.

Hatcher, T. M., & Vasconcelos, J. G. (2014). Alternatives for flow solution at the leading edge of gravity currents using the shallow water equations. *Journal of hydraulic research*, *52*(2), 228–240.

Heineman, M. C. (2004). Netstorm-a computer program for rainfall-runoff simulation and precipitation analysis. *Critical transitions in water and environmental resources management* (pp. 1–14).

Herr, R., & Gheith, H. (2015). *Blueprint columbus collection system model.*

Hinze, J. (1975). *Turbulence mcgraw* (Vol. 2). Hill Publishing Co., New York.

Hirt, C. W., & Nichols, B. D. (1981). Volume of fluid (vof) method for the dynamics of free boundaries. *Journal of computational physics*, *39*(1), 201–225.

Hodges, B. R., Liu, F., & Rowney, A. C. (2019). *A New Saint-Venant Solver for SWMM* (Vol. 1). Springer International Publishing. https://doi.org/10.1007/978-3-319-99867-1

Huang, B., Fan, M., Liu, J., & Zhu, D. Z. (2021). Cfd simulation of air–water interactions in rapidly filling horizontal pipe with entrapped air. *World Environmental and Water Resources Congress 2021*, 495–507.

Huber, W., & Roesner, L. (2012). The history and evolution of the epa swmm" in "fifty years of watershed modeling - past, present and futur. *Engineering Conferences International Symposium Series. http://dc.engconfintl.org/watershed/29*.

Jackson, T. J., Lai, C., Schmugge, T. J., & Yen, B. C. (1986). *Advances in hydroscience* (Vol. 14). Elsevier.

Khalaj, M. R., Noor, H., & Dastranj, A. (2021). Investigation and simulation of flood inundation hazard in urban areas in iran. *Geoenvironmental Disasters*, *8*(1), 1–13.

Kim, H. I., Keum, H. J., & Han, K. Y. (2019). Real-time urban inundation prediction combining hydraulic and probabilistic methods. *Water*, *11*(2), 293.

Kim, S. E., Lee, S., Kim, D., & Song, C. G. (2018). Stormwater inundation analysis in small and medium cities for the climate change using epa-swmm and hdm-2d. *Journal of Coastal Research*, (85 (10085)), 991–995.

Kundzewicz, Z. W., Kanae, S., Seneviratne, S. I., Handmer, J., Nicholls, N., Peduzzi, P., Mechler, R., Bouwer, L. M., Arnell, N., Mach, K., et al. (2014). Flood risk and climate change: Global and regional perspectives. *Hydrological Sciences Journal*, *59*(1), 1–28.

Larsen, R. J., Ting, F. C., & Jones, A. L. (2011). Flow velocity and pier scour prediction in a compound channel: Big sioux river bridge at flandreau, south dakota. *Journal of Hydraulic Engineering*, *137*(5), 595–605.

Lautenbach, D. J., Vasconcelos, J. G., Wright, S. J., Wolfe, J. R., Cassidy, J. F., Klaver, P. R., & Benson, L. R. (2008). Analysis of transient surge in the proposed district of columbia water and sewer authority deep tunnel system. *Proceedings of the Water Environment Federation*, *2008*(5), 442–468.

Leandro, J., Chen, A. S., Djordjević, S., & Savić, D. A. (2009). Comparison of 1d/1d and 1d/2d coupled (sewer/surface) hydraulic models for urban flood simulation. *Journal of hydraulic engineering*, *135*(6), 495–504.

Lee, K. T., Ho, Y.-H., & Chyan, Y.-J. (2006). Bridge blockage and overbank flow simulations using hec–ras in the keelung river during the 2001 nari typhoon. *Journal of Hydraulic Engineering*, *132*(3), 319–323.

Leon, A. S., Choi, N. J., Schmidt, A. R., & Garcia, M. H. (2010). Flow dynamics in combined storm-sewer systems: Application of the illinois transient model (itm) to the calumet tarp system in chicago, illinois. *World Environmental and Water Resources Congress 2010: Challenges of Change*, 3703–3717.

Li, J., & McCorquodale, A. (1999). Modeling mixed flow in storm sewers. *Journal of hydraulic Engineering*, *125*(11), 1170–1180.

Lyu, H.-M., Shen, S.-L., Yang, J., & Yin, Z.-Y. (2019). Inundation analysis of metro systems with the storm water management model incorporated into a geographical information system: A case study in shanghai. *Hydrology and Earth System Sciences*, *23*(10), 4293–4307.

Macchione, F., & Morelli, M. A. (2003). Practical aspects in comparing shock-capturing schemes for dam break problems. *Journal of Hydraulic Engineering*, *129*(3), 187–195.

Malekpour, A., & Karney, B. W. (2015). Spurious numerical oscillations in the preissmann slot method: Origin and suppression. *Journal of Hydraulic Engineering*, *142*(3), 04015060. https://doi.org/10.1061/(asce)hy.1943-7900.0001106

Matsson, J. (2020). *An introduction to ansys fluent 2020*. SDC Publications.

Mays, L. W. (2001). *Stormwater Collection Systems Design Handbook*. McGraw-Hill Education.

Meierdiercks, K. L., Smith, J. A., Baeck, M. L., & Miller, A. J. (2010). Analyses of Urban Drainage Network Structure and Its Impact on Hydrologic Response. *Journal of the American Water Resources Association*, *46*(5).

Muller, K. Z., Wang, J., & Vasconcelos, J. G. (2017). Water displacement in shafts and geysering created by uncontrolled air pocket releases. *Journal of Hydraulic Engineering*, *143*(10), 04017043.

Munir, B. A., Ahmad, S. R., & Hafeez, S. (2020). Integrated hazard modeling for simulating torrential stream response to flash flood events. *ISPRS International Journal of Geo-Information*, *9*(1), 1.

MWRD. (2020). Mwrd's tunnel and reservoir plan. https://mwrd.org/tunnel-and-reservoir-plan (accessed: 04.18.2020)

Nazari, B., Seo, D.-J., & Muttiah, R. (2016). Assessing the impact of variations in hydrologic, hydraulic and hydrometeorological controls on inundation in urban areas. *Journal of Water Management Modeling*.

Nguyen, H. Q., Degener, J., & Kappas, M. (2015). Flash flood prediction by coupling kineros2 and hec-ras models for tropical regions of northern vietnam. *Hydrology*, *2*(4), 242–265.

Niazi, M., Nietch, C., Maghrebi, M., Jackson, N., Bennett, B. R., Tryby, M., & Massoudieh, A. (2017). Storm Water Management Model: Performance Review and Gap Analysis. *Journal of Sustainable Water Built Environment*, *3*(2). https://doi.org/10.1061/JSWBAY.0000817.

NOAA. (2021). Global hourly - integrated surface database. https://www.ncei.noaa.gov/products/land-based-station/integrated-surface-database

Obropta, C. C., & Kardos, J. S. (2007). Review of Urban Stormwater Quality Models: Deterministic, Stochastic, and Hybrid Approaches. *Journal of the American Water Resources Association*, *43*(6), 1508–1523. https://doi.org/10.1111/j.1752-1688.2007.00124.x

OpenFOAM. (2021). *Openfoam overview*. Retrieved June 4, 2021, from https://www.openfoam.com/governance/overview

Pachaly, R., Vasconcelos, J., Allasia, D., & Minetto, B. (2019). Field evaluation of discretized model setups for the storm water management model. *Journal of Water Management Modeling*.

Pachaly, R. L., Vasconcelos, J. G., & Allasia, D. G. P. (2018). ReSWMM v0.1. https://github.com/ecotecnologias/ReSWMM

Pachaly, R. L., Vasconcelos, J. G., Allasia, D. G. P., & Bocchi, J. P. P. (2020a). *Evaluating swmm capabilities to simulate closed pipe transients* [Manuscript submitted for publication].

Pachaly, R. L., Vasconcelos, J. G., Allasia, D. G., Tassi, R., & Bocchi, J. P. P. (2020b). Comparing swmm 5.1 calculation alternatives to represent unsteady stormwater sewer flows. *Journal of Hydraulic Engineering*, *146*(7), 04020046.

Palermo, S., Talarico, V., & Turco, M. (2020). On the lid systems effectiveness for urban stormwater management: Case study in southern italy. *IOP Conference Series: Earth and Environmental Science*, *410*(1), 012012.

Panos, C. L., Hogue, T. S., Gilliom, R. L., & McCray, J. E. (2018). High-resolution modeling of infill development impact on stormwater dynamics in denver, colorado. *Journal of Sustainable Water in the Built Environment*, *4*(4), 04018009.

Papaioannou, G., Loukas, A., Vasiliades, L., & Aronica, G. (2016). Flood inundation mapping sensitivity to riverine spatial resolution and modelling approach. *Natural Hazards*, *83*(1), 117–132.

Parmakian, J. (1963). *Waterhammer analysis* (Vol. 9). Prentice-Hall.

Paule-Mercado, M. C. A., Salim, I., Lee, B.-Y., Memon, S., Sajjad, R. U., Sukhbaatar, C., & Lee, C.-H. (2018). Monitoring and quantification of stormwater runoff from mixed land use and land cover catchment in response to land development. *Ecological indicators*, *93*, 1112–1125.

Pinos, J., & Timbe, L. (2019). Performance assessment of two-dimensional hydraulic models for generation of flood inundation maps in mountain river basins. *Water science and engineering*, *12*(1), 11–18.

Popescu, I. (2014). *Computational hydraulics*. IWA Publishing.

Pratt, N. (2019). Oars-osis augmentation & relief sewer tabbed as ocea finalist. https://news.asce.org/oars-osis-augmentation-relief-sewer-tabbed-as-ocea-finalist/ (accessed: 04.10.2019)

Preissmann, A. (1961). Propagation of translatory waves in channels and rivers. *Proceedings of the 1st Congress of French Association for Computation, Grenoble, France*, 432–443.

Qian, Y., Zhu, D. Z., Liu, L., Shao, W., Edwini-Bonsu, S., & Zhou, F. (2020). Numerical and experimental study on mitigation of storm geysers in edmonton, alberta, canada. *Journal of Hydraulic Engineering*, *146*(3), 04019069.

Quirogaa, V. M., Kurea, S., Udoa, K., & Manoa, A. (2016). Application of 2d numerical simulation for the analysis of the february 2014 bolivian amazonia flood: Application of the new hec-ras version 5. *Ribagua*, *3*(1), 25–33.

Rai, P. K., Dhanya, C., & Chahar, B. (2018). Coupling of 1d models (swat and swmm) with 2d model (iric) for mapping inundation in brahmani and baitarani river delta. *Natural Hazards*, *92*(3), 1821–1840.

Riaño-Briceño, G., Barreiro-Gomez, J., Ramirez-Jaime, A., Quijano, N., & Ocampo-Martinez, C. (2016). MatSWMM - An open-source toolbox for designing real-time control of urban drainage systems. *Environmental Modelling and Software*, *83*, 143–154. https://doi.org/10.1016/j.envsoft.2016.05.009

Ridgway, K., & Kumpula, G. J. (2008). Surge modeling in sewers using alternative hydraulic software programs. *Journal of Water Management Modeling*.

Ridgway, K. E. (2008). Evaluating force main transients with swmm5 and other programs. *Journal of Water Management Modeling*, *6062*, 43–54. https://doi.org/10.14796/JWMM.R236-04.

Ridgway, K. E., & Kumpula, G. (2007). Surge Modeling in Sewers using the Transient Analysis Program (TAP). *Journal of Water Management Modeling*, *6062*, 155–164. https://doi.org/10.14796/JWMM.R228-10.

Roe, P. L. (1981). Approximate riemann solvers, parameter vectors, and difference schemes. *Journal of computational physics*, *43*(2), 357–372.

Roesner, L. A., Aldrich, J. A., Dickinson, R. E., & Barnwell, T. O. (1988). *Swmm user's manual, version 4: Extran addendum*. EPA.

Rossman, L. A. (2006). Storm Water Management Model Quality Assurance Report: Dynamic Wave Flow Routing. *Storm Water Management Model Quality Assurance Report*, 1–115.

Rossman, L. A. (2015a). Storm water management model user's manual version 5.1. *U.S. Environmental Protection Agency*, 1–353. http://www.epa.gov/water-research/storm-water-management-model-swmm

Rossman, L. A. (2015b). Swmm user's manual version 5.1. *EPA*, 1–353.

Rossman, L. A. (2017a). Storm Water Management Model Reference Manual Volume II – Hydraulics. *U.S. Environmental Protection Agency*, 190.

Rossman, L. A. (2017b). Storm water management model reference manual volume ii – hydraulics. *U.S. Environmental Protection Agency*, *2*(Mayo), 190. https://www.epa.gov/water-research/storm-water-management-model-swmm

Rossman, L. A., & Huber, W. C. (2016). Storm Water Management Model Reference Manual Volume I – Hydrology. *U.S. Environmental Protection Agency*, (July).

Rusche, H. (2003). *Computational fluid dynamics of dispersed two-phase flows at high phase fractions* (Doctoral dissertation). Imperial College London (University of London).

Salvan, L., Abily, M., Gourbesville, P., & Schoorens, J. (2016). Drainage system and detailed urban topography: Towards operational 1d-2d modelling for stormwater management. *Procedia Engineering*, *154*, 890–897.

Schulz, H. E., Vasconcelos, J. G., & Patrick, A. C. (2020). Air entrainment in pipe-filling bores and pressurization interfaces. *Journal of Hydraulic Engineering*, *146*(2), 04019053.

Schulze, L., & Thorenz, C. (2014). The multiphase capabilities of the cfd toolbox openfoam for hydraulic engineering applications. *ICHE 2014. Proceedings of the 11th International Conference on Hydroscience & Engineering*, 1007–1016.

Seckin, G., Haktanir, T., & Knight, D. (2007). A simple method for estimating flood flow around bridges. *Proceedings of the Institution of Civil Engineers-Water Management*, *160*(4), 195–202.

Seyoum, S. D., Vojinovic, Z., Price, R. K., & Weesakul, S. (2012). Coupled 1D and Noninertia 2D Flood Inundation Model for Simulation of Urban Flooding. *Journal of Hydraulic Engineering*, *138*(1). https://doi.org/10.1061/(ASCE)HY.1943-7900

Sjöberg, A. (1982). Sewer network models dagvl-a and dagvl-diff. In B. C. Yen (Ed.), *Urban stormwater hydraulics and hydrology* (pp. 127–136). Water Resources Publ.

Song, C. C., Cardie, J. A., & Leung, K. S. (1983). Transient mixed-flow models for storm sewers. *Journal of hydraulic engineering*, *109*(11), 1487–1504.

Sturm, T. (2001). *Open channel hydraulics*. Mc Graw Hill.

Sturm, T. (2010). *Open channel hydraulics*. McGraw-Hill.

Svenungsson, J. (2016). Solving electric field using maxwell's equations and compressibleinterfoam solver. *CFD with OpenSource Software*.

Thorley, A. R. D. (1991). *Fluid transients in pipeline systems*. D.; L. George Ltd.

Timbadiya, P. V., Patel, P. L., & Porey, P. D. (2011). Calibration of hec-ras model on prediction of flood for lower tapi river, india. *Journal of Water Resource and Protection*, *3*(11), 805.

Toro, E. F. (2013). *Riemann solvers and numerical methods for fluid dynamics: A practical introduction*. Springer Science & Business Media.

Trajkovic, B., Ivetic, M., Calomino, F., & D'Ippolito, A. (1999). Investigation of transition from free surface to pressurized flow in a circular pipe. *Water Science and Technology*, 105–112.

Tsihrintzis, V. A., & Hamid, R. (1998). Runoff quality prediction from small urban catchments using SWMM. *Hydrological Processes*, *12*(June 1996), 311–329.

USGS. (2021). U.s. geological survey water data for the nation. http://waterdata.usgs.gov/nwis/

Vasconcelos, J. (2019). Biao huang jue wang jose vasconcelos. *Computational Fluid Dynamics*, 187.

Vasconcelos, J. G., Klaver, P. R., & Lautenbach, D. J. (2015). Flow regime transition simulation incorporating entrapped air pocket effects. *Urban Water Journal*, *12*(6), 488–501.

Vasconcelos, J. G., & Leite, G. M. (2012). Pressure surges following sudden air pocket entrapment in storm-water tunnels. *Journal of hydraulic engineering*, *138*(12), 1081–1089.

Vasconcelos, J. G., & Wright, S. J. (2006). Mechanisms for air pocket entrapment in stormwater storage tunnels. *World Environmental and Water Resource Congress 2006*, 1–10.

Vasconcelos, J. G., & Wright, S. J. (2007). Comparison between the two-component pressure approach and current transient flow solvers. *Journal of Hydraulic Research*, *45*(2), 178–187.

Vasconcelos, J. G., & Wright, S. J. (2011). Geysering generated by large air pockets released through water-filled ventilation shafts. *Journal of hydraulic engineering*, *137*(5), 543–555.

Vasconcelos, J. G., & Wright, S. J. (2017). Anticipating transient problems during the rapid filling of deep stormwater storage tunnel systems. *Journal of Hydraulic Engineering*, *143*(3), 06016025.

Vasconcelos, J. G., Wright, S. J., & Roe, P. L. (2006). Improved simulation of flow regime transition in sewers: Two-component pressure approach. *Journal of Hydraulic Engineering*, *9429*(JUNE 2006), 553–562.

Vasconcelos, J. G., Wright, S. J., & Roe, P. L. (2009). Numerical oscillations in pipe-filling bore predictions by shock-capturing models. *Journal of hydraulic engineering*, *135*(4), 296–305.

Vasconcelos, J. G., Eldayih, Y., & Jamily, J. A. (2018). Evaluating Storm Water Management Model accuracy in mixed flows conditions. *Journal of Water Management Modeling*, 1–21.

Vemula, S., Srinivasa Raju, K., & Sai Veena, S. (2020). Modelling impact of future climate and land use land cover on flood vulnerability for policy support–hyderabad, india. *Water Policy*, *22*(5), 733–747.

Von Karman, T. (1937). The fundamentals of the statistical theory of turbulence. *Journal of the Aeronautical Sciences*, *4*(4), 131–138.

Wang, J., & Vasconcelos, J. (2018). Manhole cover displacement caused by the release of entrapped air pockets. *Journal of Water Management Modeling*.

Wang, J., & Vasconcelos, J. G. (2020). Investigation of manhole cover displacement during rapid filling of stormwater systems. *Journal of Hydraulic Engineering*, *146*(4), 04020022.

Wanielista, M. P., & Yousef, Y. A. (1992). *Stormwater management*. John Wiley & Sons.

Wendt, J. F. (2008). *Computational fluid dynamics: An introduction*. Springer Science & Business Media.

Wilcox, D. C. et al. (1998). *Turbulence modeling for cfd* (Vol. 2). DCW industries La Canada, CA.

Wright, S. J., Vasconcelos, J., & Ridgway, K. (2003). Surges associated with filling of stormwater storage tunnels. *Journal of Water Management Modeling*.

Wright, S. J., Lewis, J. W., & Vasconcelos, J. G. (2011). Geysering in rapidly filling storm-water tunnels. *Journal of Hydraulic Engineering*, *137*(1), 112–115.

Wylie, E. B., & Streeter, V. L. (1993). *Fluid transients in systems* (Vol. 1). Prentice Hall Englewood Cliffs, NJ.

Yalcin, E. (2019). Two-dimensional hydrodynamic modelling for urban flood risk assessment using unmanned aerial vehicle imagery: A case study of kirsehir, turkey. *Journal of flood risk management*, *12*, e12499.

Yen, B. C. (1986). Hydraulics of sewers. *Advances in hydroscience* (pp. 1–122). Elsevier.

Yi, X. (2011). A dam break analysis using hec-ras. *Journal of Water Resource and Protection*, *2011*.

Zahmatkesh, Z., Burian, S. J., Karamouz, M., Tavakol-davani, H., & Goharian, E. (2015). Low-Impact Development Practices to Mitigate Climate Change Effects on Urban Stormwater Runoff : Case Study of New York City. *Journal of Irrigation and Drainage Engineering*, *141*(1), 1–13. https://doi.org/10.1061/(ASCE)IR.1943-4774.0000770.

Zhou, F. et al. (2002). Transient flow in a rapidly filling horizontal pipe containing trapped air. *Journal of Hydraulic Engineering*, *128*(6), 625–634.